

NAVAL POSTGRADUATE SCHOOL MONTEREY, CALIFORNIA



THESIS

**OPTIMAL SOLUTION SELECTION FOR
SENSITIVITY-BASED FINITE ELEMENT
MODEL UPDATING AND STRUCTURAL
DAMAGE DETECTION**

by

Jay A. Renken

December, 1995

Thesis Advisor:

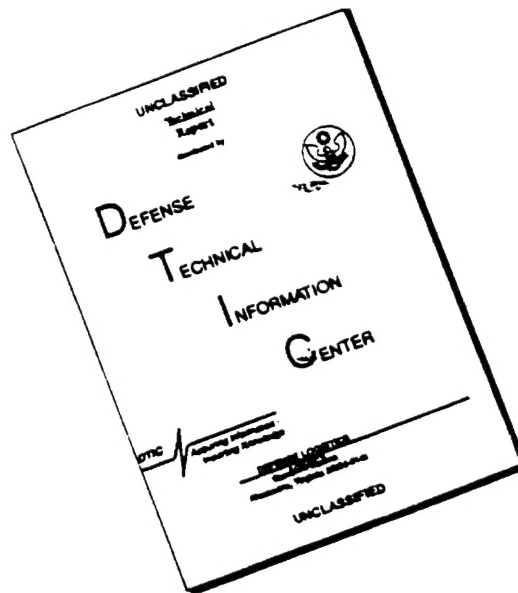
Joshua H. Gordis

Approved for public release; distribution is unlimited.

DTIC QUALITY INSPECTED 1

19960401 066

DISCLAIMER NOTICE



THIS DOCUMENT IS BEST QUALITY AVAILABLE. THE COPY FURNISHED TO DTIC CONTAINED A SIGNIFICANT NUMBER OF PAGES WHICH DO NOT REPRODUCE LEGIBLY.

REPORT DOCUMENTATION PAGE			Form Approved OMB No. 0704-0188	
Public reporting burden for this collection of information is estimated to average 1 hour per response, including the time for reviewing instruction, searching existing data sources, gathering and maintaining the data needed, and completing and reviewing the collection of information. Send comments regarding this burden estimate or any other aspect of this collection of information, including suggestions for reducing this burden, to Washington Headquarters Services, Directorate for Information Operations and Reports, 1215 Jefferson Davis Highway, Suite 1204, Arlington, VA 22202-4302, and to the Office of Management and Budget, Paperwork Reduction Project (0704-0188) Washington DC 20503.				
1. AGENCY USE ONLY (Leave blank)		2. REPORT DATE December 1995		3. REPORT TYPE AND DATES COVERED Master's Thesis
4. TITLE AND SUBTITLE OPTIMAL SOLUTION SELECTION FOR SENSITIVITY-BASED FINITE ELEMENT MODEL UPDATING AND STRUCTURAL DAMAGE DETECTION			5. FUNDING NUMBERS	
6. AUTHOR(S) Jay A. Renken				
7. PERFORMING ORGANIZATION NAME(S) AND ADDRESS(ES) Naval Postgraduate School Monterey CA 93943-5000			8. PERFORMING ORGANIZATION REPORT NUMBER	
9. SPONSORING/MONITORING AGENCY NAME(S) AND ADDRESS(ES)			10. SPONSORING/MONITORING AGENCY REPORT NUMBER	
11. SUPPLEMENTARY NOTES The views expressed in this thesis are those of the author and do not reflect the official policy or position of the Department of Defense or the U.S. Government.				
12a. DISTRIBUTION/AVAILABILITY STATEMENT Approved for public release; distribution is unlimited.			12b. DISTRIBUTION CODE	
13. ABSTRACT (maximum 200 words) The finite element model has become the standard way in which complex structural systems are modeled, analyzed, and the effects of loading simulated. A new method is developed for comparing the finite element simulation to experimental data, so the model can be validated, which is a critical step before a model can be used to simulate the system. An optimization process for finite element structural dynamic models utilizing sensitivity based updating is applied to the model updating and damage detection problems. Candidate solutions are generated for the comparison of experimental frequencies to analytical frequencies, with mode shape comparison used as the selection criteria for the optimal solution. The method is applied to spatially complete simulations and to spatially incomplete experimental data which includes the model validation of a simple airplane model, and the damage localization in composite and steel beams with known installed damage.				
14. SUBJECT TERMS Finite Element Model Update			15. NUMBER OF PAGES 214	
			16. PRICE CODE	
17. SECURITY CLASSIFICATION OF REPORT Unclassified	18. SECURITY CLASSIFICATION OF THIS PAGE Unclassified	19. SECURITY CLASSIFICATION OF ABSTRACT Unclassified	20. LIMITATION OF ABSTRACT UL	

NSN 7540-01-280-5500

Standard Form 298 (Rev. 2-89)
Prescribed by ANSI Std. Z39-18 298-102

Approved for public release; distribution is unlimited.

**OPTIMAL SOLUTION SELECTION FOR SENSITIVITY-BASED FINITE
ELEMENT MODEL UPDATING AND STRUCTURAL DAMAGE
DETECTION**

Jay A. Renken
Lieutenant Commander, United States Navy
B.S., University of Illinois, 1983

Submitted in partial fulfillment
of the requirements for the degrees of

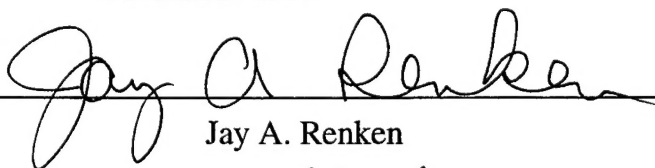
**MASTER OF SCIENCE IN MECHANICAL ENGINEERING
MECHANICAL ENGINEER**

from the

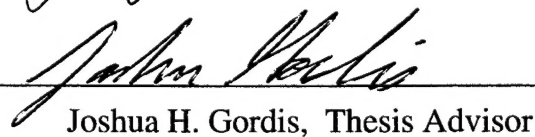
NAVAL POSTGRADUATE SCHOOL

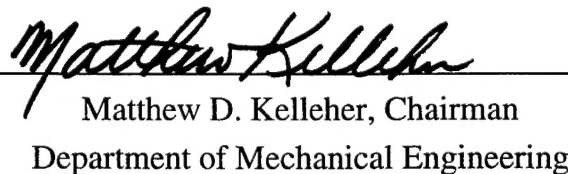
December 1995

Author:


Jay A. Renken

Approved by:


Joshua H. Gordis, Thesis Advisor


Matthew D. Kelleher, Chairman
Department of Mechanical Engineering

ABSTRACT

The finite element model has become the standard way in which complex structural systems are modeled, analyzed, and the effects of loading simulated. A new method is developed for comparing the finite element simulation to experimental data, so the model can be validated, which is a critical step before a model can be used to simulate the system. An optimization process for finite element structural dynamic models utilizing sensitivity based updating is applied to the model updating and damage detection problems. Candidate solutions are generated for the comparison of experimental frequencies to analytical frequencies, with mode shape comparison used as the selection criteria for the optimal solution. The method is applied to spatially complete simulations and to spatially incomplete experimental data which includes the model validation of a simple airplane model, and the damage localization in composite and steel beams with known installed damage.

TABLE OF CONTENTS

I.	INTRODUCTION	1
A.	BACKGROUND	2
B.	ANALYSIS METHODS	2
C.	ANALYSIS APPLICATIONS	4
1.	Model Updating	4
2.	Damage Localization	7
 II.	 THEORY	 11
A.	FREQUENCY SENSITIVITIES	11
B.	ASSESSING SENSITIVITY ANALYSIS	13
C.	OPTIMIZATION	14
D.	OPTIMIZATION SCALING	16
E.	DESIGN VARIABLE COMBINATIONS	17
F.	MODAL ASSURANCE CRITERION	19
 III.	 COMPUTER SIMULATION	 21
A.	BEAM MODEL UPDATING	21
1.	Sensitivity Linearity Assessment	22
2.	Initial Optimization Procedures	27
a.	Test Case 1 - 2 Design Variables, No Scaling	30
b.	Test Case 2 - 2 Design Variables, With Scaling ..	32
c.	Test Cases 3 and 4 - Objective Function	
	Weighting	34
3.	Advanced Optimization Procedures	36
a.	Test Case 5 - Multiple Design Variables	
	Combinations	37
b.	Test Case 6 - Prescribed Error Effects	39

c.	Test Case 7 - Alternate Objective Function	40
4.	Two Region Optimization	44
a.	Test Case 8- 4 Design Variables	45
5.	Model Updating Observations	47
B.	BEAM DAMAGE LOCALIZATION	48
1.	Damage Localization Process	50
2.	One Inch Crack	51
a.	Centered Damage - Elements 24-25	51
b.	Off Center Damage - Element 40	55
3.	2.25 Inch Crack	56
a.	Centered Damage - Elements 23-26	56
b.	Off Center Damage - Elements 30-31	57
4.	4.5 Inch Crack	58
a.	Centered Damage - Elements 22-27.	58
b.	Off Center Damage - Elements 5-8	59
5.	9 Inch Crack	60
a.	Centered Damage - Elements 20-29.	60
b.	Off Center Damage - Elements 37-45	61
6.	Damage Localization Observations	61
IV.	EXPERIMENT	63
A.	EXPERIMENTAL MEASUREMENT	63
B.	SPATIALLY INCOMPLETE DATA	64
1.	Extraction Method	65
2.	Transformation Matrix Reduction and Expansion	66
C.	MODEL UPDATING	67
1.	Test Article Description	67
2.	Finite Element Model Description	68
3.	Model Updating Problem	69

4.	Optimization Process	72
5.	Optimization Solution	73
6.	Solution Interpretation	74
D.	COMPOSITE BEAM DAMAGE LOCALIZATION	75
1.	Test Article and Finite Element Model Description	75
2.	Finite Element Model Update	76
3.	Damage Localization	77
4.	Localization Results	78
5.	Solution Interpretation	80
E.	STEEL BEAM DAMAGE LOCALIZATION	80
1.	Test Article and Finite Element Model Description	81
2.	Finite Element Model Update	82
3.	Damage Localization	83
4.	Solution Method	84
5.	Localization Results	84
6.	Simulated Experimental Damage	85
a.	Frequency Substitution	87
b.	Mode Shape Substitution	88
c.	Frequency and Mode Shape Substitution	89
7.	Solution Interpretation	90
V.	CONCLUSIONS / RECOMMENDATIONS	93
A.	SUMMARY	93
B.	CONCLUSIONS	94
C.	RECOMMENDATIONS	95
APPENDIX A.	ALUMINUM BEAM SPECIFICATIONS	99
A.	PHYSICAL DIMENSIONS AND PROPERTIES	99
B.	DYNAMIC RESPONSE	99

C.	OPTIMIZATION RESULTS	102
APPENDIX B.	COMPOSITE BEAM SPECIFICATIONS	111
A.	PHYSICAL DIMENSIONS AND PROPERTIES	111
B.	DYNAMIC RESPONSE	112
APPENDIX C.	EXPERIMENTAL SETUP	117
APPENDIX D.	AIRPLANE MODEL SPECIFICATIONS	123
A.	PHYSICAL DIMENSIONS AND PROPERTIES	123
B.	DYNAMIC RESPONSE	123
APPENDIX E.	AIRPLANE FINITE ELEMENT MODEL	135
APPENDIX F.	COMPOSITE BEAM TEST DATA	149
APPENDIX G.	STEEL BEAM SPECIFICATIONS	161
A.	PHYSICAL DIMENSIONS AND PROPERTIES	161
B.	DYNAMIC RESPONSE	161
APPENDIX H.	COMPUTER CODE	173
APPENDIX I.	IDEAS CONVERSION INFORMATION	193
A.	SENSITIVITY CONVERSION	193
B.	MODE SHAPE NORMALIZATION AND MODAL MASSES .	194

LIST OF REFERENCES	195
---------------------------------	------------

INITIAL DISTRIBUTION LIST	197
--	------------

LIST OF FIGURES

1-1	Optimization Flow Diagram	5
1-2	Damage Localization Flow Diagram	8
3-1	Absolute Value of Percentage Error for 1st Natural Frequency Update ..	24
3-2	Absolute Value of Percentage Error for 2nd Natural Frequency Update ..	24
3-3	Test Case 1 Solution Results	31
3-4	Test Case 2 Solution Results	33
3-5	Test Case 3 Solution Results	35
3-6	Test Case 4 Solution Results	35
3-7	Test Case 5 Solution Results	38
3-8	Test Case 6 Solution Results	40
3-9	Test Case 7 Solution Results	42
3-10	Test Case 8 Solution Results	46
3-11	Region Expansion, 1 inch Centered Crack	54
4-1	Analytical Model Frequency Percentage Error	70
4-2	Airplane Model Design Variable Regions	71
4-3	Frequency Error Comparison, Original and Updated Models	74
A-1	Aluminum Beam	99
A-2	Aluminum Beam, 1st Mode Shape	100
A-3	Aluminum Beam, 2nd Mode Shape	100
A-4	Aluminum Beam, 3rd Mode Shape	101
A-5	Aluminum Beam, 4th Mode Shape	101
B-1	Composite Beam	111
B-2	Composite Beam Analytical Mode Shape 1	112
B-3	Composite Beam Analytical Mode Shape 2	113
B-4	Composite Beam Analytical Mode Shape 3	113
B-5	Composite Beam Analytical Mode Shape 4	114
B-6	Composite Beam Analytical Mode Shape 5	114
B-7	Composite Beam Analytical Mode Shape 6	115
B-8	Composite Beam Analytical Mode Shape 7	115
B-9	Composite Beam Analytical Mode Shape 8	116
B-10	Composite Beam Analytical Mode Shape 9	116
C-1	Experimental Setup	117
D-1	Experimental Data Points	124
D-2	Airplane Experimental Mode Shape 1	125
D-3	Airplane Experimental Mode Shape 2	126
D-4	Airplane Experimental Mode Shape 3	127
D-5	Airplane Experimental Mode Shape 4	128
D-6	Airplane Experimental Mode Shape 5	129
D-7	Airplane Experimental Mode Shape 6	130
D-8	Airplane Experimental Mode Shape 7	131
D-9	Airplane Experimental Mode Shape 8	132
D-10	Airplane Experimental Mode Shape 9	133

D-11	Airplane Experimental Mode Shape 10	134
E-1	Airplane Finite Element Model	136
E-2	Airplane Analytical Mode Shape 1	137
E-3	Airplane Analytical Mode Shape 2	138
E-4	Airplane Analytical Mode Shape 3	139
E-5	Airplane Analytical Mode Shape 4	140
E-6	Airplane Analytical Mode Shape 5	141
E-7	Airplane Analytical Mode Shape 6	142
E-8	Airplane Analytical Mode Shape 7	143
E-9	Airplane Analytical Mode Shape 8	144
E-10	Airplane Analytical Mode Shape 9	145
E-11	Airplane Analytical Mode Shape 10	146
F-1	Composite Beam Excitation Points	150
F-2	Composite Beam Experimental Mode Shape 1	151
F-3	Composite Beam Experimental Mode Shape 2	152
F-4	Composite Beam Experimental Mode Shape 3	153
F-5	Composite Beam Experimental Mode Shape 4	154
F-6	Composite Beam Experimental Mode Shape 5	155
F-7	Composite Beam Experimental Mode Shape 6	156
F-8	Composite Beam Experimental Mode Shape 7	157
F-9	Composite Beam Experimental Mode Shape 8	158
F-10	Composite Beam Experimental Mode Shape 9	159
G-1	Steel Beam	161
G-2	Steel Beam Excitation Points	163
G-3	Steel Beam Experimental Mode Shape 1	164
G-4	Steel Beam Experimental Mode Shape 2	165
G-5	Steel Beam Experimental Mode Shape 3	166
G-6	Steel Beam Experimental Mode Shape 4	167
G-7	Steel Beam Experimental Mode Shape 5	168
G-8	Steel Beam Experimental Mode Shape 6	169
G-9	Steel Beam Experimental Mode Shape 7	170
G-10	Steel Beam Experimental Mode Shape 8	171
G-11	Steel Beam Experimental Mode Shape 9	172

LIST OF TABLES

2-1	2-Level Factorial Test, "After [Ref. 6: p. 58]"	18
3-1	Cauchy Ratio Equivalent Calculated Values	26
3-2	Damage Localization Results, First Iteration, 1 inch Crack, Elements 24-25	52
3-3	Damage Localization Results, Second Iteration, 1 inch Crack, Elements 24-25	53
3-4	Damage Localization Results, Third Iteration, 1 inch Crack, Elements 24-25	53
3-5	Damage Localization Results, 1 inch Off Center Crack	55
3-6	Damage Localization Results, 2.25 inch Centered Crack	56
3-7	Damage Localization Results, Fourth Iteration, 2.25 inch Centered Crack	57
3-8	Damage Localization Results, 2.25 inch Off Center Crack	57
3-9	Damage Localization Results, 4.5 inch Centered Crack	58
3-10	Damage Localization Results, 4.5 inch Off Center Crack	59
3-11	Damage Localization Results, 9 inch Centered Crack	60
3-12	Damage Localization Results, 9 inch Off Center Crack	61
4-1	Airplane Model Dynamic Response	69
4-2	Composite Beam Update Data	77
4-3	Composite Beam Damage Search Results, Extraction Method	78
4-4	Composite Beam Damage Search Results, Static Reduction	79
4-5	Composite Beam Damage Search Results, Static Expansion	79
4-6	Composite Beam Damage Search Results, IRS Reduction	80
4-7	Composite Beam Damage Search Results, IRS Expansion	80
4-8	Steel Beam Update Data	83
4-9	Steel Beam Damage Search Results, Extraction Method	85
4-10	Simulated Experimental Data Comparison	86
4-11	Steel Beam Damage Search Results, Simulated Experimental Data	86
4-12	Experimental Data Substitution Results	87
A-1	Test Case 1 Numerical Results	102
A-2	Test Case 2 Numerical Results	103
A-3	Test Case 3 Numerical Results	104
A-4	Test Case 4 Numerical Results	105
A-5	Test Case 5 Numerical Results	106
A-6	Test Case 6 Numerical Results	107
A-7	Test Case 7 Numerical Results	108
A-8	Test Case 8 Numerical Results	109
D-1	Airplane Model Dimensions	123
E-1	Airplane Update Frequency Comparison	147

I. INTRODUCTION

A. BACKGROUND

Finite element models are widely used to predict the response characteristics of complex structures in the area of structural dynamics. The models can be very complex and use large numbers of degrees of freedom so that the desired level of accuracy will be achieved. However, the construction of the models can be an inexact science. Variations such as non-homogeneity in physical properties within structures, difficulties in determining the stiffness of different types of structural joints, and the inability for the solution of a finite degree of freedom model to converge to the exact solution of an infinite degree of freedom system make the task of constructing an accurate model daunting.

In view of these difficulties with finite element models, methods of model updating to improve model correlation with tests have been explored [Ref. 1-3]. Methods for model updating are based on the comparison of analytical data from finite element models to that of experimentally obtained data from the structures being modeled. Dynamic response parameters used for this comparison are the natural frequencies of vibration, corresponding mode shapes, and damping behavior. The real question becomes how is the dynamic response information fed back into the model to make corrections? There are two major difficulties with updating an analytical model. The first difficulty is that when dealing with a complex model there are large numbers of variables that can be adjusted resulting in a very large search domain. Related to this problem with the search process is that there are an infinite number of design variable combination changes that

will result in a mathematically correct yet non-unique solution for the model system. The second difficulty is that the solution time to re-solve the eigenproblem for complex models can be quite large and very expensive, which limits the number of variable change combinations that can be investigated in a cost effective manner. With these difficulties in mind it is imperative that a search routine to update models will minimize iterations and therefore cost, as well as provide verifiable and accurate results.

Once a finite element model has been updated it is used to accurately predict the dynamic response characteristics of the modeled structure and to investigate the effect of design changes. This allows non-destructive testing of the structure to various simulated loads ensuring adequate strength or performance of the structure. Another application of the updated model is in the area of localizing structural damage in a structure. Measured dynamic response parameters of a structure that is believed to be damaged are compared to the updated model. The search process used to update the model is then applied to determine where differences between analysis and test occurred, thereby localizing the probable area of damage.

B. ANALYSIS METHODS

Dynamic response parameters are generated for the analytical model and the actual structure. The parameters experimentally determined from the actual structure are the natural frequencies of the structure and the corresponding mode shapes. The parameters for the initial analytical model are the natural frequencies and the associated frequency sensitivities. Finite element model sensitivities are the first derivative of the eigen problem solution set with respect to the design variables under consideration.

Frequency sensitivities are the basis for a linear approximation to compute the change in the natural frequencies of a model based on a change in a given design variable. This method of frequency updating greatly reduces the computational time required to calculate the results of a change to large finite element models by eliminating the need to re-solve the eigenproblem for each iteration. This process of frequency updating has been used extensively for model updating and is discussed further in references (1) through (3).

To search the solution domain for prospective solutions, a constrained optimization routine is employed. Optimization theory and techniques are discussed further in reference (4). The optimization routine employed searches for the minimum value of an objective function which is constructed to minimize the differences between the analytical model parameters and the experimental data. This organized approach of searching for the optimal combination of design variables minimizes the number of combinations that are investigated thereby reducing the computational requirements of this process.

The real difficulty to this method of correcting a finite element model is to determine which candidate solution most closely matches the experimental data. Multiple combinations of design variable changes can result in the same changes to the natural frequencies of the model so the accuracy of the frequencies is not the only evaluation factor. An improved method of solution evaluation is to determine the effects on the analytical mode shapes and compare them to the experimental mode shapes. This comparison of mode shapes is called the Modal Assurance Criterion (MAC) and is discussed in reference (5). The MAC is a measure of how closely two mode shapes

coincide. The candidate solution with a MAC value most close to one when compared to the experimental data most closely resembles the experimental case and is selected as the optimal solution.

C. ANALYSIS APPLICATIONS

There are two applications of this optimal solution search procedure using finite element model sensitivities and frequency differences. The first application of the procedure is updating the system finite element model. Model updating correlates the baseline model for use for system computations. The second procedure involves damage localization using a previously updated model. There are numerous non-destructive methods for testing structures but most are limited to surface defects. By comparing the change in the vibrational characteristics of a validated system as well as comparing the mode shapes the finite element model can be used as a damage localization system for internal structure defects.

1. Model Updating

Model updating is imperative to verify the accuracy of a finite element model. The method that was chosen to update the model was an optimization search utilizing sensitivity based frequency updates. Figure 1-1 is a flow diagram of the updating process. This method is similar to those as discussed in references (1) to (3) with differences in design variable scaling and choice of objective function. The initial step is to develop the finite element model of the structure to generate the analytical frequencies and design variable sensitivities. The actual structure is also tested to provide the experimental data. The objective function is then selected. The objective function is the equation that the

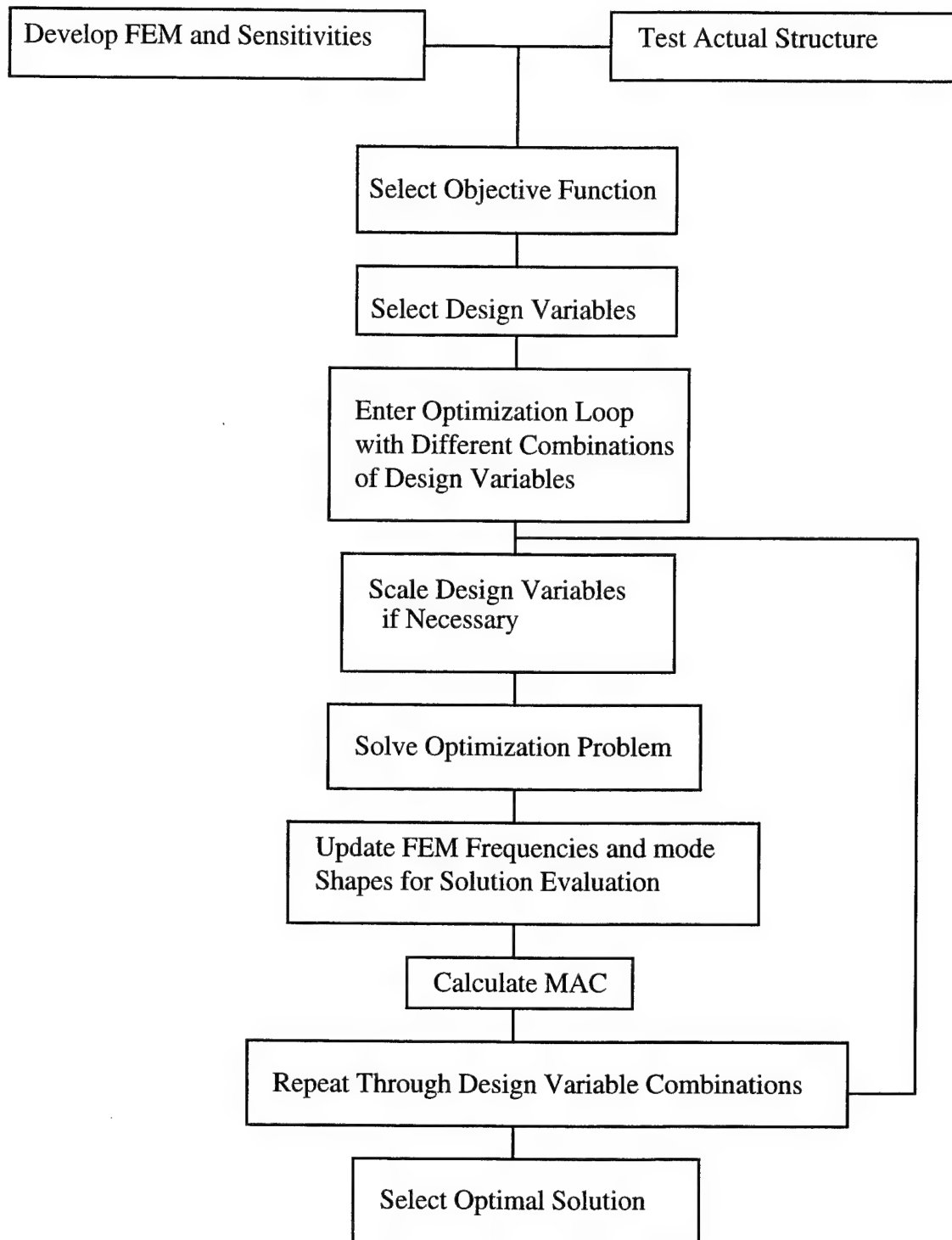


Figure 1-1 Optimization Flow Diagram

optimization process will minimize. The parameters chosen for the objective function can vary. In reference (1) the summation of the percentage difference in the system frequencies and the absolute change in the design variables were chosen. In reference (2), differences in the frequencies, the mode shapes and the static deflection were chosen. For this thesis two objective functions were investigated. The first was a scaled sum of the percentage difference in the frequencies added to the sum of the percentage change of the design variables during the domain search. The second type of objective function is the sum of the change in design variables during the domain search constrained by maintaining the difference in the analytical and experimental frequencies below a chosen tolerance.

The design variables are chosen based on the specifics of the model and the structure. These could be material property values or assumed values of joint stiffness or any other variable which was chosen with some level of uncertainty. At this point the optimization loop is entered. Combinations of the design variables are chosen so that all possible combinations are investigated. These type of search is discussed in reference (6). This type of search pattern will result in $2^n - 1$ iterations, where n is the number of design variables chosen. This drives the use of less design variables to minimize computation time.

If the design variables are of differing magnitudes they should be scaled to be the same size. This will reduce the chance that a single variable will dominate the optimization process. The scaled design variables are used with the frequency sensitivities to update the objective function. The optimization process uses a 1st order

search routine to find the minimum objective function value within the search domain. The optimized design variables are then fed back into a routine to solve the eigenproblem generating the natural frequencies and mode shapes for this variable combination. The mode shapes are compared to the experimental data by computing the MAC and are summed for the modes of interest. This process is repeated for all the combinations of the design variables. The combination of design variables with the highest MAC value is chosen as the optimal solution.

2. Damage Localization

The process chosen for damage localization utilizes the same basic optimization routine as model updating with a different search logic. This method is based on the premise that any sub-surface defects in the material will be manifested in a finite element model as a reduction in the stiffness of the structure. It was assumed that there would be no mass loss for this situation. Figure 1-2 is a flow diagram of the damage localization process. It differs from the procedures discussed in references (7) through (10) in the search methodology and evaluation methods. The process still begins with the comparison of the analytical data and the experimental data. The objective function is the same as in the validation process.

The major difference between the model updating process and the damage location process is that the design variables considered are the element stiffnesses within designated search regions. The search logic is that a selected search region is divided into sub-regions. The stiffness of a sub-region is optimized as if it had suffered a reduction resulting in the experimentally observed frequency shifts for the damaged case. The

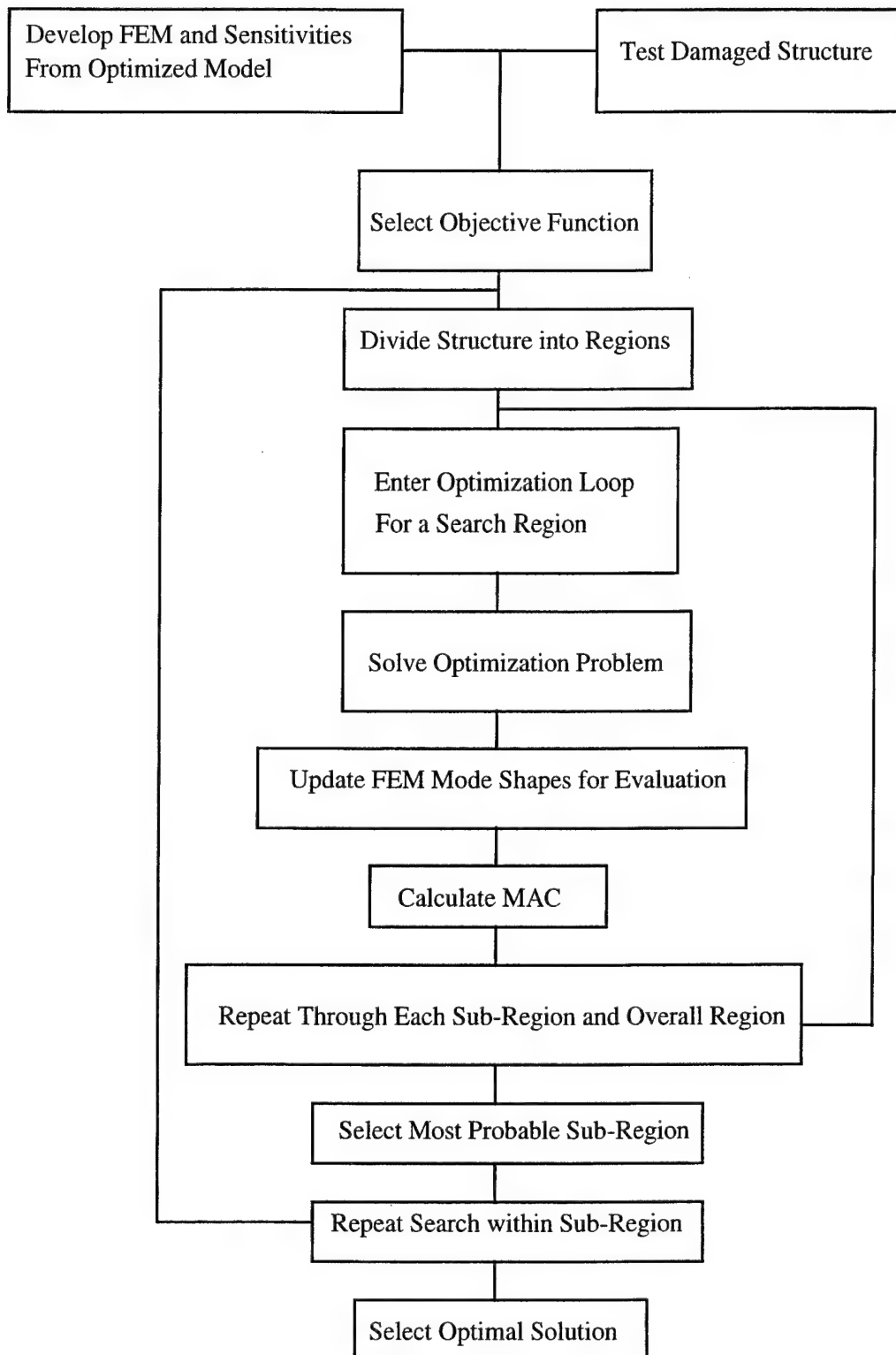


Figure 1-2 Damage Localization Flow Diagram

reduced stiffness for that sub-region is fed back into the finite element model to generate assumed damage mode shapes. These mode shapes are then compared with the experimental mode shapes with the MAC. This process is repeated for all of the search sub-regions as well as the overall region of the search. The sub-region with the highest summed MAC value is evaluated as the most probable area of damage if the MAC value does not exceed that of the entire region. The selection of the most probable sub-region is then used to start another search iteration with the smaller region. This process is repeated until the damage is localized to a single element of the analytical model or the search region is evaluated as more probable than any single sub-region. At this point the most probable area of damage is selected.

II. THEORY

A. FREQUENCY SENSITIVITIES

A typical dynamic response finite element model is a method to mathematically model the response characteristics of a structure. The properties of the structure are reduced to the eigenvalue problem for dynamic structural response as given by:

$$[K][\Phi] - [M][\Phi][\Lambda] = 0 \quad (2.1)$$

where $[K]$ is the system stiffness matrix, $[M]$ is the system mass matrix, $[\Lambda]$ is the eigenvalue matrix, and $[\Phi]$ is the eigenvector matrix. $[K]$ and $[M]$ are defined by the physical properties of the system including the physical dimensions, mass density and the Young's modulus of the materials in the structure. The stiffness and mass matrices are $n \times n$ in size where n is the number of degrees of freedom within the model. $[\Lambda]$ is a $n \times n$ diagonal matrix which contains the system eigenvalues. $[\Phi]$ is a $n \times n$ matrix whose columns define the mode shapes of the system. The natural frequencies of the system are computed from the eigenvalue matrix. The i th natural frequency of the system, in Hertz, is calculated as follows:

$$\omega_i = \sqrt{\lambda_i} \quad (2.2)$$

$$f_i = \frac{1}{2\pi} \sqrt{\omega_i} \quad (2.3)$$

where λ_i is the i th diagonal term of the eigenvalue matrix. Equation (2.1) can be rearranged and still holds for each individual mode as shown for the i th mode in the following:

$$([K] - \lambda_i[M])\{\phi_i\} = 0 \quad (2.4)$$

Now consider a change in the k th design variable, v_k , which may affect both $[K]$ and $[M]$. Differentiating Equation (2.4) with respect to v_k results in:

$$\left[\left[\frac{\partial K}{\partial v_k} \right] - \frac{\partial \lambda_i}{\partial v_k} [M] - \lambda_i \left[\frac{\partial M}{\partial v_k} \right] \right] \{\phi_i\} + ([K] - \lambda_i [M]) \left\{ \frac{\partial \phi_i}{\partial v_k} \right\} = 0 \quad (2.5)$$

Equation (2.5) is then premultiplied by $\{\phi_i\}^T$, the transpose of the i th mode shape, resulting in equation (2.6).

$$\{\phi_i\}^T \left[\left[\frac{\partial K}{\partial v_k} \right] - \frac{\partial \lambda_i}{\partial v_k} [M] - \lambda_i \left[\frac{\partial M}{\partial v_k} \right] \right] \{\phi_i\} + \{\phi_i\}^T ([K] - \lambda_i [M]) \left\{ \frac{\partial \phi_i}{\partial v_k} \right\} = 0 \quad (2.6)$$

Because of the orthogonality of eigenvectors Equation (2.7) through Equation (2.9) hold:

$$[K] = [K]^T \quad (2.7)$$

$$[M] = [M]^T \quad (2.8)$$

$$\{\phi_i\}^T ([K] - \lambda_i [M]) = 0 \quad (2.9)$$

Substituting Equation (2.9) into Equation (2.6) eliminates the second term of the left hand side. Rearranging terms yields Equation (2.10):

$$\frac{\partial \lambda_i}{\partial v_k} = \frac{\{\phi_i\}^T \left[\left[\frac{\partial K}{\partial v_k} \right] - \lambda_i \left[\frac{\partial M}{\partial v_k} \right] \right] \{\phi_i\}}{\{\phi_i\}^T [M] \{\phi_i\}} \quad (2.10)$$

If mass normalized mode shapes are utilized the denominator of Equation (2.10) is equal to 1 reducing Equation (2.10) to:

$$\frac{\partial \lambda_i}{\partial v_k} = \{\phi_i\}^T \left[\left[\frac{\partial K}{\partial v_k} \right] - \lambda_i \left[\frac{\partial M}{\partial v_k} \right] \right] \{\phi_i\} \quad (2.11)$$

Equation (2.11) is then used to calculate the sensitivity matrix, $[T]$, for the analytical model. $[T]$ is a $n \times m$ matrix where n is the number of modes used and m is the number of design variables considered. The sensitivity matrix is used to approximate the frequency shift of the analytical system within the optimization loop for small changes in the design variables with Equation (2.12):

$$\{\Delta\lambda\} = [T]\{\Delta v_k\} \quad (2.12)$$

Where Δ symbolizes small changes in the eigenvalues and the design variables.

B. ASSESSING SENSITIVITY ANALYSIS

Because Equation (2.12) is a linear approximation for a non-linear situation it is only valid for small changes in the vicinity of the system eigenvalues and original design variable values. A method to assess the applicability of the sensitivity approximation is derived in detail in reference (11). The method utilizes second-order sensitivities to evaluate if the use of first order sensitivities are appropriate. "The method is based on the use of a truncated Taylor Series extrapolation" [Ref. 11: p. 136] and "the Cauchy condition for the convergence of a general power series" [Ref. 11: p. 136]. "Analogy to the Cauchy ratio test suggests that the convergence of the Taylor series is likely to depend on the ratio" [Ref. 11: p. 136]:

$$\gamma_{ik} = \left| \Delta v_k \sum_{j=1, j \neq i}^n \frac{\{\phi_j\}^T \left[\frac{\partial K}{\partial v_k} \right] - \lambda_i \left[\frac{\partial M}{\partial v_k} \right] \{\phi_i\}}{\{\phi_i\}^T \left[\frac{\partial K}{\partial v_k} \right] - \lambda_i \left[\frac{\partial M}{\partial v_k} \right] \{\phi_i\}} \alpha_{ij} \right| \quad (2.13)$$

with

$$\alpha_{ij} = \frac{\{\phi_j\}^T \left[\left[\frac{\partial K}{\partial v_k} \right] - \left[\frac{\partial M}{\partial v_k} \right] \right] \{\phi_i\}}{(\lambda_i - \lambda_j)} \quad (2.14)$$

Where i indicates the mode of interest, j indicates all other modes, and k indicates the design variable of interest. The determination of acceptability of the first order sensitivity approximation is based on the value of γ_{ij} . "If γ_{ij} is much less than one the approximation should be accurate" [Ref. 10: p. 136].

C. OPTIMIZATION

"The purpose of numerical optimization is to aid in rationally searching for the best design to minimize a function of the design variables to satisfy constraints" [Ref. 4: p. 1]. In this instance the purpose is to match the dynamic response of a finite element model to that of the experimental response of the system of interest. "The general problem statement for a non-linear constrained optimization problem is" [Ref. 4: p. 9]:

$$\text{Minimize: } F(X) \quad \text{Objective Function} \quad (2.15)$$

Subject to:

$$g_j(X) \leq 0 \quad j = 1, m \quad \text{Inequality Constraints} \quad (2.16)$$

$$h_k(X) = 0 \quad k = 1, p \quad \text{Equality Constraints} \quad (2.17)$$

$$X_i^l \leq X_i \leq X_i^u \quad i = 1, n \quad \text{Side Constraints} \quad (2.18)$$

$$\text{where } X = \begin{Bmatrix} X_1 \\ X_2 \\ X_3 \\ \vdots \\ X_n \end{Bmatrix} \quad \text{Design Variables}$$

The vector X is the vector of design variables. The constraint equations are used to bound possible solution combinations to meet the requirements of the given situation.

Most optimization algorithms require that an initial set of design variables, X^0 , be specified. Beginning from this starting point, the design is updated iteratively. This process can be written as:

$$X^q = X^{q-1} + \alpha S^q \quad (2.19)$$

where q is the iteration number and S is a vector search direction in the design space. "The scalar quantity α defines the distance that we wish to move in direction S " [Ref. 4: p. 10]. The updated values of X are used to calculate the value of the objective function for each iteration. The search direction is chosen to decrease the value of the objective function while staying within the constraints of the system. The process continues until the objective function converges to a local minimum and the optimal solution is localized.

There are many methods to choose the search direction, S . The search direction selected for this thesis is the steepest descent method. In the steepest descent method the search direction is taken as the negative of the gradient of the objective function. That is at iteration q :

$$S^q = - \nabla F(X^q) \quad (2.20)$$

"This S^q vector is used in Equation (2.19) to perform a one-dimensional search" [Ref. 4: p. 88].

D. OPTIMIZATION SCALING

For the model optimization problem the design variables being considered can have greatly different magnitudes. To ensure that each design variable has the same effect on the optimization process it is beneficial to scale the design variables. "Scaling has the effect of putting each variable on the same basis in the sense that a 1 percent change has roughly the same meaning for each variable" [Ref. 4: p. 100]. The method of scaling chosen was to scale variables to the value of the smallest design variable. This results in the construction of a nxn diagonal scaling matrix, S_c . The kth diagonal term of the scaling matrix is X_{\min}/X_k . Scaled design variables can then be calculated with the following:

$$\{\tilde{X}\} = [S_c]\{X\} \quad (2.21)$$

where the tilde symbolizes scaled values. Rearranging Equation (2.21) results in:

$$\{X\} = [S_c]^{-1}\{\tilde{X}\} \quad (2.22)$$

Applying the scaling logic of Equation (2.22) to the particular function stated in Equation (2.12) results in the following:

$$\{\Delta\lambda\} = [T][S_c]^{-1}\{\Delta\tilde{v}_k\} \quad (2.23)$$

Combining the sensitivity matrix and the inverted scaling matrix results in the scaled change in frequency function used in the objective function for the scaled optimization problem:

$$\{\Delta\lambda\} = [\tilde{T}]\{\Delta\tilde{v}_k\} \quad (2.24)$$

E. DESIGN VARIABLE COMBINATIONS

When conducting an experiment to see how design variables effect a given function, “a logical way to manage the experiment is to change one design variable at a time, which is called the classical one-factor-at-a-time (1-F.A.A.T.) technique” [Ref. 6: p. 51]. This method, although orderly and thorough, does not take into account any interrelation between design variables, or allow for multiple factors to be considered together. Another approach to this experiment is to examine k factors, in n observations, with each factor at two levels. “This approach is called the 2-level factorial design” [Ref. 6: p. 54]. By two levels it is meant that a particular factor is either considered at a low level or a high level for each observation. “The total number of observations in such an experiment is determined by taking the number of levels (2) to the power of the number of factors (k) such that $n = 2^k$ ” [Ref. 6: p. 54]. “In this design we look at all possible combinations of the two level design variables” [Ref. 6: p. 54].

In the context of this thesis there are minor modifications to the 2-level factorial design. The first is that the low level of the design variable means that it is not adjusted. The high level of the design variable means that it is adjusted. To symbolize whether a design variable is considered or not a binary notation is used. A 0 means the design variable is not considered while a 1 indicates that the design variable is considered. With these symbols a table can be constructed to describe the design variable combinations for the experiment. Table 2-1 is an example of how a experiment would be set up for three design variables. Three design variables for two levels would result in 2^3 or 8

Observation	Design Variable (1)	Design Variable (2)	Design Variable (3)
1	0	0	0
2	1	0	0
3	0	1	0
4	1	1	0
5	0	0	1
6	1	0	1
7	0	1	1
8	1	1	1

Table 2-1 2-Level Factorial Test, “After [Ref. 6: p. 58]”

observations. Some observations on the 2-level factorial test table design from reference

(6): p. 57 are included:

“Note the pattern in the columns in Table 2-1. The first column varies the 0’s and 1’s alternately, while the second column varies them in pairs and third in fours. In general, we can reduce the pattern of the digits in any column to a formula: The number of like digits in a set = 2^{n-1} where n is the column in the matrix.

for $n=1$, $2^{1-1} = 2^0 = 1$

for $n=2$, $2^{2-1} = 2^1 = 2$

for $n=3$, $2^{3-1} = 2^2 = 4$

for $n=4$, $2^{4-1} = 2^3 = 8$, etc.

The convention of alternating 0’s and 1’s produces an order in the experimental design, which is useful in the design and analysis. It is called Yates order after the British statistician.”

In the context of the finite element updating problem, the first combination listed in Table 2-1 is the original model and as such is not considered. Therefore the number of design variable combinations to be considered for model updating is $2^k - 1$ with k being the number of design variables of interest.

F. MODAL ASSURANCE CRITERION

“The Modal Assurance Criterion (MAC) is a scalar constant relating the causal relationship between two modal vectors” [Ref. 5: p. 113]. For this thesis the MAC is used as a means to compare analytically and experimentally obtained vibrational mode shapes. The MAC will have a value between 0 and 1. A value of 0 indicates that the two modal vectors are not consistent while a value of 1 indicates the modal vectors are consistent. The method of calculating the MAC for comparing the i th mode of the analytical (a) system to the i th mode of the experimental (x) system is:

$$MAC_i = \frac{\left\| \{\phi_i^a\}^T \{\phi_i^x\} \right\|^2}{\left\| \{\phi_i^a\}^T \{\phi_i^a\} \right\| \left\| \{\phi_i^x\}^T \{\phi_i^x\} \right\|} \quad (2.25)$$

The individual MAC values for each vibrational mode of interest are then summed to provide a scalar “rating” of the solution. The iteration with the highest summed MAC rating is then selected as the optimal solution.

The following chapters will demonstrate the application of these theories. Optimization theory with scaling will be applied to both model updating and damage localization based on sensitivity updating of the finite element model. The applicability of the sensitivity updates will be evaluated with the Cauchy ratio. The design variable combinations are chosen with the 2-level factorial method. The results of the search iterations will be evaluated with the MAC value.

III. COMPUTER SIMULATIONS

The investigation of model updating and damage localization was initially conducted with computer simulations. A baseline finite element model was created to be used as the analytical model. The baseline model was then modified by making changes to specific model parameters, yielding a simulated experimental model with known differences in the design variables. By comparing the baseline model and the simulated experimental model the operation of the optimization and localization processes could be studied and verified. The types of models, design variables modified, and the procedures for the simulations will be discussed in further detail in this chapter.

A. BEAM MODEL UPDATING

The initial process to be examined is model updating. In order to determine the size of design variable changes for which frequency sensitivity calculations are appropriate and to verify optimization processes a simple finite element model was utilized. This baseline model was constructed for an aluminum beam with damping neglected to simplify the model. This model considered two degrees of freedom at each node, one translation and one rotation, and contained eight elements and nine nodes. The boundary conditions for the test cases was fixed-free, that is the left end of the beam was clamped. The material was assumed to have homogenous physical properties. Specific beam data is included in Appendix A.

In the simple beam model, two model parameters were chosen to be manipulated as the design variables for the optimization investigation. The design variables chosen were the Young's modulus and the mass density for the entire beam. The optimization

process is developed to determine what set of changes to the design variables in the finite element model would result in an “updated” analytical model matching the dynamic response of the simulated experimental model. The values of the two design variables for the baseline finite element model will be referred to as the original values of the design variables and the known changes to the design variables will be referred to as the design variable errors. The original values of the design variable were either reduced, held constant, or increased, in all possible combinations, to generate the simulated experimental data. For two design variables, examined at three levels, there are 3^2 or nine possible combinations. The combination with no changes to either design variable is trivial, so eight different design variable error combinations were investigated. For example, one error combination was a decrease in density while modulus was held constant. The use of different error combinations was to determine if the type of errors in the design variables affected the optimization solution. The design variable errors for the simulated experimental models were at least five percent of the original values to ensure that a noticeable difference in the dynamic response parameters was observed. The different aspects of the optimization process were investigated with multiple test cases. Each test case examined a particular solution aspect and consisted of eight trials, one for each of the design variable error combinations. This allowed the isolation of the effects for the items changed from test case to test case.

1. Sensitivity Linearity Assessment

The first and foremost issue which must be validated in the optimization process is the sensitivity-based update of the finite element model. The sensitivity matrix is used

to approximate the change to the natural frequencies of the analytical system based on a change to designated design variables. The relation for the frequency change was identified in Equation (2.12). The updated analytical natural frequencies are computed as shown in Equation (3.1). Note that the second term in the right hand side is the frequency change as identified in Equation (2.12).

$$\{f_u^a\} = \{f^a\} + [T]\{\Delta DV\} \quad (3.1)$$

where $\{f\}$ indicates the system natural frequencies and DV represents design variables. This approximation for the updated analytical natural frequencies is used in the numerical optimization process to evaluate possible design variable values. The purpose of using this approximation is to reduce the computational time to accomplish the optimization. If the approximation was not used, the numerical optimization routine would have to re-solve the eigenproblem for every iteration, increasing the computational time required to solve the problem. With this in mind, it is imperative that the linearity of the sensitivity-update be assessed to ensure that it is accurate within the solution domain.

The range of validity for the frequency sensitivity-update approximation was assessed for the aluminum beam test model in 2 fashions both of which will be discussed in following sections. The first method was a direct comparison of the updated natural frequencies calculated from Equation (3.1) to that of the eigenproblem re-solve for a given set of errors to the design variables. The design variables were varied up to plus or minus 10 percent from the original values in the finite element model. Figure 3-1 and Figure 3-2 are plots of the absolute value of percentage error between the eigenproblem re-solve and the sensitivity based frequency update for the first two natural frequencies of

Error for Sensitivity update for 1st Natural Frequency

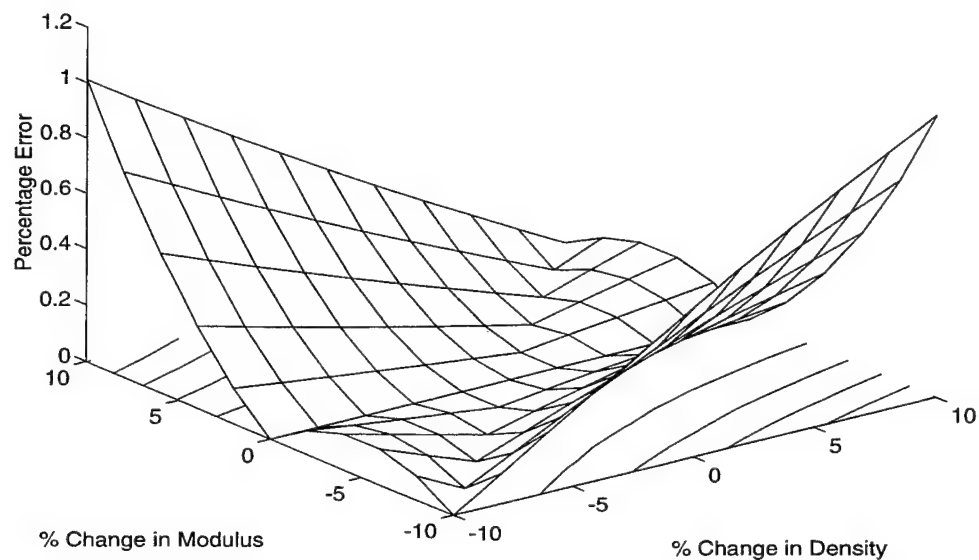


Figure 3-1 Absolute Value of Percentage Error for 1st Natural Frequency Update

Error for Sensitivity update for 2nd Natural Frequency

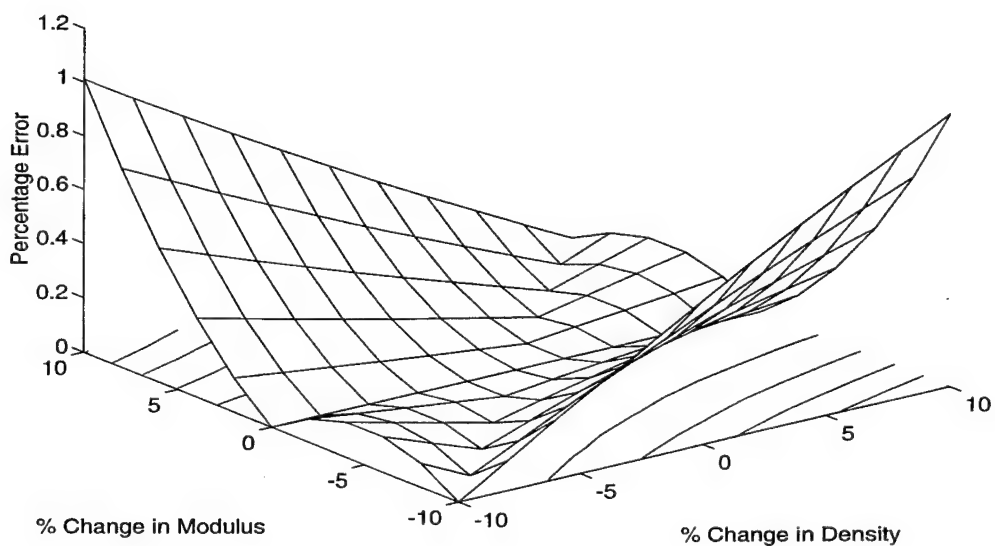


Figure 3-2 Absolute Value of Percentage Error for 2nd Natural Frequency Update

the beam versus the percentage changes to the design variables. Both cases have a maximum error of approximately one percent. An item to notice in the figures is that the error is at the highest level when the design variables are adjusted in the opposite fashion. This is because the changes in design variables have opposite effects on the system frequencies. For example, when the modulus is increased the frequencies increase, and when the density increases the frequencies decrease. Therefore when the design variables are shifted in opposite directions, one positive and one negative, the overall change to the natural frequencies is larger in magnitude and the corresponding error is larger. Conversely when the design variables are shifted in the same direction, either both positive or both negative, the overall change to the natural frequencies is smaller because the changes cancel and the corresponding error is also smaller. This indicates that the approximation error is based more on the magnitude of the change to the natural frequencies themselves as opposed to the magnitude of the changes to the design variables. The error levels of approximately 1 percent calculated by direct comparison of frequencies is considered acceptable for the optimization procedure.

The second method of verifying the acceptability of the sensitivity updating approximation was to calculate the Cauchy ratio equivalent for the model. This ratio was defined in Equation (2.13) and Equation (2.14) included in Chapter II on page 13. The ratio uses the magnitude of the second term in a Taylor series expansion to determine if using the first term alone is a valid approximation. This ratio is computed for a specific design variable change in the model, and for all of the natural frequencies of interest. The acceptability measure for this method is if the ratio has a value much less than one. This

ratio was calculated here for the first two natural frequencies and up to 20 percent changes in the density and modulus. This method of assessment does not take into consideration a combination of changes to both design variables simultaneously. The single largest calculated ratio values are included as Table 3-1. The ratio exceeds 0.1 when the mass density changes by eight percent and when the modulus changes by 12 percent, both for the second natural frequency. The question with this validation method is what value of the ratio actually indicates that the accuracy limits have been exceeded? Reference (11) only refers to a value of much less than one. Without a well defined definition of an acceptable value the results of this method of assessment are open to interpretation.

Percent Change	1st Frequency		2nd Frequency	
	Mass Density	Modulus	Mass Density	Modulus
1	0.0083	0.0072	0.013	0.0091
2	0.017	0.014	0.026	0.018
3	0.022	0.025	0.027	0.039
4	0.033	0.029	0.052	0.036
5	0.041	0.036	0.064	0.045
6	0.050	0.043	0.077	0.054
7	0.058	0.070	0.090	0.064
8	0.066	0.058	0.103	0.073
9	0.074	0.065	0.115	0.082
10	0.083	0.072	0.130	0.091
11	0.091	0.080	0.142	0.099
12	0.099	0.086	0.155	0.109

Table 3-1 Cauchy Ratio Equivalent Calculated Values

Based on the results of the numerical linearity assessment ("Method 1", above), that up to a 10 percent change in either or both of the design variables is acceptable, the

maximum ratio value for the 10 percent shift is chosen as the acceptable ratio value. This value is 0.13. In view of the two methods of evaluating the sensitivity updating approximation, the error of the approximation is at an acceptable level within a limit of 10 percent change to either or both design variables.

2. Initial Optimization Procedures

As mentioned above, different aspects of the optimization procedure were considered in order to determine their effect on the process. The first set of test cases were intended to validate basic methods of the optimization solution. The test cases for this phase of testing considered the first two natural frequencies and both design variables, mass density and modulus for the entire beam. Substituting these particular variables into Equation (2.12) results in the following expression for the frequency changes.

$$\begin{Bmatrix} \Delta f_1 \\ \Delta f_2 \end{Bmatrix} = [T] \begin{Bmatrix} \Delta E \\ \Delta \rho \end{Bmatrix} \quad (3.2)$$

where f are the natural frequencies, E is Young's modulus, ρ is mass density, and $[T]$ is a 2x2 sensitivity matrix. The prescribed errors in the design variables for the simulated experimental model were a five percent change to the mass density and a eight percent change in the modulus.

One of the aspects investigated was a possible solution method that did not require the iterative optimization process. A direct solution was calculated due to its simplicity. The use of the same number of design variables and natural frequencies results in a square sensitivity matrix. The square sensitivity matrix allows Equation (3.2),

to be solved directly by premultiplying both sides of the equation by the inverse of the sensitivity matrix resulting in Equation (3.3):

$$\begin{Bmatrix} \Delta E \\ \Delta \rho \end{Bmatrix} = [T]^{-1} \begin{Bmatrix} \Delta f_1 \\ \Delta f_2 \end{Bmatrix} \quad (3.3)$$

Although this method is quick and mathematically correct, in this instance the solution has no physical significance. That is the design variable errors calculated from this solution method are of a significantly different magnitude than the known error values. This was true whether the design variables were scaled or not.

Therefore the primary solution method considered was a constrained optimization routine, as defined as in Equations (2.15) through (2.18) in Chapter II on page 14. The purpose of the optimization routine is to locate the minimum value of an objective function subject to imposed constraints. The process begins with a start point within the solution domain and then uses an iterative search logic to numerically converge to a solution. Some specifics of the optimization process can be modified to alter the results of the search. Some items which were considered include:

- Design variable scaling
- Alternate objective functions
- Objective function scaling
- Solution constraints
- Iteration start point

The specifics of these items will be addressed in the following paragraphs.

One of the areas for evaluation is whether design variables should be scaled or not. Scaling can improve the performance of the optimization routine by modifying the problem so that the design variables are of similar magnitudes. For this beam case the mass density and modulus differ in magnitude by a factor of 10^{11} so scaling may be beneficial. Design variable scaling is investigated in Test Cases 1 and 2.

Another item to be investigated is the objective function. The objective function used for initial optimization evaluation is of the form:

$$OF = A * \sum_{i=1}^n \frac{f_i^x - f_i^a}{f_i^x} + B * \sum_{k=1}^m \frac{\Delta DV_k}{DV_k} \quad (3.4)$$

where n is the number of frequencies of interest, m is the number of design variables, and A and B are scalar multipliers used as weighting factors in the objective function. The analytical frequencies in Equation (3.4) are computed using the current state variables and Equation (3.1), i.e. at each iteration of the optimization process, the analytical frequencies are updated to determine the effect of possible design changes. This process will decrease the difference between the experimental and updated analytical frequencies until convergence to the minimum value of the objective function is obtained. The optimization routine will return the design variable changes required such that the finite element model frequencies will match the experimental frequency data. These design variable changes are used to calculate the value of optimum design variables by adding the changes to the original design variable values. The weighting factors, A and B , are to enhance the effect of one term versus the other in the objective function and can be altered to determine the effect on the optimization process of either term. Weighting of

the objective function terms is investigated in Test Cases 3 and 4. The only constraint imposed at this stage was a limit of 10 percent change from the original design variable values during the search iterations. The starting point values to begin the iterative search were the original design variable values for all of the trials within each test case.

a. Test Case 1 - 2 Design Variables, No Scaling

The scalar multipliers in the objective function for this case were $A = 1$ and $B = 1$. There was no scaling of the design variables. The results for Test Case 1 are included numerically in Appendix A as Table A-1 and graphically in Figure 3-3. The axes for the plot are the percentage changes in the two design variables from the original values of the finite element model. The set of points labeled as "Prescribed" are the eight combinations of known design variable errors that comprise the simulated experimental trials. The set of points labeled as "Solution" are the changes to the original design variable values that were returned as the optimized solution by the optimization routine. Lines connect the data point of a known error to the data point of the corresponding optimization solution. The distance between the two data points is a measure of the accuracy of the solution. The shorter the distance the better the solution matched the known error condition. If a solution was within 2.5 percent of the known error for both design variables it was judged as reasonable and noted with an ellipse enclosing both the error data point and the solution data point. The start point for all of the trials was at the original design variable values and is plotted at the origin of the axes.

Only two of the eight solutions are within a reasonable tolerance from the known error values. These are not acceptable results. As shown in Figure 3-3 all of the

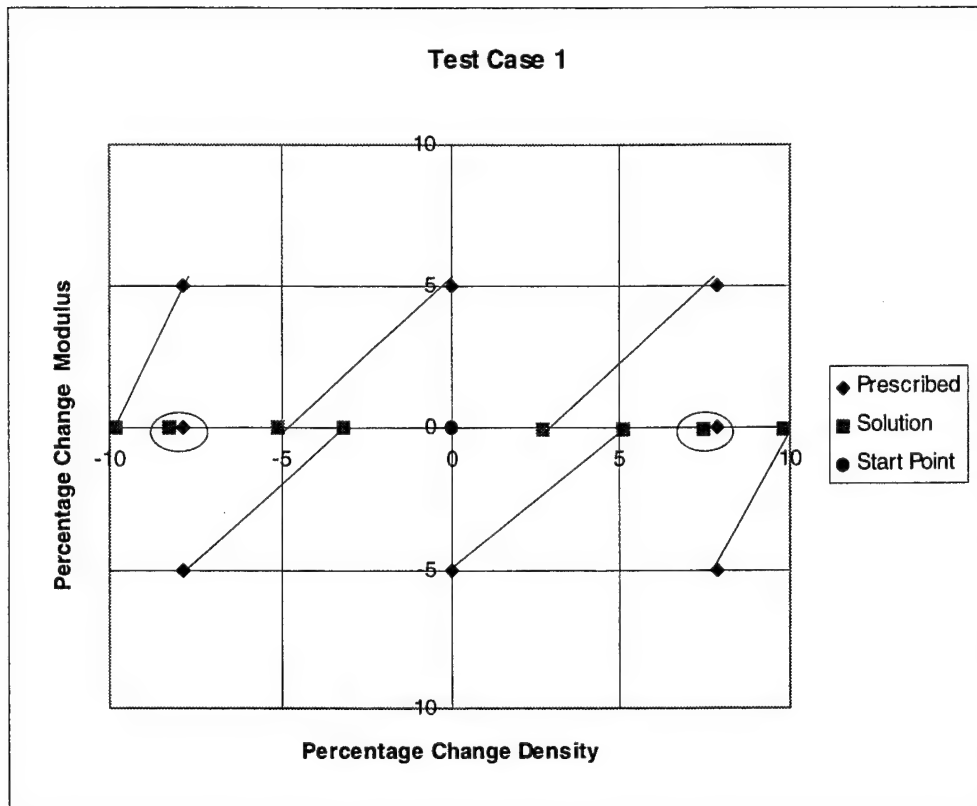


Figure 3-3 Test Case 1 Solution Results

solutions lie on the horizontal line corresponding to the zero value of the vertical axis. This indicates that the modulus was not altered by any significant amount for any of the trials. The optimization routine minimized the frequency differences between the analytical and experimental models by only manipulating the mass density of the beam. This is probably due to the large difference in magnitudes between the two design variables.

The results from Test Case 1 indicate the need to scale the design variables to equalize their effect on the design optimization process. The optimization process will not operate correctly for this situation when the design variables are greatly different in

magnitude. A method to correct this deficiency will be addressed in the following test case.

b. Test Case 2 - 2 Design Variables, With Scaling

Test Case 2 was used to verify the effectiveness of scaling the design variables to correct the solution deficiency identified in Test Case 1. The scaling method chosen was to scale the modulus value down to the magnitude of mass density. This also results in the need to scale the sensitivity matrix so that Equation (3.2) remains valid. The scaling matrix for this situation and the general scaling procedure is demonstrated in the following group of equations.

$$[S_c] = \begin{bmatrix} \frac{\rho}{E} & 0 \\ 0 & 1 \end{bmatrix} \quad (3.5)$$

$$\{\Delta DV_s\} = [S_c]\{\Delta DV\} \quad (3.6)$$

Where $[S_c]$ is the scaling matrix, and the subscript s indicates scaled values. This scaling results in a scaled design variable vector that has all terms on the same basis. Rearranging Equation (3.6) and substituting into the change in system frequency, Equation (2.12) results in:

$$\{\Delta DV\} = [S_c]^{-1}\{\Delta DV_s\} \quad (3.7)$$

$$\{\Delta f^a\} = [T][S_c]^{-1}\{\Delta DV_s\} \quad (3.8)$$

The sensitivity matrix can be combined with the scaling matrix to form the scaled sensitivity matrix and result in the scaled version of the frequency change equation:

$$[T_s] = [T][S_c]^{-1} \quad (3.9)$$

$$\{\Delta f^a\} = [T_s]\{\Delta DV_s\} \quad (3.10)$$

Equation (3.10) is then used for frequency updating for the scaled design variable problem in Equation (3.1). This scaling logic is valid for other cases and can be applied for larger design variable vectors by increasing the number of terms in the scaling matrix.

For Test Case 2 the scalar multipliers in the objective function were the same as for Test Case 1. The results for Test Case 2 are included numerically in Appendix A as Table A-2 and graphically in Figure 3-4.

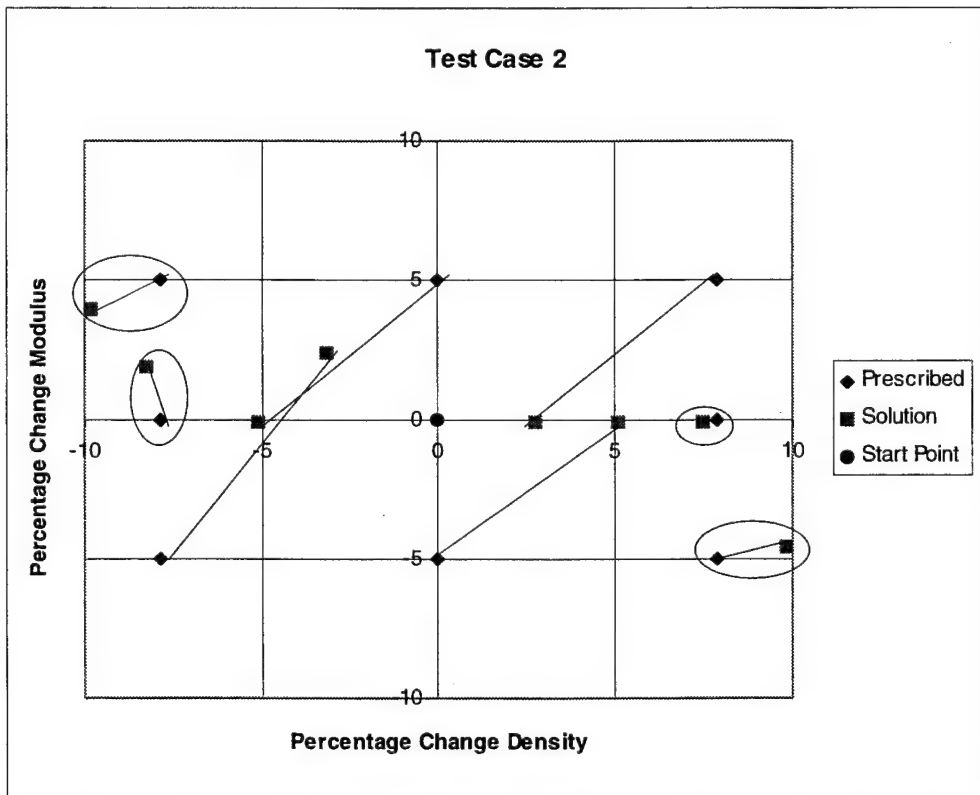


Figure 3-4 Test Case 2 Solution Results

The results for Test Case 2 show improvement over the results for Test Case 1. Four of the eight trials yielded reasonable solutions, but the overall accuracy is still not acceptable. Scaling of the design variables and the sensitivity matrix was

effective in that it allowed both design variables to be shifted during optimization. The modulus was shifted by as much as five percent for one of the trials demonstrating that modulus had been manipulated during the optimization process. Although scaling allowed both design variables to be manipulated, this in itself did not guarantee that all of the trials in the test case would achieve successful results. Scaling will be used for all subsequent test cases.

c. Test Cases 3 and 4 - Objective Function Weighting

The next test cases investigated the effects of changing the relative weighting of the objective function terms. This was to determine if emphasizing the frequency term versus the design variables term would improve optimization accuracy. Different values for A and B, the scalar multipliers in the objective function, were used for evaluation. A values were varied such that, $5 \leq A \leq 50$, while B was held constant at $B = 1$. Test Case 3 uses $A = 10$ and $B = 1$. The results for Test Case 3 are included numerically in Appendix A as Table A-3 and graphically in Figure 3-5. Test Case 4 was similar to Test Case 3 except that the change in variable term of the objective function was removed, or B was set to zero. The results for Test Case 4 are included numerically in Appendix A as Table A-4 and graphically in Figure 3-6.

The Test Case 3 results have reasonable solutions for four of the eight trials. This is not an improvement over Test Case 2. Test Case 4 has reasonable solutions for five of the eight trials. This is an improvement over Test Case 2 but the overall effectiveness of the optimization is still not at an acceptable level. Test Case 3 is inconclusive while Test Case 4 indicates that increasing relative weighting of the

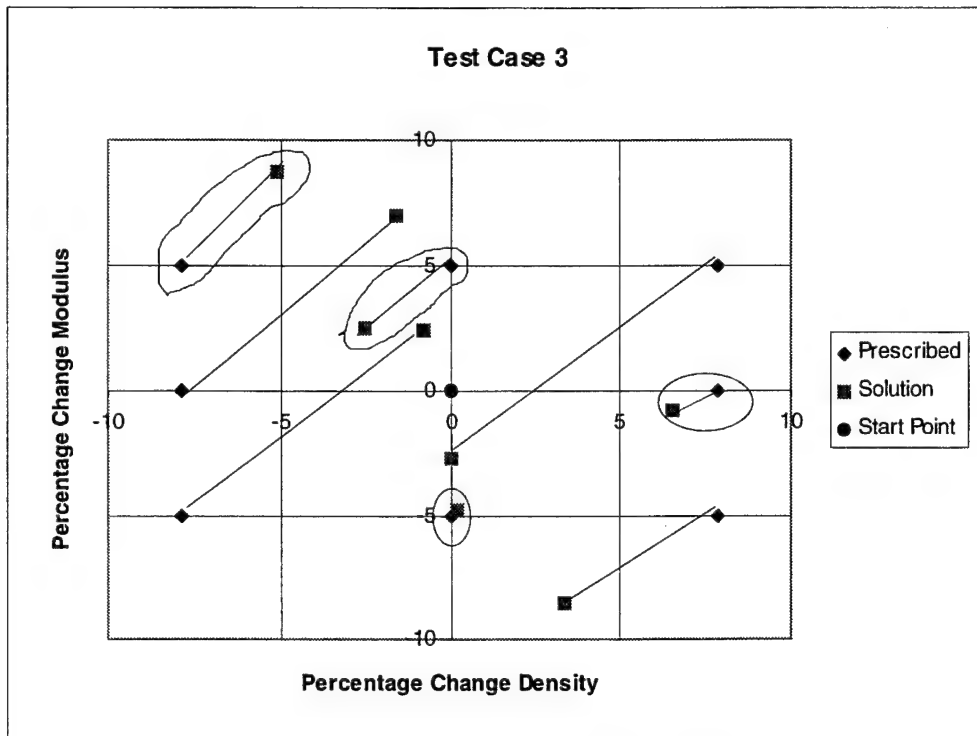


Figure 3-5 Test Case 3 Solution Results

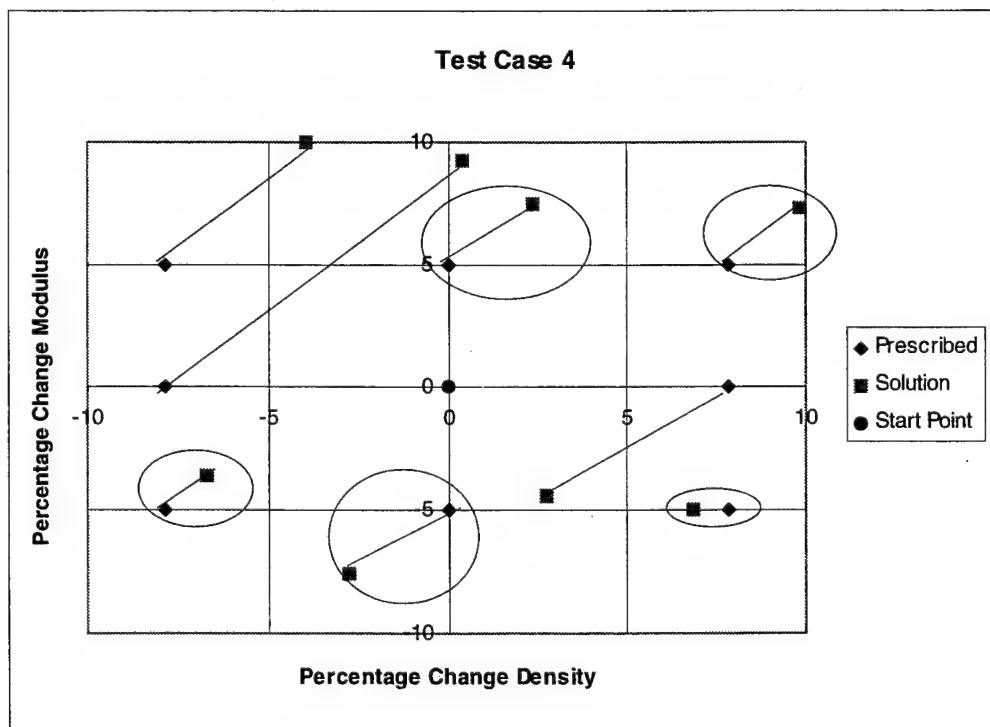


Figure 3-6 Test Case 4 Solution Results

frequency term versus the design variable term in the objective function improves overall performance of the optimization routine somewhat.

3. Advanced Optimization Procedures

At this point in the evaluation of the optimization procedure a new method was needed to ensure that the prescribed errors could be identified. In previous test cases, both design variables were considered simultaneously but not individually. This limitation in the search logic contributed to a less than adequate optimization search performance. This lack of performance prompted the use of the 2-level factorial algorithm. The 2-level factorial approach was discussed in Chapter II, Section E, pages 16-18. In this case with two design variables, this approach requires three independent iterations of the optimization procedure to search for a single set of prescribed errors. Each independent iteration uses a different combination of the two design variables. The first iteration only considers the modulus, the second iteration only considers the density, and the final iteration considers both modulus and density. The use of multiple independent iterations drives the need for some method to evaluate the candidate solutions for the different design variable combinations. A comparison of just the natural frequencies themselves was not an effective measure for evaluation. This is because the optimization process forced the analytical and experimental frequencies to converge whether or not the optimized design variable values were the prescribed errors. This is possible because of the non-uniqueness of the eigenproblem solution, that is there are an infinite number of density and stiffness combinations that will result in the same frequencies. This overlap of candidate solutions necessitated that another method of evaluation be developed.

The initial method of solution evaluation was to test the orthogonality of the updated modes shapes with respect to the simulated experimental mode shapes. When the mode shapes are mass normalized the following holds:

$$[\Phi]^T[M][\Phi] = [I] \quad (3.11)$$

where $[I]$ is the identity matrix. After the solution for the optimization process was obtained for a design variable combination the eigenproblem was re-solved with the optimized design variable values. This generated a set of optimized analytical mode shapes. The optimized analytical mode shapes were substituted for the first term of Equation (3.11) while the experimental mass matrix and experimental mode shapes were input as the remaining terms:

$$[\Phi^o]^T[M^x][\Phi^x] \quad (3.12)$$

where superscript "o" symbolizes an optimized solution. It was thought that the closer that the value of this triple product was to duplicating the identity matrix, the better that the optimized mode shapes matched the experimental mode shapes.

Another factor that was altered for the following test cases was that the number of natural frequencies considered was increased from two to four. This was to bring more system information into the optimization process.

a. Test Case 5 - Multiple Design Variable Combinations

Test Case 5 was used to implement the 2-level factorial algorithm and the orthogonality test. The objective function for Test Case 5 was the same as for Test Case 3, that is the weighting factors were $A = 10$ and $B = 1$. The results for Test Case 5 are included numerically in Appendix A as Table A-5 and graphically in Figure 3-7.

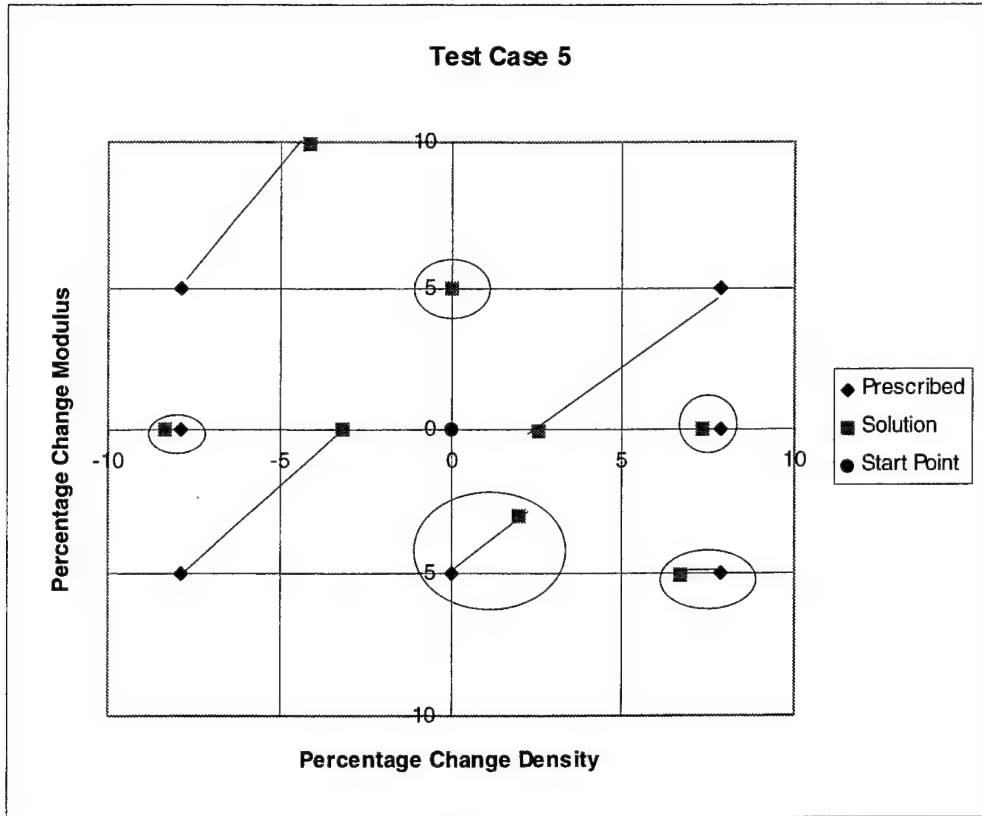


Figure 3-7 Test Case 5 Solution Results

Test Case 5 has reasonable solutions for five of the eight prescribed error combinations. The prescribed error data point for the trial with modulus increased and density unchanged is not visible because it and the solution data point are coincident. The results for this test case show improvement in the accuracy of the solutions for the trials where the error was prescribed to only one of the design variables, such as the case with the overlapping data points. This is because the 2-level search algorithm considered iterations with each design variable individually, allowing the process to isolate error to a single design variable. The overall ability to identify errors did not improve with only one reasonable solution for the trials where both design variables had errors. The results of the orthogonality check were also studied. The matrix result of the triple product was

diagonal as would be expected for similar systems. The diagonal terms were not however equal to one. In fact the iterations most closely matching the known differences were not necessarily the iterations with diagonal terms closest to one. There was not a recognizable pattern within the orthogonality test that could be used to identify the correct solution.

b. Test Case 6 - Prescribed Error Effects

Test Case 6 was used to further study the 2-level search procedure and the orthogonality test for solution evaluation. A slight change was made to the prescribed design variable errors to see if this affected the results of the optimization procedure. The first 5 test cases had used a eight percent error in mass density and a five percent error in modulus for the prescribed errors. For the remainder of the test cases the prescribed errors were eight percent for modulus and six percent for mass density. For the objective function, $B = 0$, or only the frequency difference term was considered. The results for Test Case 6 are included numerically in Appendix A as Table A-6 and graphically in Figure 3-8.

The results for Test Case 6 contain reasonable solutions for six of the eight trials. The prescribed error data points for the two trials where density is not changed but the modulus is increased or decreased are coincident to the solution data points and are not visible. The solutions for the trials where the prescribed errors only affected a single variable are excellent. All four of these trials are within one half percent of the prescribed errors. The trials with errors to both design variables show improvement as compared to the results for other test cases. The trials where the prescribed errors are of opposite sign have solutions within two and one half percent of the known values. The trials where the

prescribed errors are of different signs do not provide solutions of any quality. The orthogonality check results were very similar to that of Test Case 5. The matrices were diagonal but again there was no recognizable pattern that could be used to evaluate the different candidate solutions for each trial.

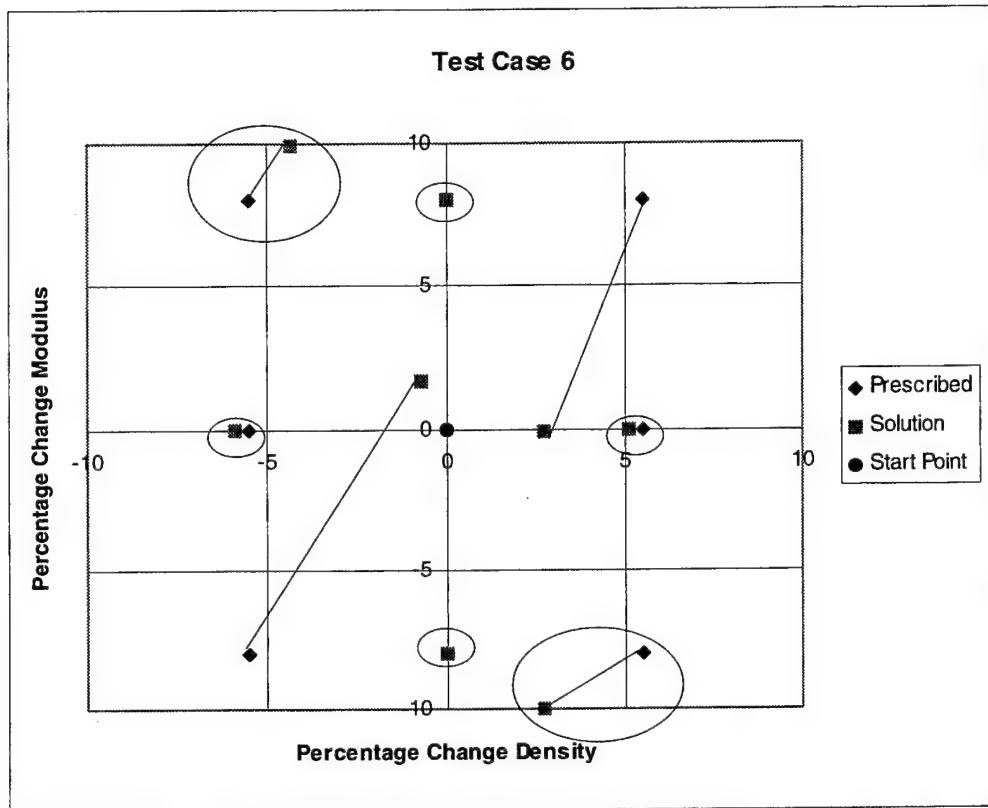


Figure 3-8 Test Case 6 Solution Results

c. Test Case 7 - Alternate Objective Function

Test Case 7 was used to evaluate a different set of objective function and optimization constraints to attempt to get viable solutions for the trials that had not been converging. The objective function was changed so that only the design variable difference term was used, or the A value in Equation 3.3 was set to zero. The frequency differences between the analytical model and the simulated experimental data were

applied in the optimization routine as an inequality constraint. The constraint was that the relative frequency differences was not to exceed a specified tolerance. These equations for the objective functions and the constraint are shown below:

$$OF = B^* \sum_{k=1}^m \frac{\Delta DV_k}{DV_k} \quad (3.13)$$

$$\left| \left\{ \frac{f^x - f^a}{f^x} \right\} \right| - tol \leq 0 \quad (3.14)$$

The design variables were still limited to a solution domain of ten percent change from the original values.

Another method of solution evaluation was also investigated in this test case. The Modal Assurance Criterion (MAC), which was discussed in Chapter II, Section F, measures the independence of two mode shapes. The MAC formula, Equation (2.25), is utilized to compare the optimum solution mode shapes to the simulated experimental mode shapes to determine if they are similar. The MAC is then summed for all of the mode shapes to develop a single number with which to rate the candidate solutions. The search procedure itself was not altered. The results for Test Case 7 are included numerically in Appendix A as Table A-7 and graphically in Figure 3-9.

The results for Test Case 7 do not show any improvement in the optimization procedure. In fact the solutions are less accurate than the results for Test Case 6 with only five of the eight trials within reasonable limits of the known errors. The prescribed error data points for the two trials where density is not changed but the modulus is increased or decreased are coincident to the solution data points and are not

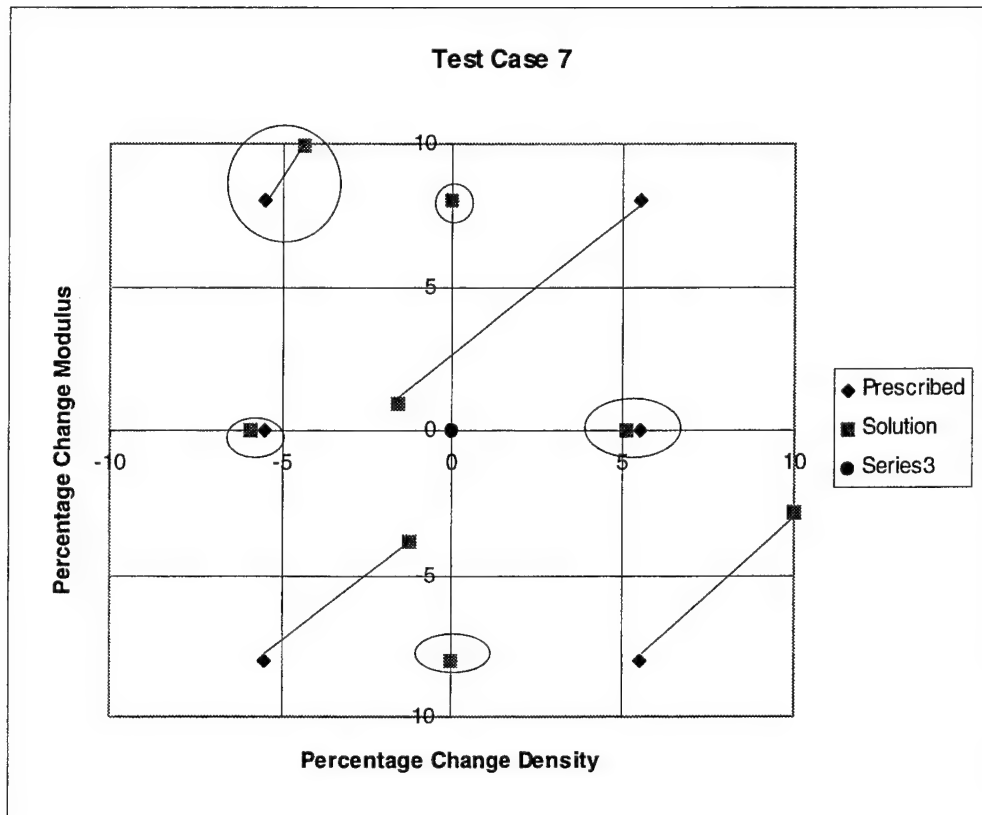


Figure 3-9 Test Case 7 Solution Results

visible. The trials where the prescribed errors are made to a single variable have good accuracy. The trials where prescribed errors are made to both design variables are not as accurate. When the prescribed error are of the same sign, the solution is not of any value. When the prescribed errors are of the opposite sign the solutions are less accurate than in Test Case 6. The higher accuracy achieved in Test Case 6 demonstrates that a combination of the frequency differences and the design variable changes in the objective function, is a better form for the objective function than the design variable changes as used in Test Case 7.

The results for all of the 2-level factorial test cases demonstrate certain significant points. The first point is that all of the test cases were very successful at

identifying the trials where the prescribed errors are applied to a single design variable. The use of all the possible design variable combinations isolates the situations where only a single design variable is effected and results in accurate solutions. The second point concerns the situation where the prescribed errors are made to both design variables, but are of opposite sign. The results for these trials were generally adequate but were not as accurate as the trials where the prescribed errors where to only one design variable. This is because these trials are in the region of the solution domain with the highest error for sensitivity updating. Although the solution process converged to a reasonable answer, the error for the sensitivity-based frequency approximation caused optimization solution inaccuracy. The final point concerns the trials where the prescribed errors are made to both design variables, but are of the same sign. These trials are not very accurate at all. This is due to the fact that the prescribed errors to the design variables have opposite effects on the system frequencies. The resultant changes to the natural frequencies from the errors are not very large, so the optimization routine tends to make small changes to the design variables for the solutions in these trials. This results in solutions that are very inaccurate. These routine limitations are significant for understanding and applying the optimization routine.

The orthogonality test for solution evaluation had the same results as previous test cases. The matrix was diagonal but the highest value was not always the known solution. One interesting thing to note is that for the solutions that match the prescribed errors orthogonality test had a highest value of approximately 0.815. The significance of this value is not understood. The theory of the test dictates that the closer

this value is to one the better the solution, but that was not the case. This evaluation method assumes that the mode shape scaling for the optimal solution set is the same as for the simulated experimental set which is not necessarily the case.

The MAC test was ineffective for the homogenous test case. This was due to the fact that small changes in beam properties over the entire beam have negligible effects on the mode shapes. Therefore all of the candidate solutions had the same results for the MAC test. The value of the MAC computed for the updated finite element mode shapes compared to the simulated experimental mode shapes, was one for all of the modes and all of the candidate solutions so the valid solution could not be discerned MAC. Further tests are necessary to validate the MAC method of solution evaluation.

4. Two Region Optimization

Up to this point the model updating process has been tested on a homogenous beam. These tests have provided insight into a simple two design variable case. The need for scaling, the effects of objective function weighting, design variable combinations, solution limitations, and methods of solution evaluation have been investigated. To further test some of the concepts for model updating a test case was run on a more complex beam model. Instead of using a homogenous beam and two design variables, the beam was divided into two regions and the number of design variables was doubled. The density and modulus in the left half of the beam were made independent of the density and modulus in the right half of the beam, resulting in four design variables. The assumed values for both halves of the beam are the same, but the errors for the simulated experimental models are input into only one half of the beam.

The optimization process for a four design variable case is essentially the same as for the two variable case. The form of the objective function is the same but will have more elements to sum in the design variable term. One difference in the process is that the number of design variable combinations for each trial of the test case increases. As discussed in Chapter II, for the 2-level factorial algorithm with four design variables the number of design variable combinations increases to $2^4 - 1$ or 15. This obviously increases the time and expense of the model updating computation.

a. Test Case 8 - 4 Design Variables

Test Case 8 was intended to verify the optimization process for the four design variable problem. The 2-level factorial search was again utilized. The prescribed errors for the simulated experimental data were made to the left half of the beam model while the properties of the right half of the beam were unchanged. The objective function considered only the frequency difference terms, that is the B weighting factor in Equation (3.4) had a value of zero. Both the orthogonality and MAC methods of solution evaluation were calculated. The results for Test Case 7 are included numerically in Appendix A as Table A-7 and graphically in Figure 3-9.

The results for Test Case 8 are excellent. All eight of the trials yielded very accurate solutions, with the solution data points virtually coincident with the prescribed error data points. The ability to isolate the two halves of the beam improved the capability of the optimization process to identify the prescribed errors. The problems with the canceling effects for prescribed errors with the same sign were eliminated. This is probably due the enhanced ability to focus the effects of a change in an area. With the

design variable errors in only half of the beam, the frequency shifts are not as uniform through all the modes as the error cases for the homogeneous beam. Because of this, the corrections to only half of the beam would be easier for the process to recognize.

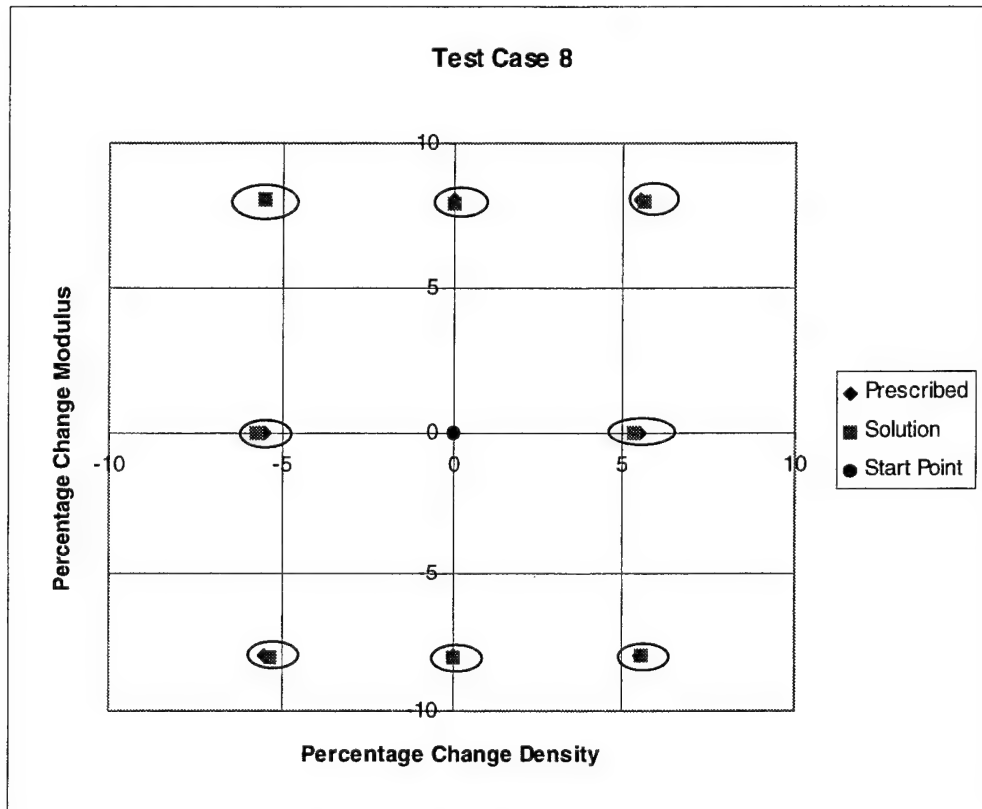


Figure 3-10 Test Case 8 Solution Results

The orthogonality method for solution evaluation was not effective for this problem. The triple product matrix was diagonal but the values on the diagonal did not isolate the known solution. The highest value was not necessarily the correct design variable combination nor was there a consistent “correct” value identified such as in the homogenous beam cases.

The MAC method of evaluation was effective in identifying the correct solution. All of the trial combinations that matched the correct solutions were the highest

MAC value for that trial. The MAC was effective in this case because the error in only halve of the beam caused a non-symmetric change to the mode shapes which was easier to detect. This demonstrates the effectiveness of the MAC method for solution identification as long as the design variables for the optimization process are not homogenous over the entire beam or model.

5. Model Updating Observations

The test cases that have been discussed in the previous sections provide significant information for the utilization of the optimization procedure for finite element model updating. The different aspects that have been investigated with simple beam models will allow the procedure to be applied to more complex systems. Significant findings include:

- Sensitivity based updating of finite element models is an effective approximation for the change in natural frequencies for small changes in design variables.
- The accuracy of the sensitivity based update appears to be more dependent on the amount of the frequency change vice the design variable change.
- The Cauchy ratio equivalent for sensitivity assessment is not conclusive in this case because the guidelines are open to interpretation.
- Scaling of the design variables is necessary if the variables are of significantly different magnitudes.
- Increasing the relative weighting of the frequency difference term in the objective function improves the solution quality.

- The 2-level factorial experiment allows the investigation of all design variable combinations to improve model error identification.
- The 2-level factorial experiment is particularly effective for the trials where the prescribed errors are applied to one design variable only.
- The ability of the optimization process to identify differences is dependent on how the differences combine to effect the system frequencies.
- For the homogeneous case, when the prescribed errors to the two design variables have opposite signs, the process will converge to a reasonable solution but it will not be as accurate because of sensitivity error.
- For the homogeneous case, when the prescribed errors to the two design variables have the same sign, the process does not converge to a reasonable solution.
- The ability of the optimization process to localize errors was improved when the design variables and the prescribed errors were divided into sections.
- The orthogonality method for solution evaluation is not effective because there was no discernible trend to indicate the known errors.
- The Modal Assurance Criterion method of solution evaluation is effective when the design variables considered are not applied over the entire structure of the model.

B. BEAM DAMAGE LOCALIZATION

The second application of the optimization procedure is damage localization for a structure with a updated finite element model in the undamaged state. The damage

localization routine builds upon the lessons learned in the model updating process. The baseline finite element model to investigate damage localization processes was constructed for a composite beam. Damping was neglected to simplify the model. The model considered two degrees of freedom at each node, one translation and one rotation. The model contained 48 elements, each one inch in length, and 49 nodes. The elements are labeled from 1 to 48 and will be referred by number in later sections. The boundary conditions for the model were free-free. This resulted in two rigid body modes which were ignored in the computations. The material was assumed to have homogenous physical properties. Specific beam data is included in Appendix B.

The damage localization process is based on the premise that any internal damage to a structure can be represented in a finite element model as a reduction in the material's modulus, or stiffness. It is assumed that there will be no corresponding reduction in mass. With this in mind, the experimental data for the damaged condition was simulated by reducing the stiffness for effected elements in the baseline finite element model. These will be referred to as the prescribed damage conditions. Four different sizes of damage were simulated. These ranged in size from one inch to nine inches. Each crack length was simulated in the center of the beam and at an off center location to verify the ability to localize the damage. The simulated experimental data from the prescribed damage conditions provided the damaged system dynamic parameters for comparison to the undamaged finite element model.

1. Damage Localization Process

As stated above the damage localization procedure is an application of the model optimization process. For damage localization the optimization process is modified in how it searches for model differences. For this application the only design variable considered is the modulus of the model. Because there is only one design variable the need for the 2-level factorial experiment is eliminated. There is however the need for some logical method of conducting a search of the model. A search method will be presented following the description of the optimization problem. The objective function for the damage localization process is the same as was used for model updating with the frequency term weighted. This emphasizes the frequency difference term of the objective function. The sensitivity matrix is still used to calculate updated analytical frequencies during the optimization process. The first eight modes of vibration are considered for the optimization routine and the mode comparison. The two major issues of the damage localization routine is developing a logical search plan and determining how to evaluate possible solutions. The optimization process will force the analytical frequencies and the experimental frequencies to match so that a frequency comparison is not necessarily the best measure. The Modal Assurance Criterion (MAC) is again investigated as a means to compare possible solutions to the experimental data.

The damage localization process is characterized by dividing the beam into three sectors for investigation. For this model with 48 elements, each sector contained 16 elements. The modulus of each sector, as well as the entire section, is optimized to match the experimental frequencies assuming that the sector is damaged. This optimized

damage stiffness for each sector is used to calculate new vibrational mode shapes for the model. The optimized analytical mode shapes for the overall length and each sector are then compared to the experimental mode shapes with the MAC. The sub-section with the highest MAC sum is taken as the most probable region of damage. This most probable sector is further divided into three smaller sectors and the process is repeated. This process continues until the damage is localized to a single element, or if a region has a higher MAC value than any of its three sub-regions, the entire region is selected as the area of damage. This process will be represented graphically in Figure 3-11 following a detailed description of the process. In this example with 48 elements, no more than 4 iterations of the search procedure are necessary to reduce the damage to a single element. A comment to be made about this procedure is that the location of the optimized stiffness value is more important than the value itself. This procedure does not attempt to evaluate the extent of damage, just the location of the damage. The first test case will be discussed in detail to illustrate the search procedure. Other cases are conducted in the same fashion but only the results will be included and discussed.

2. One Inch Crack

a. Centered Damage - Elements 24-25

The first simulated damage case tested was a one inch crack, centered on the beam. The finite element model has a node located at the center of the beam so the damage affected the elements on both sides of the center node. These elements are labeled as elements 24 and 25. The experimental damage data set was simulated by reducing the

modulus in the two elements for the baseline model. For the first search iteration the 48 beam elements were divided into three sectors. These sectors are comprised of elements 1 to 16, elements 17 to 32, and elements 33 to 48. Error in the modulus value was calculated with the optimization routine for each of the sectors and the entire beam. The results for the first iteration are shown in Table 3-2. Eight modes are considered so the maximum possible MAC value is eight.

Sector	1-16	17-32	33-48	1-48
Summed MAC	7.9894	7.9983	7.9888	7.9993

Table 3-2 Damage Localization Results, First Iteration, 1 inch Crack, Elements 24-25

As shown in Table 3-2, the MAC value for the entire beam is the highest with the center sector being the next highest. This would seem to indicate the entire beam should be taken as the area of damage. On the other hand, in the case of the homogenous beam for the model updating application, the MAC was ineffective for evaluation over the entire beam. Because of this ineffectiveness over the entire beam the higher rating of the overall beam will be discarded and the center section will be taken for the next iteration.

The region for the second iteration contains elements 17 to 32. This region is divided into three sectors. With 16 elements the region can not be divided into three sectors of the same size. To maintain symmetry the extra element is put into the center sector. If there had been two extra elements they would have been put in the two end sectors. The sectors for this iteration are comprised of elements 17 to 21, elements 22 to 27, and elements 28 to 32. The results for the second iteration are shown in Table 3-3.

The sector with the highest MAC value is again the center sector. For this iteration the sector MAC value exceeds that of the overall region of interest, which would validate the decision to ignore a high MAC rating for the first iteration. Based on the highest MAC value elements 22 to 27 are chosen as the sector to be expanded for the third iteration.

Sector	17-21	22-27	28-32	17-32
Summed MAC	7.9983	7.9992	7.9981	7.9983

Table 3-3 Damage Localization Results, Second Iteration, 1 inch Crack, Elements 24-25

The region for the third iteration is then divided into the three sectors. These sectors contain elements 22 and 23, elements 24 and 25, and elements 26 and 27 respectively. The results for the third iteration are shown in Table 3-4.

Sector	22-23	24-25	26-27	22-27
Summed MAC	7.9989	7.9999	7.9991	7.9992

Table 3-4 Damage Localization Results, Third Iteration, 1 inch Crack, Elements 24-25

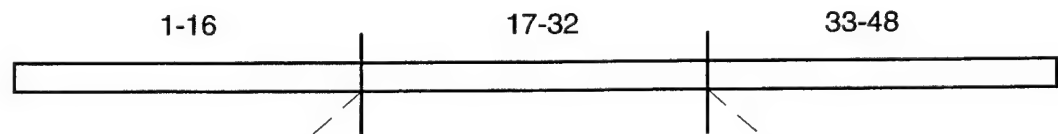
The sub-sector with the highest MAC value is again the center sector. For this iteration the center sector MAC value again exceeds that of the overall region of interest. The sector with the highest MAC is the region of the simulated damage condition for this trial. At this point another iteration could be run by adding a third element to elements 24 and 25 so that the region could be divided into thirds.

This initial trial demonstrates that the idea of subdividing the beam into sectors and then evaluating the sectors until a probable region of damage is identified displays some promise. The use of the MAC value as the solution evaluation appears to be an

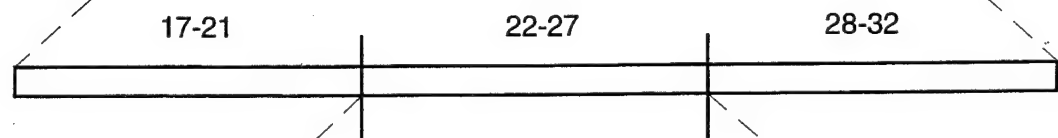
effective tool for this application. However, the overall beam for the first iteration should not be selected because of the difficulty with the homogenous beam shapes.

Figure 3-11 shows pictorially how the search procedure flows from the entire beam to smaller sectors. For the simulated damage condition of a one inch centered crack there are three iterations. The first iteration considers the entire beam and three sectors of 16 elements. After the first iteration the center sector is expanded into three smaller sectors with either five or six elements. Following the second iteration the center sector is again expanded into three smaller sectors with two elements apiece. This method of searching a beam model will quickly reduce the beam into small sections.

1st Iteration



2nd Iteration



3rd Iteration

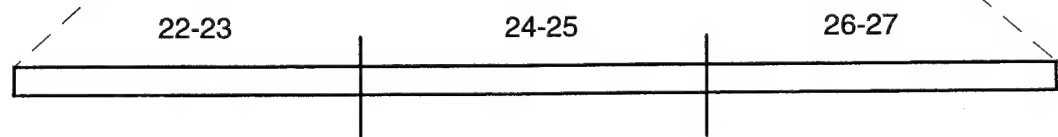


Figure 3-11 Region Expansion, 1 inch Crack, Elements 24-25

b. Off Center Damage - Element 40

To verify that the search logic was valid on damage away from the center of the beam and to eliminate any effects of symmetry, off center damage condition was simulated. The damaged experimental data set was simulated by reducing the stiffness in element 40 of the baseline model. The search procedure was identical to that used for the centered crack. Results for this case are included in Table 3-5. The highest MAC value is highlighted for each iteration and shows the subsection chosen for the next iteration.

Damage in Element 40				
Sector 1st Iteration MAC Values	1-16 7.9994	17-32 7.9997	33-48 7.9998	1-48 7.9997
Sector 2nd Iteration MAC Values	33-37 7.9998	38-42 7.9999	43-48 7.9997	33-48 7.9998
Sector 3rd Iteration MAC Values	33-37 7.9997	38-42 7.9997	43-48 7.9997	33-48 7.9999

Table 3-5 Damage Localization Results, 1 inch Off Center Crack

The damage localization routine identified the beam section from elements 38 to 42 as the area of probable damage. This search selected more elements than the prescribed damage for the simulated experimental data, but the selected region did include the correct location of the damage. The search did reduce the 48 inch beam to a probable damage region of five inches in length which is a large improvement in reducing the area that would need to be further investigated

3. 2.25 Inch Crack

a. Centered Damage - Elements 23-26

The next set of tests were for a crack length of 2.25 inches. The prescribed damage for the simulated experimental data set affected the first two elements on either side of the center node. These elements are numbered 23 to 26. The search procedure results are included in Table 3-6.

Damage in Elements 23-26				
Sector	1-16	17-32	33-48	1-48
1st Iteration	7.9851	7.9986	7.9847	7.9981
MAC Values				
Sector	17-21	22-27	28-32	17-32
2nd Iteration	7.9976	7.9997	7.9974	7.9986
Elements 17-32				
Sector	22-23	24-25	26-27	22-27
3rd Iteration	7.9982	7.9991	7.9986	7.9997
Elements 22-27				

Table 3-6 Damage Localization Results, 2.25 inch Centered Crack

These search procedure identified elements 22 to 27 as the region of probable damage. The region is again larger than the known damage but does include the elements with the prescribed damage for the experimental case. To determine if the process could discern the damage to a smaller region a fourth iteration was run was a different region. Elements 20 to 29 were chosen so that the center section, elements 23 to 26, could be isolated. The results for the fourth iteration are included as Table 3-7. The process did identify elements 23 to 26 as the most probable region of damage

Damage in Elements 23-26				
Sector	20-22	23-26	27-29	20-29
4th Iteration	7.9980	7.9998	7.9980	7.9988
MAC Values				

Table 3-7 Damage Localization Results, 4th Iteration, 2.25 inch Centered Crack

b. Off Center Damage - Elements 30-31

For this test condition the prescribed damage for the simulated experimental data set affected the elements numbered 30 and 31. A fourth iteration was again included to attempt to isolate the known damage. The search procedure results are included as Table 3-8.

Damage in Elements 30-31				
Sector	1-16	17-32	33-48	1-48
1st Iteration	7.9988	7.9995	7.9993	7.9994
MAC Values				
Sector	17-21	22-27	28-32	17-32
2nd Iteration	7.9986	7.9994	7.9998	7.9995
MAC Values				
Sector	22-23	24-25	26-27	22-27
3rd Iteration	7.9991	7.9994	7.9994	7.9998
MAC Values				
Sector	26-28	29-31	32-34	26-34
4th Iteration	7.9990	7.9999	7.9992	7.9995
Elements 26-34				

Table 3-8 Damage Localization Results, 2.25 inch Off Center Crack

The first three iterations isolate the region of damage to elements 28 to 32 which does include the region with prescribed damage for the simulated experimental

data. The fourth iteration reduces the most probable region of damage to elements 29 to 31 further isolating the prescribed damage. This indicates how the selection of the search region by the analyst is significant effects the ability to locate damage. The sectors need to be set up so that the damage is within a sector. This will probably require that a model be tested numerous times with different starting regions.

4. 4.5 Inch Crack

a. *Centered Damage - Elements 22-27*

The next set of tests were for a crack length of 4.5 inches. The centered damage condition effected the first three elements on either side of the center node. The prescribed damage, the reduction of modulus, was made in elements numbered 22 to 27 to generate the simulated experimental data set. The search procedure results are included in Table 3-9.

Damage in Elements 22-27				
Sector	1-16	17-32	33-48	1-48
1st Iteration	7.9942	7.9997	7.9941	7.9990
MAC Values				
Sector	17-21	22-27	28-32	17-32
2nd Iteration	7.9983	8.000	7.9982	7.9997
MAC Values				
Sector	22-23	24-25	26-27	22-27
3rd Iteration	7.9991	7.9995	7.9993	8.000
MAC Values				

Table 3-9 Damage Localization Results, 4.5 inch Centered Crack

This test selected elements 22 to 27 as the region of probable damage. This is the prescribed damage condition for this test. The method did stop the search in the

third iteration by identifying that the larger region was the area with the highest MAC. This allows the procedure to identify damage conditions larger than one or two elements.

b. Off Center Damage - Elements 5-8

The prescribed damage for the simulated experimental data set affected the first elements 5 to 8. A fourth iteration was included to better isolate the prescribed damage condition. The search procedure results are included as Table 3-10.

Damage in Elements 5-8				
Sector 1st Iteration MAC Values	1-16 7.9987	17-32 7.9930	33-48 7.9854	1-48 7.9946
Sector 2nd Iteration MAC Values	1-5 7.9973	6-11 7.9989	12-16 7.9961	1-16 7.9987
Sector 3rd Iteration MAC Values	6-7 7.9946	8-9 7.9946	10-11 7.9946	6-11 7.9989
Sector 4th Iteration MAC Values	1-4 7.9965	5-8 7.9999	9-12 7.9965	1-12 7.9989

Table 3-10 Damage Localization Results, 4.5 inch Off Center Crack

The first three iterations isolate the most probable damage condition to elements 6 to 11 which overlaps the prescribed region of damage. The fourth iteration reduces the most probable region of damage to elements 5 to 8 which is the prescribed damage. The fourth iteration again indicates that the process performance is based on selection of the search sectors.

5. 9 Inch Crack

a. Centered Damage - Elements 20-29

The next set of tests were for a crack length of 9 inches. The centered damage condition affected the first five elements on either side of the center node. The prescribed errors were made to these elements which are numbered 20 to 29. The search procedure results are included in Table 3-11.

Damage in Elements 20-29				
Sector	1-16	17-32	33-48	1-48
1st Iteration	7.9938	7.9997	7.9936	7.9994
MAC Values				
Sector	17-21	22-27	28-32	17-32
2nd Iteration	7.9986	7.9997	7.9987	7.9997
MAC Values				
Sector	22-23	24-25	26-27	22-27
3rd Iteration	7.9994	7.9996	7.9994	7.9997
MAC Values				

Table 3-11 Damage Localization Results, 9 inch Centered Crack

The second iteration of the process selected elements 22 to 27 or the entire region. At this point a decision was made to continue to the smaller region to determine if a more conclusive solution could be achieved. The third iteration selected the region with elements 22 to 27. This could indicate that the damage is in those six elements. The results of the second iteration seem to indicate that the damaged area is larger than the individual sectors. Because of the conflicting indications from the two iteration it was decided to change the search region to investigate larger sectors. Another test which included elements 1 to 29 identified elements 20 to 29 as the area of probable damage.

b. Off Center Damage - Elements 37-45

The off center damage case for this crack size was simulated by reducing the modulus for elements 37 to 45 in the baseline model generating the simulated experimental data. The search procedure results are included as Table 3-12.

Damage in Elements 37-45				
Sector	1-16	17-32	33-48	1-48
1st Iteration	7.9385	7.9727	7.9989	7.9810
MAC Values				
Sector	33-37	38-42	43-48	33-48
2nd Iteration	7.9868	7.9954	7.9912	7.9989
Elements 33-48				

Table 3-12 Damage Localization Results, 9 inch Off Center Crack

The second iteration identifies elements 33 to 48 as the region of most probable damage. For these results the next step would be to offset the search pattern to better define the region with the prescribed damage conditions.

6. Damage Localization Observations

The test cases for damage localization that have been discussed in the previous sub-sections provide significant information for the utilization of the optimization procedure for finite element model damage localization. Significant findings include:

- The process of dividing the model into sub-regions for examination provides a logical method for the damage search process.
- The search process has the ability to identify the region most probably containing the damage down to a single element.

- The inclusion of the overall region in the sector comparison provides a means to stop the damage search process and allow detection of damage to more than one or two elements.
- The MAC method of solution evaluation is an effective evaluation method although the results for first iteration may falsely indicate the entire model. Because of the ineffectiveness of the MAC for homogenous cases this indication is to be ignored.
- The search process is effected by the selection of the start regions. The overlap of damage into more than one sector can and will cause the results to be contradictory.
- When results are contradictory, new regions should be identified to begin a new series of search iterations.

The following chapter will discuss the application of the lessons demonstrated for both model updating and damage localization with the simulated experimental data to actual experimental pieces.

IV. EXPERIMENT

The second phase of the investigation of model updating and damage localization procedures consisted of experimental test cases. This was to apply the observations from Chapter III to determine the effectiveness of the processes for both applications. A simple airplane model was used to study the model updating process. Continuous carbon fiber/epoxy composite beams were tested for the damage localization problem. An undamaged composite beam and a composite beam with a known 2.25 inch delamination were used for the analysis. A separate test case using a steel beam was also used to study the damage localization process. The steel beam was tested in the undamaged condition to update the finite element model. The beam was then damaged and tested. The specifics of the experimental cases will be discussed in greater detail in this chapter.

A. EXPERIMENTAL MEASUREMENT

Planning was necessary to determine the most effective measurement techniques for data collection prior to the actual measurements. All of the vibration tests were similar in configuration with only the number and locations of the response points differing between samples. A free-free arrangement was used for all of the test articles to eliminate any effects of boundary conditions for the finite element models. The test articles were suspended with light weight filament tackline and rubber bands. This resulted in rigid body modes which were at much lower frequencies than the observed flexible vibrational modes. Impulse excitation was used to generate dynamic responses by striking the test articles with a instrumented hammer. A load cell in the hammer measured force input, while accelerometers mounted on the test articles measured the resulting acceleration.

Only out of plane translational response was measured. The response locations were chosen to maximize the number of the vibrational modes that would be observable in the test data.

The system information was processed with a dynamic signal analyzer and IDEAS test software which generated the frequency response functions. Multiple driving points and a single response point were used to develop one row of the system response matrix. A single degree of freedom polynomial curve fit was then used to generate the experimental mode shapes from the observed response data. Ensemble averaging was employed to smooth noise effects in the measured frequency responses. Test equipment and experimental setup are detailed in Appendix C.

B. SPATIALLY INCOMPLETE DATA

The computer simulations in the previous chapter demonstrated that the optimization processes could effectively be used to update a finite element model or to localize damage. One unrealistic aspect of the computer simulations for these processes is that the modal information provided for the experimental data sets was spatially complete. That is to say that the simulated experimental mode shapes contained deflection data for translation and rotation at every node of the finite element model. In the actual experimental mode shape data set this is not the case. It is not practical to measure deflection data at every point that corresponds to a node of the finite element model, so the experimental mode shapes will be spatially incomplete. Because of the difference in the amount of data between the analytical model mode shapes and the test data mode shapes, some method is needed to match the number degrees of freedom

between the two data sets. One technique is to reduce the analytical mode shapes down to the number of degrees of freedom of the experimental mode shapes. The other method is to expand the experimental mode shapes up to the number of degrees of freedom of the analytical mode shapes. Three different methods for either the reduction of the analytical mode shape data set or the expansion of the experimental mode shape data set were examined.

1. Extraction Method

The first and simplest method of matching the mode shape degrees of freedom is to extract those elements of each analytical mode shape that correspond to the points where the experimental mode shape were measured. The points for measurement on the experimental model will be called the "aset" or "analysis set." The experimental data set will contain the relative deflection at these points. The measurement points are chosen to correspond to some of the nodes in the analytical model. The "oset" or "omitted set" are the degrees of freedom of the analytical model that are not measured in the experiment. The extraction method of analytical mode shape reduction is to simply extract the aset data points needed for comparison while ignoring the oset data points. Then the experimental and the analytical sets can be compared on a one to one basis. The following equations apply:

$$\{\phi^a\} = \begin{Bmatrix} \phi_a^a \\ \phi_o^a \end{Bmatrix} \quad (4.1)$$

take

$$\{\phi^a\} = \{\phi_a^a\} \quad (4.2)$$

for comparison to the experimental data set. The superscript “a” refers to analytical set, the subscript “a” refers to the aset, and the subscript “o” refers to the oset.

2. Transformation Matrix Reduction and Expansion

Other methods for expanding or reducing the data sets are based on partitioning the mass and stiffness matrices. The subject is discussed in depth in references (12) and (13). The methods for partitioning the matrices are the Static Reduction Method, detailed in reference (12), and the Improved Reduction System (IRS) Method, which is detailed in reference (13). The methods use alternate means to derive a transformation matrix from the mass and stiffness matrices. The transformation matrix can be used to either reduce the analytical system or to expand the experimental system.

The mass and stiffness matrices are initially partitioned based on the aset and oset. These partitioned mass and stiffness matrices are then manipulated to develop a matrix equation relating deflections for the oset to those of the aset as shown below:

$$\{x_o\} = [t]\{x_a\} \quad (4.3)$$

where t can be derived by either the Static Reduction Method or the IRS method. The transformation matrix is then formed by combining an $n \times n$ identity matrix, where n is the number of degrees of freedom for the experimental system, with $[t]$ as shown below.

$$[Tr] = \begin{bmatrix} I_{n \times n} \\ t \end{bmatrix} \quad (4.4)$$

This transformation matrix is then used to form the reduced mass and stiffness matrices from the partitioned mass and stiffness matrices as shown in the following:

$$[K^R] = [Tr]^T [K^P] [Tr] \quad (4.5)$$

$$[M^R] = [Tr]^T [M^P] [Tr] \quad (4.6)$$

The reduced mass and stiffness matrices can then be solved to provide an analytical set with the same number of degrees of freedom as the experimental set.

The same transformation matrix described above can also be used to expand the experimental mode shapes by direct matrix multiplication as shown below.

$$\begin{Bmatrix} x_a \\ x_o \end{Bmatrix} = [Tr] \{x_a\} \quad (4.7)$$

The transformation matrix is multiplied times the experimental mode shape matrix and the resulting partitioned matrix contains the expanded experimental mode shapes. This results in experimental mode shapes with the same number of degrees of freedom as the spatially complete analytical mode shapes. The different reduction or expansion methods will be applied to determine if one provides an advantage in its use during the optimization process.

C. MODEL UPDATING

1. Test Article Description

The test article to verify the optimization process for model updating was an aluminum airplane model. The model consisted of a square beam fuselage, with a plate metal wing, and a plate metal tail, both attached to the fuselage with screws. Component dimensions and masses were measured directly. Specific airplane physical data is included in Appendix D.

The dynamic response of the plane was measured using a bandwidth of 625 Hertz. The excitation force was applied in 42 different locations on the plane, including points

on the wing, the tail, and the fuselage. A diagram of the excitation point layout for data collection is included in Appendix D as Figure 1. The response of the airplane test article was measured in two locations. These locations were at outermost excitation points on the right main wing and the left horizontal stabilizer. A polyreference curve fit procedure in the IDEAS software was used to generate the experimental mode shapes for the test article. The experimental mode shapes are included in Appendix D as Figures D-2 through D-11.

2. Finite Element Model Description

The finite element model to study the airplane was built using IDEAS simulation software. The measured physical dimensions and an assumed value of Young's modulus were the basis for representing the features of the airplane. The wings and tail were represented as thin shell elements while the fuselage was modeled as square section beam elements. The beam elements at the joints were created with the same nodes as used for the wing elements. The beam elements were then offset to account for the actual positioning of the fuselage. No other compensation to the stiffnesses was included to account for the joints on the wing or the tail. Specific finite element information is included in Appendix E, including a plot of the model elements in Figure E-1. The model was used to predict the first ten flexible modes of vibration. Analytical mode shape plots are included in Appendix E as Figures E-2 through E-11. The six rigid body modes were at frequencies, 10^{-6} or thereabouts, much lower than the flexible modes and were ignored. The analytically predicted natural frequencies and basic mode description as well as the corresponding experimental natural frequencies are included in Table 4-1.

Mode	Experimental Frequency	Analytical Frequency	Mode Description
1	103.906	135.637	Symmetric 1st Wing Bending
2	128.125	96.751	Antisymmetric 2nd Wing Bending with Ampinage torsion
3	140.625	126.072	Fuselage Horizontal 1st Bending
4	223.047	217.966	Fuselage Vertical 1st Bending
5	272.266	268.562	Wing Torsion
6	335.156	293.406	Symmetric 1st Tail Bending and Wing Torsion/Peeling
7	355.469	336.579	Antisymmetric 2nd Wing Bending and Antisymmetric 2nd Tail Bending
8	384.984	361.009	Wing Torsion - Fuselage Vertical 1st Bending - Tail 1st Bending
9	404.297	416.758	Fuselage Horizontal 2nd bending
10	553.125	518.864	Wing Symmetric 2nd Bending

Table 4-1 Airplane Model Dynamic Response

Figure 4-1 is a plot of the percentage error of the analytical model versus the experimental data. This demonstrates the accuracy of the original finite element model in representing the basic dynamic responses of the airplane. The average of the absolute value of the percentage error is 4.87 percent. The largest error occurs for mode six and is over 12 percent in magnitude. The model tends to predict the system's natural frequencies lower than observed in the test.

3. Model Updating Problem

With the data from the analytical model and experimental measurements the optimization problem could be constructed. The first step was to select the design variables to be considered for optimization. The different sections of the airplane were

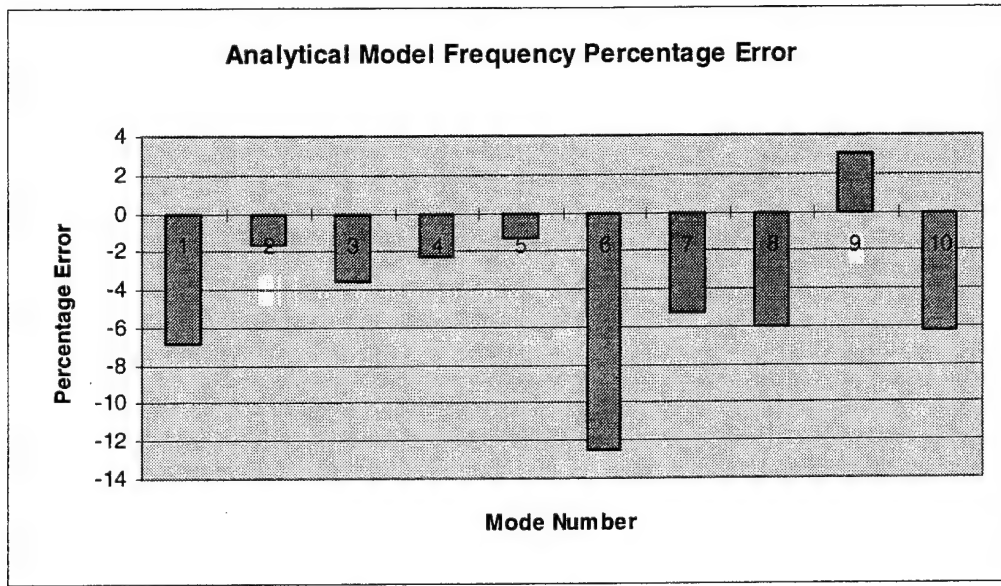


Figure 4-1 Analytical Model Frequency Percentage Error

weighed separately, so the mass density values were reasonably accurate and as such were not considered as design variables. On the other hand the Young's modulus of the materials for the plane were assumed. Because of the lower confidence in the modulus values they were considered for modification as design variables. The plane was divided into 11 regions to be considered separately. The modulus for the elements making up those regions were selected as the design variables. Figure 4-2 shows how the plane was divided into regions for the design variables. Note that the wing and the tail regions are symmetric with respect to the fuselage. The division of the plane into the different regions provided great flexibility for the optimization process. The design variables could be considered individually or linked together with other design variables. For instance the four regions of the wing that are not on the joint could be linked to form a separate design variable. This allowed the investigation of more than just the case with 11 design variables.

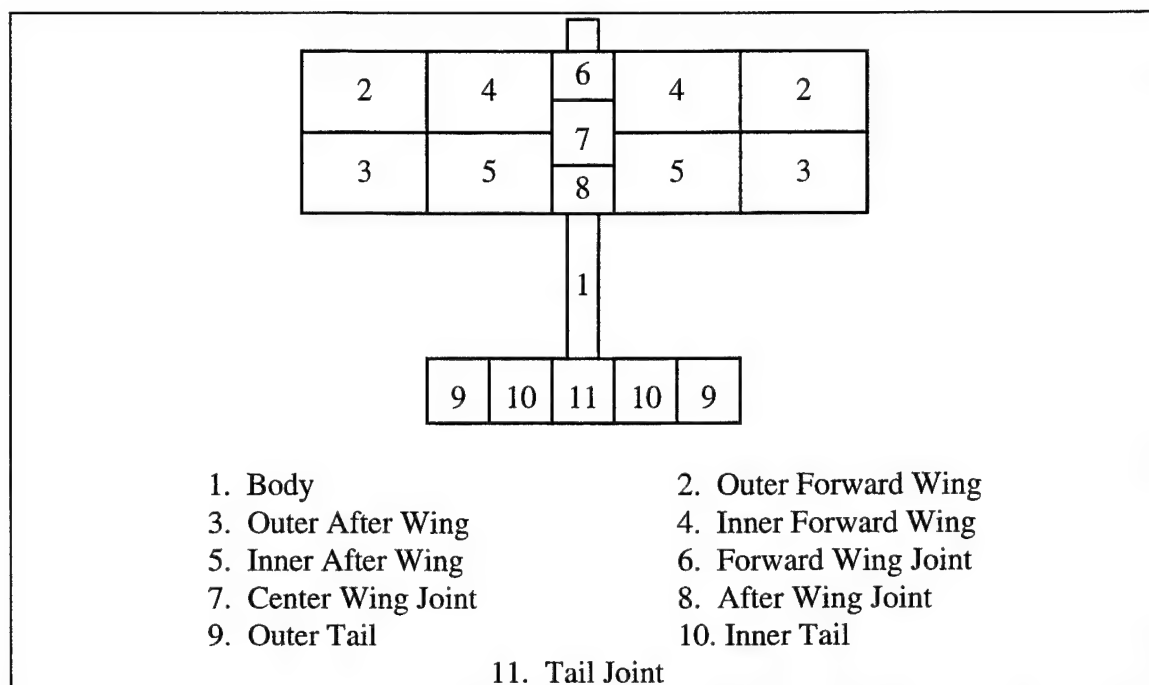


Figure 4-2 Airplane Model Design Variable Regions

The sensitivity update method was used to update the finite element model frequencies during the optimization iterations. The sensitivity values were computed by the IDEAS software. The objective function for the optimization process was of the form as shown in Equation (3-4), which is repeated below:

$$OF = A * \sum_{i=1}^n \frac{f_i^x - f_i^a}{f_i^x} + B * \sum_{k=1}^m \frac{\Delta DV_k}{DV_k} \quad (4.8)$$

where n is the number of modes and m is the number of design variables. The objective function contains a frequency difference term and a change in design variables term. The frequency term weighting multiplier, A , was set to ten while the change in design variable term weighting multiplier, B , was set to zero. The constraints imposed on the solution were that the individual frequency error terms were to be less than 5 percent and the design variables were allowed to vary up to 40 percent.

There was another issue for the optimization process with the airplane model which was not present for the computer simulation. The issue was which natural frequencies to consider for the optimization process. The finite element model predicted 10 vibrational modes in the bandwidth for the test. However, not all of them were out-of-plane modes. For example mode 9 was horizontal bending of the fuselage, with very little deflection in the direction that the response accelerometers were set up to measure. Modes 2 and 3 were also predominantly in-plane modes, but the wing and tail deflection was significant enough to detect experimentally. Because of the difficulties in measuring all of the modes, some optimization iterations were conducted with one or more of the modes omitted.

4. Optimization Process

The optimization process was run numerous times to calculate candidate solution sets. The sensitivities for the 11 regions of the airplane were combined to form as few as five and as many as 11 design variables for an optimization run. The 2-level factorial algorithm was used within the optimization run to investigate the different combinations of the active design variables. The solution process was more volatile with multiple design variables. The A multiplier needed to be adjusted frequently to ensure the solution process would run to completion. There was a problem encountered within the constrained optimization routine in MATLAB. If the multiplier for the frequency term was not high enough, the routine would crash due to a magnitude error. While the routine was attempting to go to the next iteration point, a fatal error would occur because one of

the numbers in the process would go to zero. Changing the A multiplier changes the slope of the objective function preventing the deficiency in the routine from occurring.

Following the completion of the optimization runs a value for average frequency error was calculated to be used as an initial evaluation method for each solution. Because the finite element model was computed within IDEAS, the optimization process could not automatically update the original finite element model. The candidate solutions were entered by hand into IDEAS to calculate the new analytical frequencies and mode shapes for comparison and final solution evaluation. The analytical mode shapes were reduced to the same number of degrees of freedom of the experimental model by the extraction method. This method was chosen because of the earlier simulations which showed no advantage in solution accuracy for the other more complex methods.

5. Optimization Solution

The solution which was selected as optimal was computed with five design variables and all ten frequencies. This solution had the lowest average error for all ten frequencies and the highest MAC value of all of the runs. The specific frequency values and errors are included in Appendix E in Table E-1. The design variable regions for this solution and their designations in Figure 4-2 are:

- Fuselage (1)
- Wing - except for joint region (2,3,4, and 5)
- Wing joint region (6,7, and 8)
- Tail - except for joint region (9 and 10)
- Tail joint region (11)

The maximum change made to any of the design variables was for the tail, and was a 31 percent increase from the original value. All of the design variable values were increased with the exception of the fuselage. Figure 4-3 shows the effects of the updating process on the frequency errors for the finite element model. The original model errors are plotted with the updated model errors. The finite element model average frequency error was reduced from 4.87 percent to 1.92 percent.

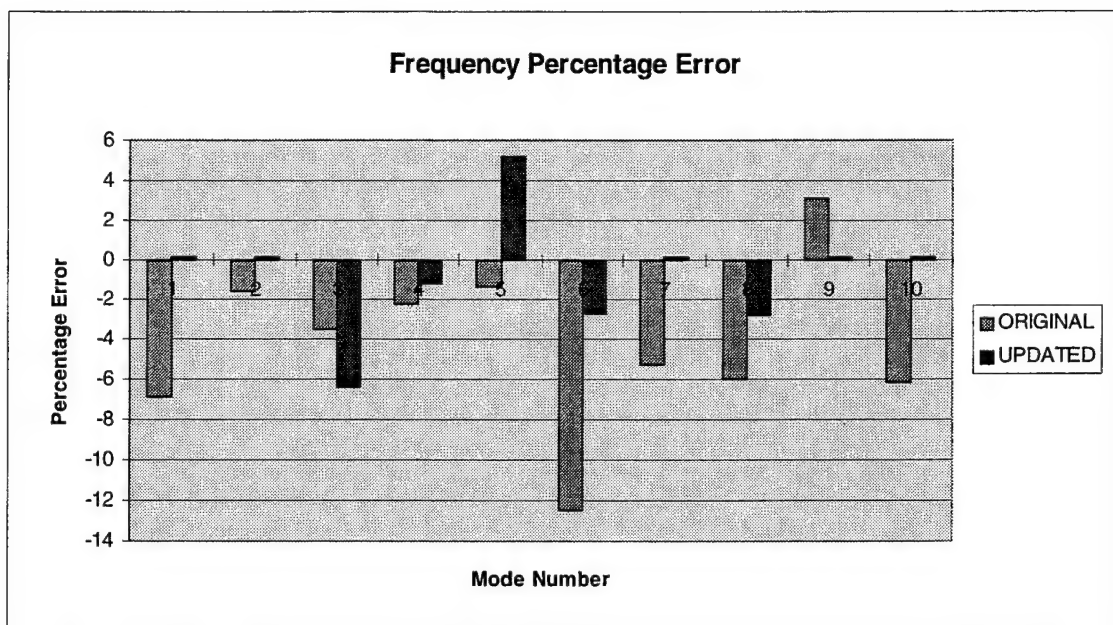


Figure 4-3 Frequency Error Comparison, Original and Updated Models

6. Solution Interpretation

The optimization process provided a solution set to update and improve the performance of the finite element model. But what do the changes to the design variables signify? The process indicates that the modulus in the wing, tail, and both joints should be increased. The plate material and the joint characteristics are stiffer than assumed for the original model. This gives an indication why most of the natural frequencies were

originally predicted low by the model. These stiffness increases resulted in most of the natural frequencies increasing in value. The wing and wing joint stiffness was increased which raised the predicted frequencies for the wing modes; 1,5,7, and 10. The increases in stiffness improved the accuracy for modes 1, 7 and 10 but overcompensated for mode 5 and actually increased the error magnitude. This demonstrates that it is difficult to isolate particular modes with fairly large design variable regions. Smaller design variable regions may have more success in correcting that model deficiency. The tail stiffness was increased dramatically. This was to compensate for mode 6, which is tail bending, being predicted rather low. The model prediction for this mode was probably quite low because the mass density had been increased to compensate for a weld bead on the tail. The body modulus was reduced to lower the frequencies that were fuselage dominated because mode 9 was predicted high. In retrospect, the recommended changes to the material properties tend to show where the mistakes were made in the construction of the finite element model. This goes to demonstrate how hard some properties are to represent accurately in the model. It also highlights the assumptions that were made for property values or dimensions that incorrectly represented the true values.

D. COMPOSITE BEAM DAMAGE LOCALIZATION

1. Test Article and Finite Element Model Description

The experimental verification of the damage localization process was conducted with two composite beams. One of the beams was undamaged while the other had a known delamination 2.25 inches in length at its center. The beams were measured to determine physical dimensions. These articles were the basis for the composite beam

models and the properties used in the Chapter III computer simulations. The assumed value for Young's modulus of the beam is the value identified in Reference (14). Specific beam data is included in Appendix B.

Beam dynamic response was measured experimentally with a frequency bandwidth of 1200 Hertz. The response of the each beam was measured at a single point, which was located at the left end of the beam. The excitation force was applied in 25 different locations along the length of the beams. A diagram of the excitation point layout for data collection is included in Appendix F as Figure F-1. A polynomial curve fit procedure was used to generate the experimental mode shapes for the test pieces. The experimental mode shapes for the damaged beam are included in Appendix F as Figures F-2 through F-10.

2. Finite Element Model Update

The experimental data from the undamaged beam was used to update a finite element model to develop the baseline model for the beam. The updated model could then be used to detect and localize damage in a similar beam. The design variable for the model updating procedure was Young's modulus of the composite beam. The first five natural frequencies were utilized in the update procedure. The optimization process increased the value of the modulus to match the experimental frequencies of the undamaged beam. The results of the optimization process are included in Table 4-2.

Mode	Experimental Frequency	Initial Analytical Frequency	Percentage Error	Updated Analytical Frequency	Percentage Error
1	29.06	27.95	-3.82	29.04	-0.07
2	79.69	77.06	-2.62	80.05	-0.45
3	156.56	151.05	-3.51	156.93	-0.23
4	259.38	249.66	-3.80	259.36	0.01
5	386.25	372.83	-3.47	387.32	-0.04

Table 4-2 Composite Beam Update Data

3. Damage Localization

The damage localization problem with experimental data was set up identical to the problem set up using the simulated experimental data as discussed in Chapter III. The objective function was weighted to emphasize the frequency difference term, and the design variable under consideration was the modulus for the sectors of the beam. The only difference was in the use of the experimental frequencies and mode shapes and the use of spatially incomplete data. The experimental data included translation at 25 points while the finite element model contained translation and rotation information for 49 nodes. All three of the data reduction or expansion methods were used to equalize the number of degrees of freedom for the analytical and experimental mode shapes. The summed MAC rating for all of the modes was used to evaluate the solutions. The optimization routine was run with the first nine natural frequencies. The 2.25 inch crack is located at the center of the beam and overlaps the four center elements of the beam. Elements 24 and 25 contain most of the known damage but elements 23 and 26 could also display decreased stiffness.

4. Localization Results

The first trial investigated the localization process with spatially incomplete data. The method used for mode shape equalization was analytical mode shape reduction using the extraction method. The aset data from the analytical model mode shapes was extracted and compared to the experimental mode shapes to compute the MAC. The results of the search procedure are included in Table 4-3. The MAC values themselves are not included in the table but the region with the highest rating is highlighted to indicate the search results. Extraction provided the correct identification of the damage in the center elements.

Damage in Elements 24-25				
1st Iteration Sectors	1-16	17-32	33-48	1-48
2nd Iteration Sectors	17-21	22-27	28-32	17-32
3rd Iteration Sectors	22-23	24-25	26-27	22-27

Table 4-3 Composite Beam Damage Search Results, Extraction Method

The next trial investigated the localization process with the reduction of the analytical mode shapes using the Static Reduction transformation matrix. Results are contained in Table 4-4.

Damage in Elements 24-25				
1st Iteration Sectors	1-16	17-32	33-48	1-48
2nd Iteration Sectors	17-21	22-27	28-32	17-32
3rd Iteration Sectors	22-23	24-25	26-27	22-27

Table 4-4 Composite Beam Damage Search Results, Static Reduction

The next trial investigated the localization process with expansion of the experimental mode shapes using the Static Reduction transformation matrix. Results are contained in Table 4-5.

Damage in Elements 24-25				
1st Iteration Sectors	1-16	17-32	33-48	1-48
2nd Iteration Sectors	17-21	22-27	28-32	17-32
3rd Iteration Sectors	22-23	24-25	26-27	22-27

Table 4-5 Composite Beam Damage Search Results, Static Expansion

The next trial investigated the localization process with the reduction of the analytical mode shapes using the Improved Reduction System (IRS) transformation matrix. Results are contained in Table 4-6.

Damage in Elements 24-25				
1st Iteration Sectors	1-16	17-32	33-48	1-48
2nd Iteration Sectors	17-21	22-27	28-32	17-32
3rd Iteration Sectors	22-23	24-25	26-27	22-27

Table 4-6 Composite Beam Damage Search Results, IRS Reduction

The next trial investigated the localization process with expansion of the experimental data using the Improved Reduction System (IRS) transformation matrix. Results are contained in Table 4-7.

Damage in Elements 24-25				
1st Iteration Sectors	1-16	17-32	33-48	1-48
2nd Iteration Sectors	17-21	22-27	28-32	17-32
3rd Iteration Sectors	22-23	24-25	26-27	22-27

Table 4-7 Composite Beam Damage Search Results, IRS Expansion

5. Solution Interpretation

All five of the solutions from the damage localization routines converge to the two center elements as the most probable location of damage, which is the location of the known damage. This successful demonstration of the localization process shows that the sector search logic combined with the optimization routine can locate damage in a simple

test structure using spatially incomplete data. As far as the methods of compensating for spatially incomplete data all of the techniques investigated were successful. Without a performance advantage for any of the methods the one that requires the least computational time should be used. The extraction method requires no computations other than identifying and extracting the aset data points so that method should be employed.

Four other composite beams with known damages were also tested to determine if the damage could be localized. The experimental frequency data for the beams was not consistent enough to allow the process to succeed. That is, the frequency shifts induced by the reduction of stiffness in the beam did not provide a consistent downward trend for all natural frequencies as compared to the undamaged beam. Without consistent frequency shifts the optimization and damage localization process will not be successful. Therefore the extent of the damage will remain unknown.

E. STEEL BEAM DAMAGE LOCALIZATION

1. Test Article and Finite Element Model Description

The experimental verification of the damage localization process was also investigated with a steel beam test piece. The beam was tested in the undamaged state to update the finite element model and then notched to simulate stiffness reduction. The beam was measured directly to determine physical dimensions. The assumed value for Young's modulus of the beam was the standard value used for steel. Specific beam data is included in Appendix G.

Beam dynamic response was measured experimentally with a frequency bandwidth of 2500 Hertz. The response of the beam was measured at a single point, which was located at the left end of the beam. The excitation force was applied in 25 different locations along the length of the beam. A diagram of the excitation point layout for data collection is included in Appendix G as Figure G-2. A polynomial curve fit procedure was used to generate the experimental mode shapes for the test pieces. The experimental mode shapes for the damaged beam are included in Appendix G as Figures G-3 through G-12.

2. Finite Element Model Update

The experimental data from the beam in the undamaged condition was used to update a finite element model to develop the baseline model for the beam. The updated model could then be used to detect and localize damage in the test piece. The design variable from the model updating procedure was Young's modulus of the beam. The first five natural frequencies were utilized in the update procedure. The optimization process decreased the value of the modulus to match the experimental frequencies of the undamaged beam. A MAC calculation was done to determine how well the analytical mode shapes matched the experimental mode shapes. All five of the mode shapes had MAC values greater than 0.99 indicating very good correlation of the analytical results to the experimental mode shapes. The results of the optimization process are included in Table 4-8.

Mode	Experimental Frequency	Initial Analytical Frequency	Percentage Error	Updated Analytical Frequency	Percentage Error
1	56.25	57.54	2.29	56.186	-0.11
2	155.00	158.62	2.33	154.89	-0.01
3	303.75	310.97	2.37	303.66	-0.01
4	501.25	514.08	2.56	502.0	0.01
5	746.875	768.00	2.83	749.96	0.01

Table 4-8 Steel Beam Update Data

3. Damage Localization

The damage localization problem for the steel beam was set up identical to the problems explored for simulated tests in Chapter III and for the experimental composite beam test. The objective function was weighted to emphasize the frequency difference term, and the design variable under consideration was the modulus for the sectors of the search. The experimental data included relative translation at 25 points while the finite element model contained translation and rotation information for 49 nodes. All three of the data reduction or expansion methods were used equalize the number of degrees of freedom for the analytical and experimental mode shapes. The summed MAC rating for all of the modes was used to evaluate the solutions. The optimization routine was run with the first nine natural frequencies. The damage condition was induced by notching the beam. The reduction in cross sectional area was made in element 25 and resulted in a decrease of 9.22 percent to the moment of inertia in that element, effectively reducing the stiffness of the beam.

4. Solution Method

The initial trials for the steel beam optimization routine did not provide a solution for the change to the design variable needed to update the model. The solution process continually returned the initial value of the design variable as the optimal solution. This was due to the errors in the analytical frequencies versus the experimental frequencies. The analytical model predicted the low frequencies high and the high frequencies low. The relative error was about equal so the routine determined that the system was at the optimal solution. To compensate for the inability of the optimization process to solve for the change to the design variable another method was used. This method is similar to the direct solve method discussed in Chapter III and is called the pseudo-inverse method. This method uses an overdetermined matrix equation to solve for the change to a single design variable. The sensitivity matrix, $[T]$, is reduced to a 9×1 vector. The vector is transposed and the individual terms are inverted. This procedure is called the pseudo-inverse of a non-square matrix. The solution for the single design variable change can then be computed as follows:

$$\Delta DV = [\text{pinv}(T)]\{\Delta f\} \quad (4.9)$$

where pinv indicates the pseudo-inverse procedure. This procedure does provide a solution for the reduction in the design variable that is used for the sector search.

5. Localization Results

The use of the pseudo-inverse solution method did allow the routine to compute a value for the change to the modulus within a region. The search procedure was not

successful though. The process tended to select the overall regions instead of one of the three sectors for the search. The results for this damage case are shown in Table 4-9.

Damage in Element 25				
1st Iteration Sectors	1-16	17-32	33-48	1-48
2nd Iteration Sectors	17-21	22-27	28-32	17-32

Table 4-9 Steel Beam Damage Search Results, Extraction Reduction

The process indicates the overall region for the second iteration. In fact the next highest MAC value was for the right sector, elements 28 to 32, so even if the overall region selection was ignored the known solution would not be selected. None of the methods of compensating for the spatially incomplete data made the results improve in accuracy.

6. Simulated Experimental Damage

To investigate why the process did not work for this test piece, the experimental damage condition was simulated by making adjustments to the baseline finite element model. The simulated experimental data set was then compared to the experimental data. The comparison data is contained in Table 4.10. The simulated experimental data was reduced to be spatially incomplete by the extraction method, that is the aset points were extracted from the simulated modal data.

Mode	Experimental Frequency	Simulated Frequency	Percentage Error	MAC
1	56.25	56.02	-0.41	0.9987
2	154.688	154.89	0.13	0.9974
3	303.125	302.99	-0.04	0.9972
4	501.562	501.97	0.09	0.9973
5	746.88	748.33	0.19	0.9924
6	1042.19	1047.37	0.50	0.9921
7	1381.25	1391.88	0.77	0.9823
8	1768.75	1791.16	1.27	0.9907
9	2201.56	2233.85	1.47	0.9917

Table 4-10 Simulated Experimental Data Comparison

The major differences are observed in the simulated frequencies as compared to the experimental frequencies. The MAC values rate how well the individual simulated modes correlate to the experimental modes. Ratings in excess of 0.99 indicate very good correlation. The solution process was then run with the simulated experimental data. The simulated experimental mode shapes were spatially complete. The aset data was extracted to generate spatially incomplete experimental mode shapes. The results for that case are included in Table 4-11.

Damage in Element 25				
1st Iteration Sectors	1-16	17-32	33-48	1-48
2nd Iteration Sectors	17-21	22-27	28-32	17-32
3rd Iteration Sectors	22-23	24-25	26-27	22-27
4th Iteration Sectors	23	24	25	23-25

Table 4-11 Steel Beam Damage Search Results, Simulated Experimental Data

The process successfully identified the damage for the simulated experimental case. At this point the natural frequencies and mode shapes of the actual experimental data set were substituted for the simulated experimental data to determine which factors caused the actual experiment to fail in damage localization. Table 4-12 summarizes the results of inserting the experimental data into the simulated experimental data set.

Modes	Frequency	Shapes	Both
1	25	25	25
2	25	25	25
3	25	25	25
4	25	17-32/24-25	17-32/24-25
5	25	31	31
6	25	30	30
7	17-32/24-25	30	17-32/24-25
8	17-32/24-25	22-27	17-32/24-25
9	17-32/26-27	25	17-32/22-27
1-3	25	25	25
4-6	25	30	30
7-9	17-32/22-27	30	17-32/22-27
1-9	17-32/22-27	30	17-32/28-32

Table 4-12 Experimental Data Substitution Results

a. Frequency Substitution

The experimental frequencies were substituted into the simulated experimental data set both one at a time and in groups. Changing the frequencies for the first six modes of the simulated data set individually, had no effect on the solution. The process converged to element 25 as had been previously observed for the simulated data. When the frequencies for mode seven or mode eight were substituted into the data set, the process selected elements 17 to 32 instead of the center sector. This result was ignored to determine if the problem existed in the rating of the overall region. Selecting the highest

sector, which was the center, iterations were continued to see if a single element could be identified. The next iteration selected elements 24 and 25 but a final iteration did not select element 25.

The natural frequencies were then substituted in groups. The first group consisted of the frequencies for first three modes. This did not change the results. Substituting the frequencies for modes 4 to 6 did not change the results either. Substituting the frequencies for modes 7 to 9 again caused the process to select elements 17 to 32. This response was ignored and another iteration was run which selected sector 22 to 27. Substituting the frequencies for all nine modes had the same effect as substituting the frequencies for modes 7 to 9.

This substitution process indicates that the frequencies for the high modes contaminate the solution process in some fashion to create error. The probable problem is that the large frequency difference between the analytical and experimental results force the pseudo-inverse solution to be too large. This creates error when the updated mode shapes are calculated and results in the MAC selecting the larger region.

b. Mode Shape Substitution

The experimental mode shapes were then substituted into the simulated experimental data set one at a time and in groups. Substituting the first three mode shapes individually had no effect. Substituting the fourth mode shape caused the process to select elements 17 to 32. If that selection was ignored the next iteration selected elements 24 and 25. Substituting the fifth mode shape resulted in the selection of element 31 as the damage location. Substituting both the sixth and seventh mode shapes resulted in the

selection of element 30 as the damage location. The eight mode shape resulted in the selection of elements 22 to 27 and the ninth mode shape had no effect.

The mode shapes were then substituted in groups. Mode shapes 1 to 3 had no effect on the solution. Substituting mode shapes 4 to 6 caused the process to select element 30. Substituting mode shapes 7 to 9 and 1 to 9 both lead to the process selecting element 30.

The substitution of the mode shapes indicates that the mode shapes are not the same as those predicted by the simulated damage finite element model. Even though the MAC between the simulated damage mode shapes and experimental modes shapes indicates a good match it is not good enough. Also the higher modes are less similar to the experimental data. The higher mode shapes contaminate the solution so the process selects the wrong elements. This could be caused by noise, faulty data taking, or an error in the process used to calculate the mode shapes.

c. Frequency and Mode Shape Substitution

The experimental frequencies and mode shapes were then substituted into the simulated experimental data set one mode at a time and in groups. Substituting the first three modes individually had no effect. Substituting the fourth mode caused the process to select elements 17 to 32. If that selection was ignored the next iteration selected elements 24 and 25. Substituting the fifth mode resulted in the selection of element 31 as the damage location. Substituting the sixth mode resulted in the selection of element 30 as the damage location. Substituting the seventh mode or the eight mode resulted in the selection of elements 17 to 32. This was ignored and another iteration

selected elements 24 and 25. Substituting the ninth mode resulted in selecting elements 22-27.

The modes were then substituted in groups. Modes 1 to 3 had no effect on the solution. Substituting modes 4 to 6 caused the process to select element 30. Substituting mode shapes 7 to 9 caused the process to select elements 17 to 32. Another iteration selected elements 22 to 27. Substituting modes 1 through 9 lead to the process selecting elements 28 to 32.

The substitution of both the frequencies and the mode shapes indicates that the data from the experimental data set is not “clean” enough to select the known damage location. The problem with the data could be any one of the items cited for the mode shape problems. The results for the lower modes would seem to indicate that if a solution was run just considering the lower modes that the correct damage location would be identified, but that was not the case.

7. Solution Interpretation

The unsuccessful trials for the steel beam indicate that the sector search method does have some limitations. The experimental data set needs to be extremely clean or the search process will be ineffective. Even the smallest noise or other contamination will cause errors in the process. Another problem is the inability of the optimization routine to run for the steel beam. The frequency differences should cause the routine to search for an optimum value but it does not. This may be due to a problem in the sensitivity matrix, but that does not account for the process working for beam optimization or the pseudo-

inverse solve procedure. This test case does indicate that further study is necessary on the sector search form damage localization.

V. CONCLUSIONS / RECOMMENDATIONS

A. SUMMARY

Sensitivity-based finite element model updating and numerical optimization procedures were developed to improve finite element model performance and to detect structural damage. Experimentally measured dynamic responses were compared to analytically predicted dynamic responses to provide a basis to make corrections to design parameters of the finite element model. The investigation of updating procedures and applications have shown the following:

- The updating and optimization procedures provide a means to modify finite element models to improve their accuracy, or to determine structural damage by a comparison of experimentally measured dynamic responses to those predicted by the finite element model.
- Sensitivity based updating of analytical natural frequencies for small changes to design parameters is a valid method of approximation that reduces computational requirements during the optimization process.
- Numerical optimization methods provide a logical search procedure and enhance computational efficiency in the determination of the corrections that need to be made in order to update finite element models.
- The 2-level factorial search algorithm provides a thorough means to test different combinations of design variables to ensure the best solution is attained. However, the number of iterations for this method increases

exponentially with the number of design variables, precluding its use for problems with large numbers of design variables.

- The sector search methodology provides a logical search procedure to isolate damage to a specific region of structure.
- The Modal Assurance Criterion provides a means to select the optimal solution during the optimization process by evaluating which candidate solution mode shapes most closely match the experimental data.
- The effectiveness of these procedures is directly dependent on the quality of the experimental measurements.

B. CONCLUSIONS

The processes investigated for model updating were effective in determining changes to be made to a finite element model to more closely resemble the response of the structure being modeled. These processes not only improve the performance of the finite element model but enhance the analyst's understanding of the finite element model and the structure itself. The process of identifying the design parameters and examining the specifics of the system dynamic responses, increases the level of understanding of how individual sections and their physical properties affect the overall characteristics of the system. The two applications highlight different points about the process.

The model update problem is dependent on the number and type of design parameters chosen for evaluation. The parameters should be chosen with care to ensure that they allow the isolation of specific mode shapes and frequencies while at the same time not overloading the computational capabilities in the process. The modifications to

model parameters determined by the process tended to highlight faulty assumptions or property values which could not be represented with high confidence. The solutions are also dependent on the bandwidth of experimental data available for comparison.

The composite beam damage localization process demonstrated that the sector search logic and model updating could be used to locate damage. This process is highly dependent on the structure having a previously validated finite element model to provide baseline response data. This process is also dependent on the damage condition inducing a consistent pattern of frequency errors from the baseline model.

The damage localization problem with the steel beam highlights some of the problems in comparing the analytical responses to the experimental response. The frequencies predicted by the finite element model for the undamaged beam diverged from the actual results. The higher system frequencies of the baseline model had relatively high error levels and contaminated the solution process preventing damage localization. The accuracy of the mode shape measurements also played a role in this test not being successful. Without highly accurate experimental mode shapes the process will identify the wrong location for damage.

C. RECOMMENDATIONS

The model updating procedures and routines developed showed positive results both for simulated and actual experimental data. However, there were limitations in the ability to pass data from one software type to another for the model update procedure, and the damage localization procedure did not work on both test pieces. Recommendations to address these and other shortcomings of these processes include:

- Continue to develop routines to pass data directly between the software used for optimization, MATLAB, and the software used for finite element model simulation, such as IDEAS.
- Modify the optimization processes to utilize mode shape sensitivities for use with MAC solution evaluation vice re-solving the eigenproblem.
- Modify the optimization routine to allow more flexibility in its application, by allowing for direct user interface with the use of pull down menus or prompts removing the need to hardcode for a given model type.
- Continue to investigate the process of model updating by applying the baseline software to more complex structures.
- Develop more efficient methods of combining design variables to allow isolation of all modeling errors while not requiring excessive iterations.
- Continue to research the sector search method of damage localization to both isolate why the method failed for the steel beam, and to apply the logic to larger and more complex structures.
- Employ aset and oset information to effectively increase the bandwidth of experimental testing.
- Employ more advanced means of measurement to remove possible errors due to noise or other signal contamination.

The ability to pass mode shape or design variable data directly from IDEAS to MATLAB or vice versa would greatly enhance the efficiency of the updating process. The time required to format data to put into MATLAB or to feedback design variable

modifications into simulation software greatly limits the size and number of solutions that can be investigated during optimization. Direct conversion will be required for larger models.

Mode shape sensitivities can be used to approximate the change to the mode shapes of a system based on the change to design parameters. By using this approximation the need to re-solve the eigenproblem to evaluate every candidate solution is removed and would greatly increase computational efficiency.

The computer codes used in this thesis were hardcoded to the specific situation. Although all of the processes would be similar, the ability to apply this method to other situations requires user modification of the code. Methods to improve user interface should be developed.

The processes developed could be expanded to handle larger and more complex systems. The updating logic could be applied to finite element models generated by other students for specific pieces of equipment. This would improve both the models being analyzed and the optimization code. The sector search logic could be expanded to include a way to deal with shell elements or for complex geometry than the beam elements tested.

The 2-level factorial algorithm employs large numbers of iterations to investigate all possible design variable combinations. Other methods of examining design variable combinations that allow isolation of errors while not requiring excessive computer time should be developed. This would greatly improve the computational efficiency of the optimization process.

The ability to extract more data from a test bandwidth could be explored through the use of aset and oset system frequencies. Basically the methods allow the analyst to process test data as if measurement points were fixed, effectively introducing a new set of boundary conditions. This would increase the number of system frequencies that could be used in the sensitivity equations.

The ability of a process to accurately update a model or to localize damage are dependent on the quality of the measured test data. Without accurate natural frequencies and mode shapes the process can not be expected to succeed for either application.

APPENDIX A. ALUMINUM BEAM SPECIFICATIONS

A. PHYSICAL DIMENSIONS AND PROPERTIES

The aluminum beam used for the Chapter III computer simulations was not patterned after a actual test piece. The dimensions of the beam were chosen at random and the physical properties were chosen from standard material data for aluminum. The beam orientation for the simulations was as depicted in Figure A-1. The degrees of freedom were the vertical translation, upward in the figure, and rotation around a vector out of the plane of the page.

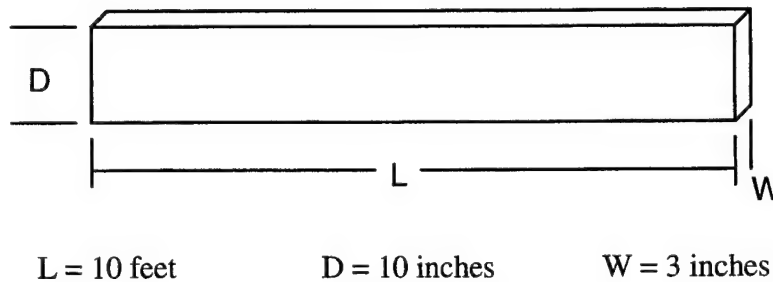


Figure A-1 Aluminum Beam

The physical properties chosen for the beam were:

Young's modulus	$E = 10 \times 10^6$	PSI
mass density	$\rho = 0.000254$	lbf-sec ² /in ⁴

B. DYNAMIC RESPONSE

The system natural frequencies predicted by the finite element model are:

Mode 1	22.26 Hz
Mode 2	139.50 Hz
Mode 3	390.82 Hz
Mode 4	767.11 Hz

The mode shapes predicted by the finite element are included in Figures A-2 through A-5.

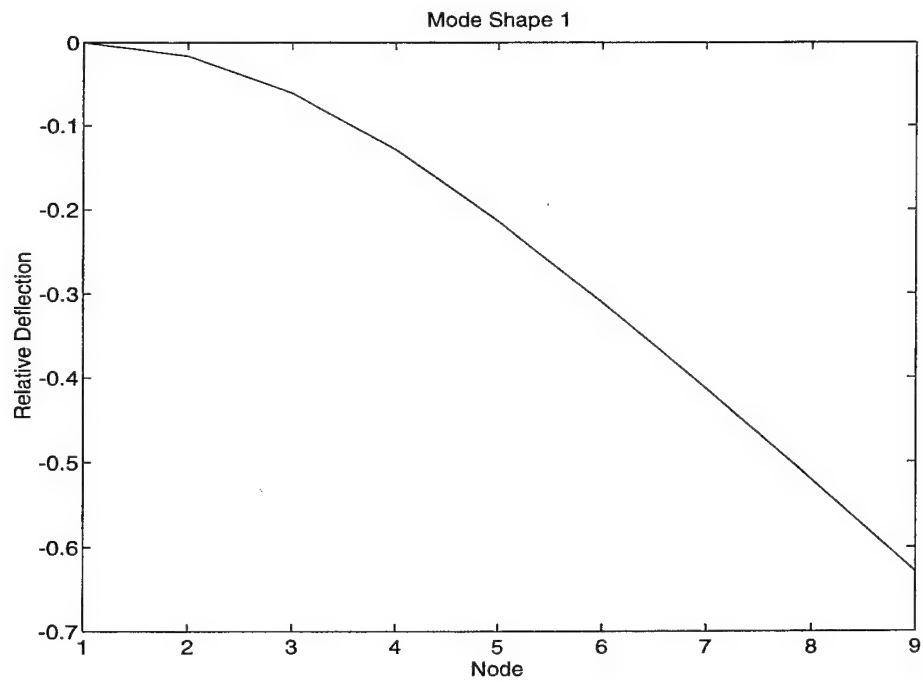


Figure A-2 Aluminum Beam, 1st Mode Shape

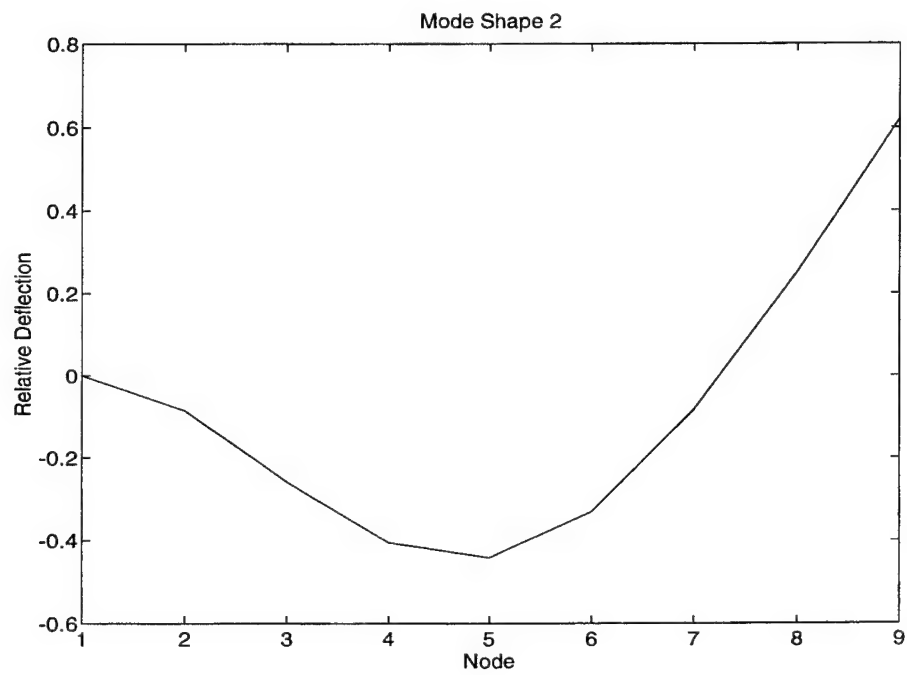


Figure A-3 Aluminum Beam, 2nd Mode Shape

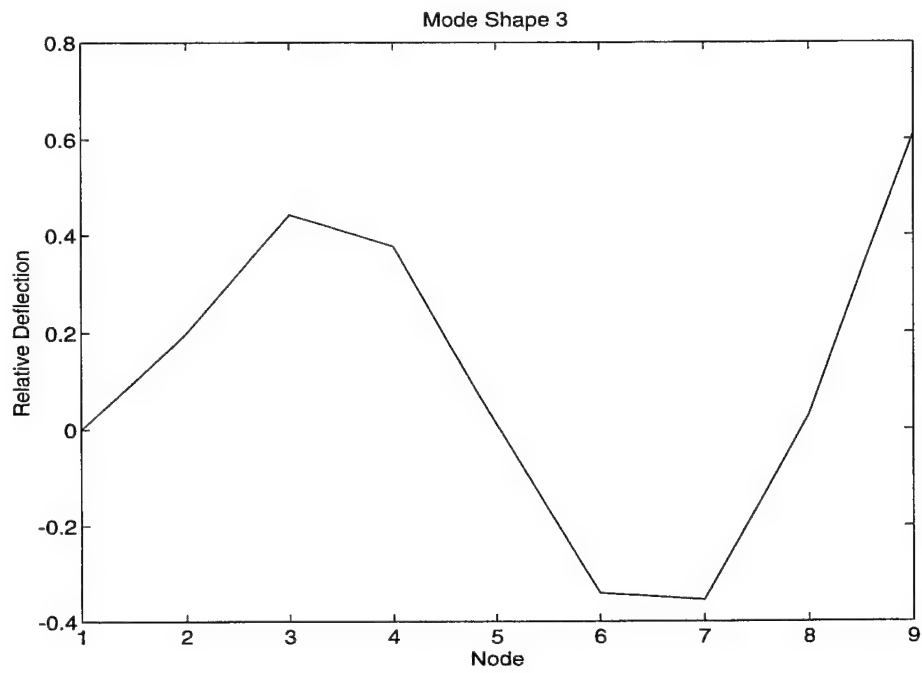


Figure A-4 Aluminum Beam, 3rd Mode Shape

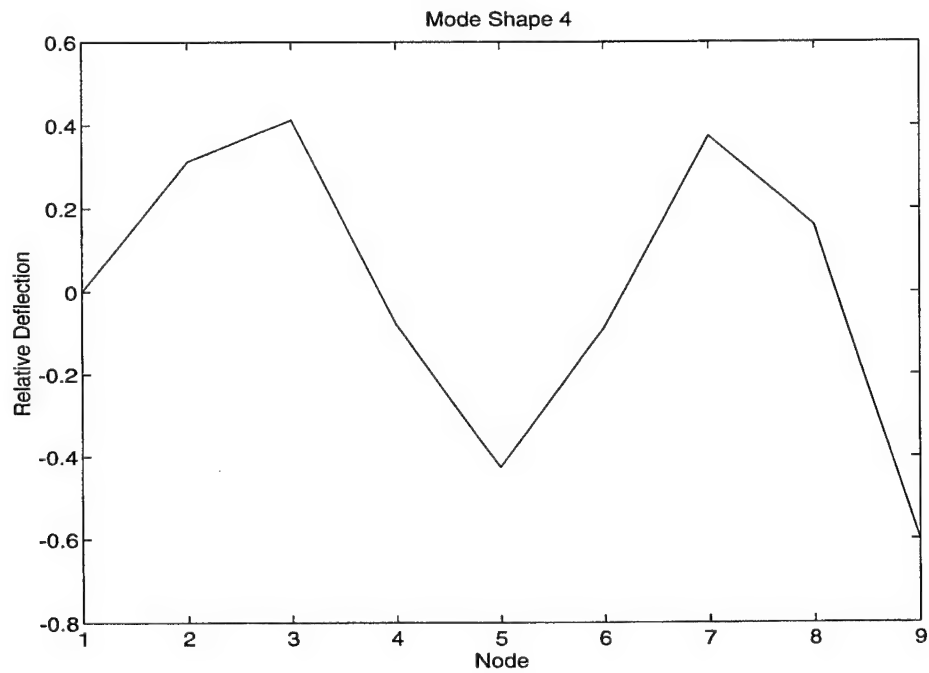


Figure A-5 Aluminum Beam, 4th Mode Shape

C. OPTIMIZATION RESULTS

Numerical results for Test Cases 1 to 8 in Chapter III are included in the following tables.

	Prescribed		Percentage Difference	
	Mass	Modulus	Mass	Modulus
Mass Down	0.000234	1.00E+07	-7.8740157	0
Mass Down, Mod Down	0.000234	9.50E+06	-7.8740157	-5
Mass Down, Mod Up	0.000234	1.05E+07	-7.8740157	5
Mod Down	0.000254	9.50E+06	0	-5
Mod Up	0.000254	1.05E+07	0	5
Mass Up	0.000274	1.00E+07	7.8740157	0
Mass Up, Mod Down	0.000274	9.50E+06	7.8740157	-5
Mass Up, Mod Up	0.000274	1.05E+07	7.8740157	5
	Solution		Percentage Difference	
	Mass	Modulus	Mass	Modulus
Mass Down	0.000233	1.00E+07	-8.2677165	0
Mass Down, Mod Down	0.000246	1.00E+07	-3.1496063	0
Mass Down, Mod Up	0.000229	1.00E+07	-9.8425197	0
Mod Down	0.000267	9.99E+06	5.1181102	-0.1
Mod Up	0.000241	1.00E+07	-5.1181102	0
Mass Up	0.000273	9.99E+06	7.480315	-0.1
Mass Up, Mod Down	0.000279	9.99E+06	9.8425197	-0.1
Mass Up, Mod Up	0.000261	9.99E+06	2.7559055	-0.1

Table A-1 Test Case 1 Numerical Results

	Prescribed		Percentage Difference	
	Mass	Modulus	Mass	Modulus
Mass Down	0.000234	1.00E+07	-7.8740157	0
Mass Down, Mod Down	0.000234	9.50E+06	-7.8740157	-5
Mass Down, Mod Up	0.000234	1.05E+07	-7.8740157	5
Mod Down	0.000254	9.50E+06	0	-5
Mod Up	0.000254	1.05E+07	0	5
Mass Up	0.000274	1.00E+07	7.8740157	0
Mass Up, Mod Down	0.000274	9.50E+06	7.8740157	-5
Mass Up, Mod Up	0.000274	1.05E+07	7.8740157	5
	Solution		Percentage Difference	
	Mass	Modulus	Mass	Modulus
Mass Down	0.000237	1.02E+07	-6.6929134	1.9
Mass Down, Mod Down	0.000252	1.02E+07	-0.7874016	2.4
Mass Down, Mod Up	0.000229	1.04E+07	-9.8425197	3.97
Mod Down	0.000267	9.99E+06	5.1181102	-0.1
Mod Up	0.0002413	9.99E+06	-5	-0.1
Mass Up	0.0002725	9.99E+06	7.2834646	-0.1
Mass Up, Mod Down	0.000273	9.54E+06	7.480315	-4.6
Mass Up, Mod Up	0.000261	9.99E+06	2.7559055	-0.1

Table A-2 Test Case 2 Numerical Results

	Prescribed		Percentage Difference	
	Mass	Modulus	Mass	Modulus
Mass Down	0.000234	1.00E+07	-7.8740157	0
Mass Down, Mod Down	0.000234	9.50E+06	-7.8740157	-5
Mass Down, Mod Up	0.000234	1.05E+07	-7.8740157	5
Mod Down	0.000254	9.50E+06	0	-5
Mod Up	0.000254	1.05E+07	0	5
Mass Up	0.000274	1.00E+07	7.87401575	0
Mass Up, Mod Down	0.000274	9.50E+06	7.87401575	-5
Mass Up, Mod Up	0.000274	1.05E+07	7.87401575	5
	Solution		Percentage Difference	
	Mass	Modulus	Mass	Modulus
Mass Down	0.00025	1.07E+07	-1.5748031	7
Mass Down, Mod Down	0.000252	1.02E+07	-0.7874016	2.4
Mass Down, Mod Up	0.000241	1.09E+07	-5.1181102	8.7
Mod Down	0.000255	9.52E+06	0.19685039	-4.8
Mod Up	0.000248	1.02E+07	-2.519685	2.49
Mass Up	0.000271	9.92E+06	6.53543307	-0.8
Mass Up, Mod Down	0.000263	9.15E+06	3.38582677	-8.55
Mass Up, Mod Up	0.000254	9.73E+06	0	-2.7

Table A-3 Test Case 3 Numerical Results

	Prescribed		Percentage Difference	
	Mass	Modulus	Mass	Modulus
Mass Down	0.000234	1.00E+07	-7.874016	0
Mass Down, Mod Down	0.000234	9.50E+06	-7.874016	-5
Mass Down, Mod Up	0.000234	1.05E+07	-7.874016	5
Mod Down	0.000254	9.50E+06	0	-5
Mod Up	0.000254	1.05E+07	0	5
Mass Up	0.000274	1.00E+07	7.8740157	0
Mass Up, Mod Down	0.000274	9.50E+06	7.8740157	-5
Mass Up, Mod Up	0.000274	1.05E+07	7.8740157	5

	Solution		Percentage Difference	
	Mass	Modulus	Mass	Modulus
Mass Down	0.000255	1.09E+07	0.3937008	9.3
Mass Down, Mod Down	0.0002369	9.64E+06	-6.732283	-3.6
Mass Down, Mod Up	0.0002439	1.10E+07	-3.976378	10
Mod Down	0.000247	9.24E+06	-2.755906	-7.6
Mod Up	0.00026	1.08E+07	2.3622047	7.5
Mass Up	0.000261	9.56E+06	2.7559055	-4.4
Mass Up, Mod Down	0.0002715	9.50E+06	6.8897638	-5.02
Mass Up, Mod Up	0.000279	1.07E+07	9.8425197	7.3

Table A-4 Test Case 4 Numerical Results

	Prescribed Value		Percentage Difference				
	Mass	Modulus	Mass	Modulus			
Mass Down	0.000234	1.00E+07	-7.874	0			
Mass Down, Mod Down	0.000234	9.50E+06	-7.874	-5			
Mass Down, Mod Up	0.000234	1.05E+07	-7.874	5			
Mod Down	0.000254	9.50E+06	0	-5			
Mod Up	0.000254	1.05E+07	0	5			
Mass Up	0.000274	1.00E+07	7.874	0			
Mass Up, Mod Down	0.000274	9.50E+06	7.874	-5			
Mass Up, Mod Up	0.000274	1.05E+07	7.874	5			
	Solution Value		Percentage Difference				
	Mass	Modulus	Mass	Modulus	DV	Combo	Single
Mass Down	0.000233	1.00E+07	-8.307	0	M only		0.814
Mass Down, Mod Down	0.000246	1.00E+07	-3.15	0	K only		0.837
Mass Down, Mod Up	0.000244	1.10E+07	-4.094	9.9	Both		0.833
Mod Down	0.000259	9.70E+06	1.969	-3.02	Both		0.824
Mod Up	0.000254	1.05E+07	0	5	K only		0.8165
Mass Up	0.000273	1.00E+07	7.323	0	M only		0.814
Mass Up, Mod Down	0.000271	9.49E+06	6.693	-5.13	Both		0.812
Mass Up, Mod Up	0.000261	9.99E+06	2.559	-0.1	Both		0.796

Table A-5 Test Case 5 Numerical Results

	Prescribed		Percentage Difference				
	Mass	Modulus	Mass	Modulus			
Mass Down	0.00024	1.00E+07	-5.5118	0			
Mass Down, Mod Down	0.00024	9.20E+06	-5.5118	-8			
Mass Down, Mod Up	0.00024	1.08E+07	-5.5118	8			
Mod Down	0.000254	9.20E+06	0	-8			
Mod Up	0.000254	1.08E+07	0	8			
Mass Up	0.000268	1.00E+07	5.5118	0			
Mass Up, Mod Down	0.000268	9.20E+06	5.5118	-8			
Mass Up, Mod Up	0.000268	1.08E+07	5.5118	8			
	Solution		Percentage Difference				
	Mass	Modulus	Mass	Modulus	DV Combo	Single	
Mass Down	0.000239	1.00E+07	-5.9055	0	M only	0.8151	
Mass Down, Mod Down	0.000261	9.99E+06	2.7559	-0.1	Both	0.8509	
Mass Down, Mod Up	0.000243	1.10E+07	-4.3701	9.9	Both	0.8215	
Mod Down	0.000254	9.20E+06	0	-8	K only	0.8156	
Mod Up	0.000254	1.08E+07	0	8	K only	0.8165	
Mass Up	0.000267	1.00E+07	5.1181	0	M only	0.8153	
Mass Up, Mod Down	0.000261	9.00E+06	2.7559	-10	Both	0.8059	
Mass Up, Mod Up	0.000252	1.02E+07	-0.7087	1.67	Both	0.7921	

Table A-6 Test Case 6 Numerical Results

	Prescribed Value		Percentage Difference				
	Mass	Modulus	Mass	Modulus			
Mass Down	0.00024	1.00E+07	-5.5118	0			
Mass Down, Mod Down	0.00024	9.20E+06	-5.5118	-8			
Mass Down, Mod Up	0.00024	1.08E+07	-5.5118	8			
Mod Down	0.00025	9.20E+06	0	-8			
Mod Up	0.00025	1.08E+07	0	8			
Mass Up	0.00027	1.00E+07	5.5118	0			
Mass Up, Mod Down	0.00027	9.20E+06	5.5118	-8			
Mass Up, Mod Up	0.00027	1.08E+07	5.5118	8			
	Solution Value		Percentage Difference				
	Mass	Modulus	Mass	Modulus	DV	Single	
					Combo		
Mass Down	0.00024	1.00E+07	-5.9055	0	M only	0.815	
Mass Down, Mod Down	0.00025	9.62E+06	-1.2205	-3.82	Both	0.835	
Mass Down, Mod Up	0.00024	1.10E+07	-4.3307	9.9	Both	0.821	
Mod Down	0.00025	9.20E+06	0	-8	K only	0.816	
Mod Up	0.00025	1.08E+07	0	8	K only	0.816	
Mass Up	0.00027	1.00E+07	5.1181	0	M only	0.815	
Mass Up, Mod Down	0.00028	9.72E+06	10	-2.81	Both	0.833	
Mass Up, Mod Up	0.00025	1.01E+07	-1.5748	0.9	Both	0.789	

Table A-7 Test Case 7 Numerical Results

	Prescribed Value		Percentage Difference			
	Mass	Modulus	Mass	Modulus		
Mass Down	0.00024	1.00E+07	-5.51	0		
Mass Down, Mod Down	0.00024	9.20E+06	-5.51	-8		
Mass Down, Mod Up	0.00024	1.08E+07	-5.51	8		
Mod Down	0.000254	9.20E+06	0	-8		
Mod Up	0.000254	1.08E+07	0	8		
Mass Up	0.000268	1.00E+07	5.512	0		
Mass Up, Mod Down	0.000268	9.20E+06	5.512	-8		
Mass Up, Mod Up	0.000268	1.08E+07	5.512	8		
	Solution Value		Percentage Difference			
	Mass	Modulus	Mass	Modulus	DV	MAC
					Combo	
Mass Down	0.00024	1.00E+07	-5.71	0	M1 only	4
Mass Down, Mod Down	0.00024	9.20E+06	-5.35	-8.05	M1 + K1	4
Mass Down, Mod Up	0.00024	1.08E+07	-5.51	7.99	M1 + K1	4
Mod Down	0.000254	9.19E+06	0	-8.11	K1 only	4
Mod Up	0.000254	1.08E+07	0	7.9	K1 only	4
Mass Up	0.000268	1.00E+07	5.354	0	M1 only	4
Mass Up, Mod Down	0.000268	9.20E+06	5.551	-8.01	M1 + K1	4
Mass Up, Mod Up	0.000268	1.08E+07	5.63	7.95	M1 + K1	4

Table A-8 Test Case 8 Numerical Results

APPENDIX B. COMPOSITE BEAM SPECIFICATIONS

A. PHYSICAL DIMENSIONS AND PROPERTIES

The composite beam used for the Chapter III computer simulations was patterned after sample test pieces. The beams are made of a continuous carbon fiber/epoxy. The dimensions and the mass of the beam were measured. The original Young's modulus value was the value calculated in Reference (14). The beam orientation for the simulations was as depicted in Figure B-1. The degrees of freedom for the beam were vertical translation, upward in the figure, and rotation around a vector out of the plane of the page.

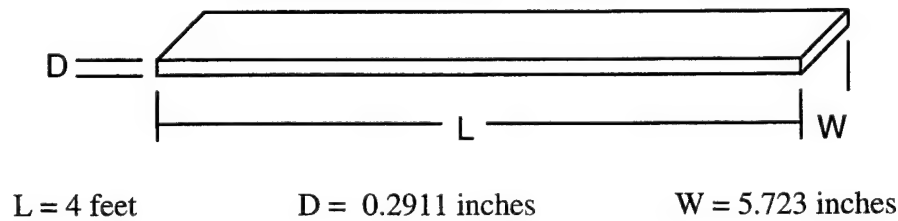


Figure B-1 Composite Beam

The original physical properties assumed for the beam were:

Young's modulus	$E = 6.33 \times 10^6$	PSI
mass density	$\rho = 0.0001328$	lbf-sec ² /in ⁴

Young's modulus was updated using the optimization procedure and comparison to the undamaged beam's dynamic response. The updated value was:

Young's modulus	$E = 6.76 \times 10^6$	PSI
-----------------	------------------------	-----

B. DYNAMIC RESPONSE

The system natural frequencies predicted by the finite element model are:

Mode 1	28.96 Hz
Mode 2	79.85 Hz
Mode 3	156.6 Hz
Mode 4	258.9 Hz
Mode 5	386.9 Hz
Mode 6	540.5 Hz
Mode 7	719.8 Hz
Mode 8	924.8 Hz
Mode 9	1155.6 Hz

The mode shapes predicted by the finite element are included in Figures B-2 through B-10.

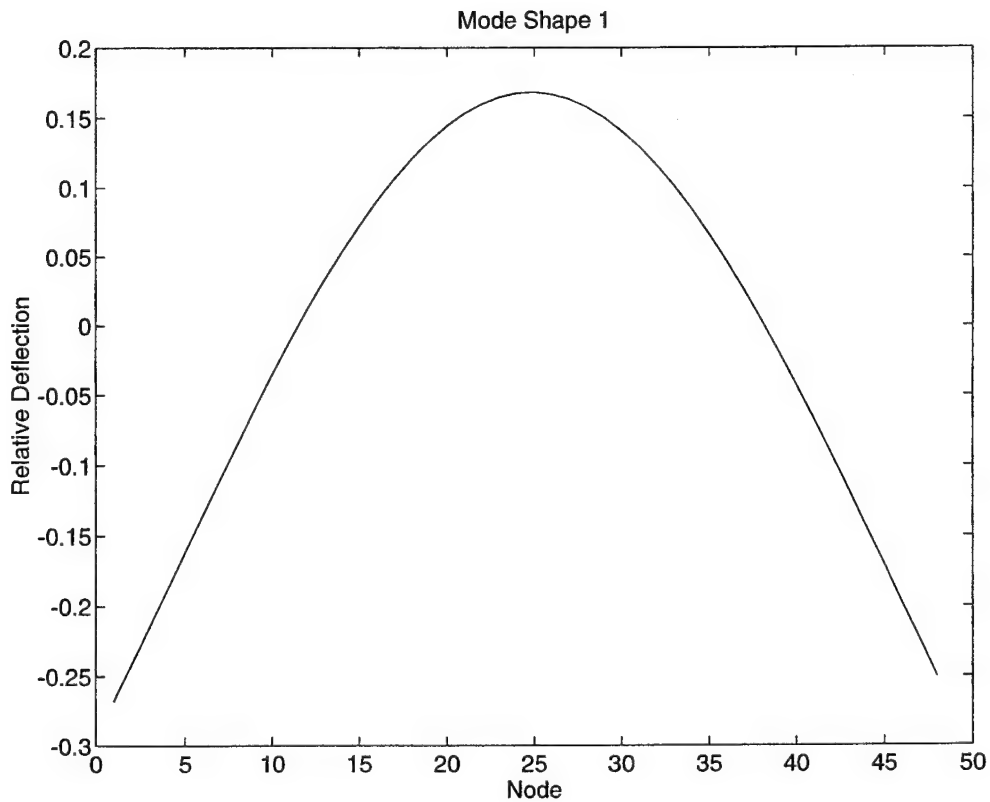


Figure B-2 Composite Beam Analytical Mode Shape 1

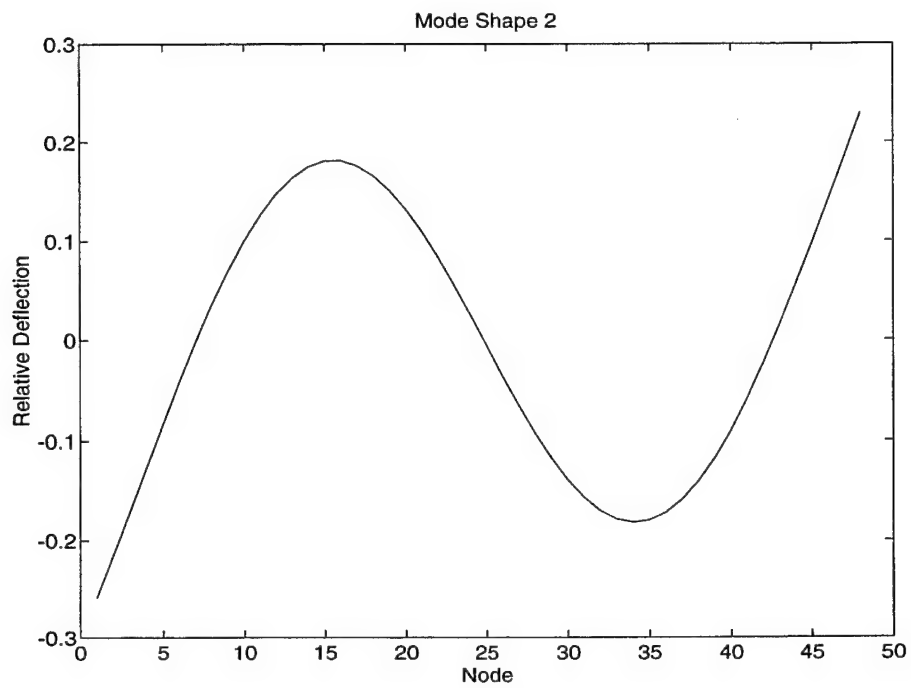


Figure B-3 Composite Beam Analytical Mode Shape 2

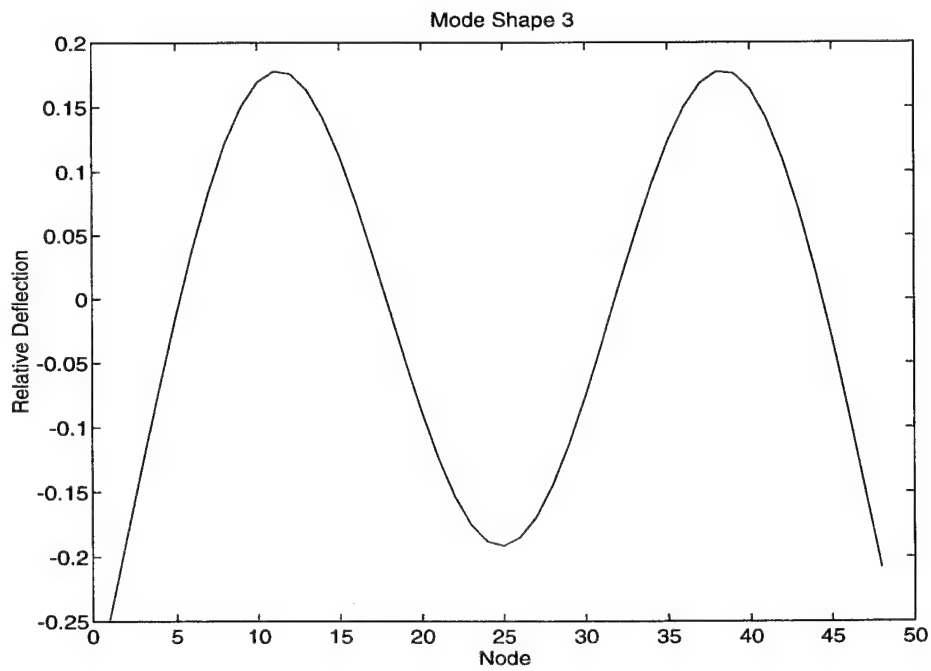


Figure B-4 Composite Beam Analytical Mode Shape 3

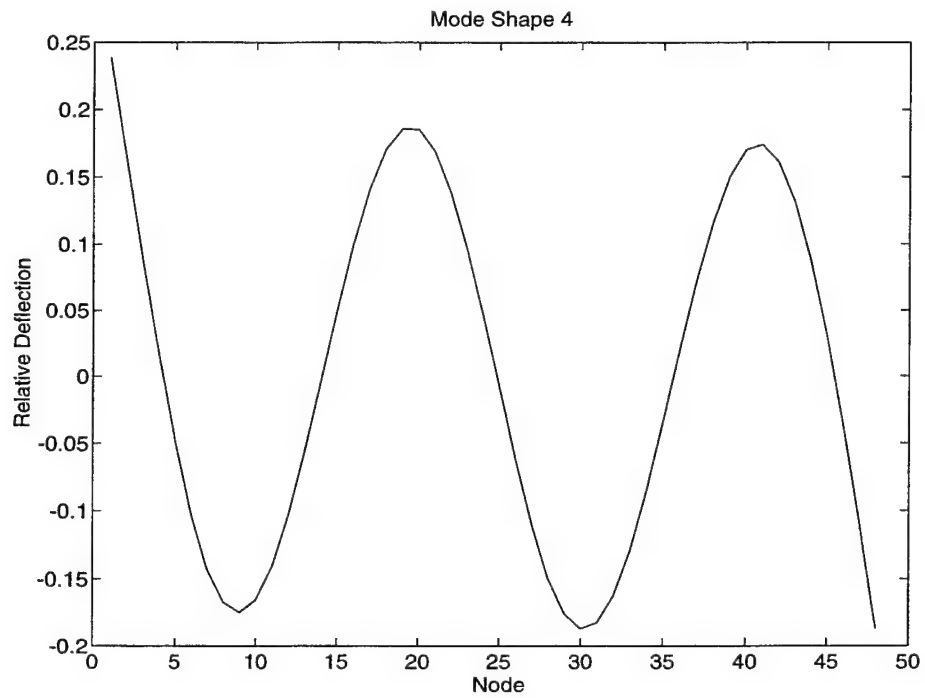


Figure B-5 Composite Beam Analytical Mode Shape 4

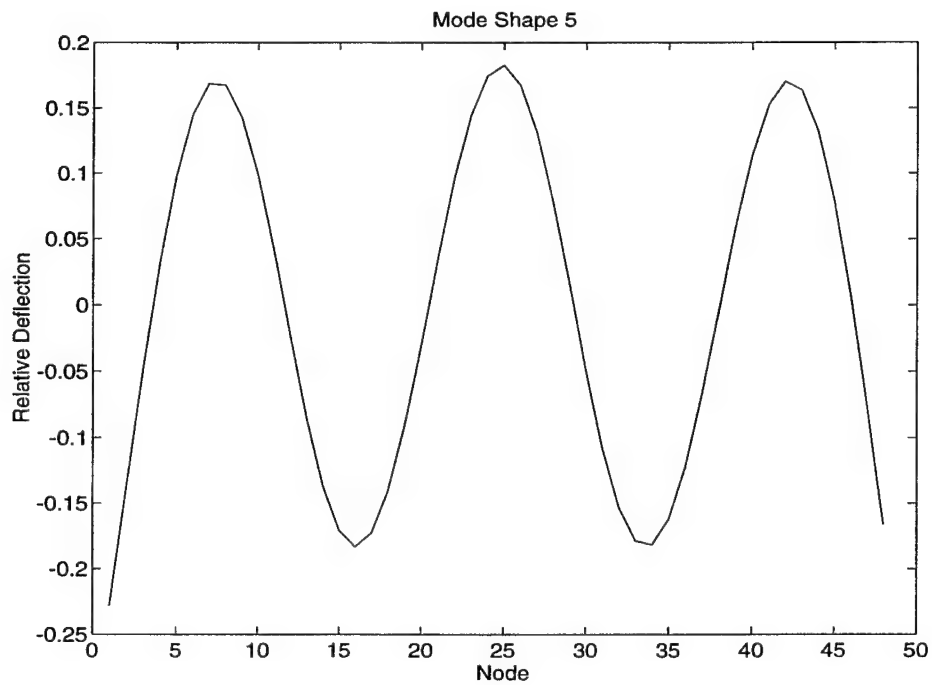


Figure B-6 Composite Beam Analytical Mode Shape 5

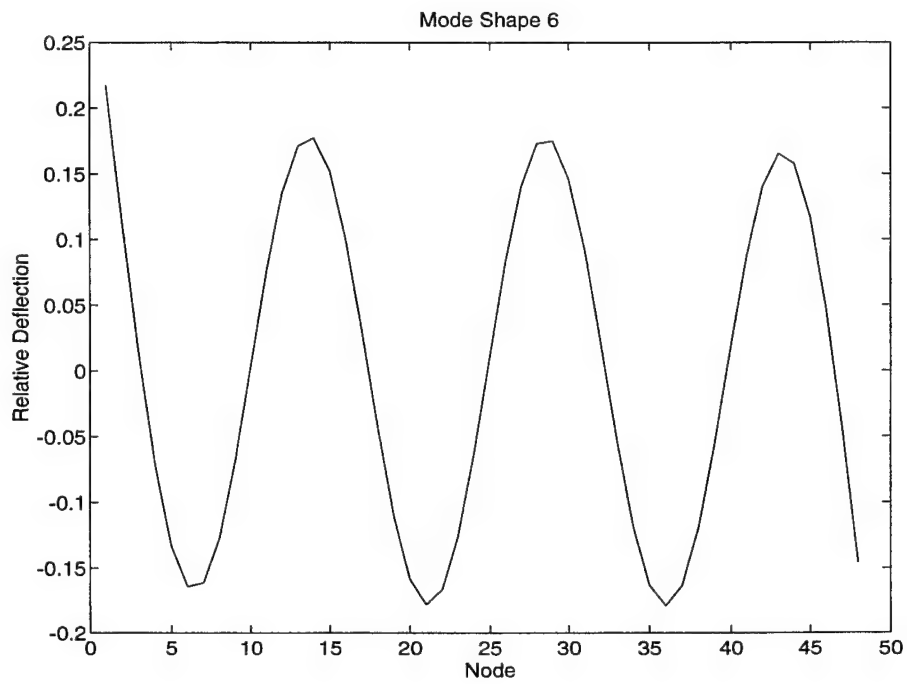


Figure B-7 Composite Beam Analytical Mode Shape 6

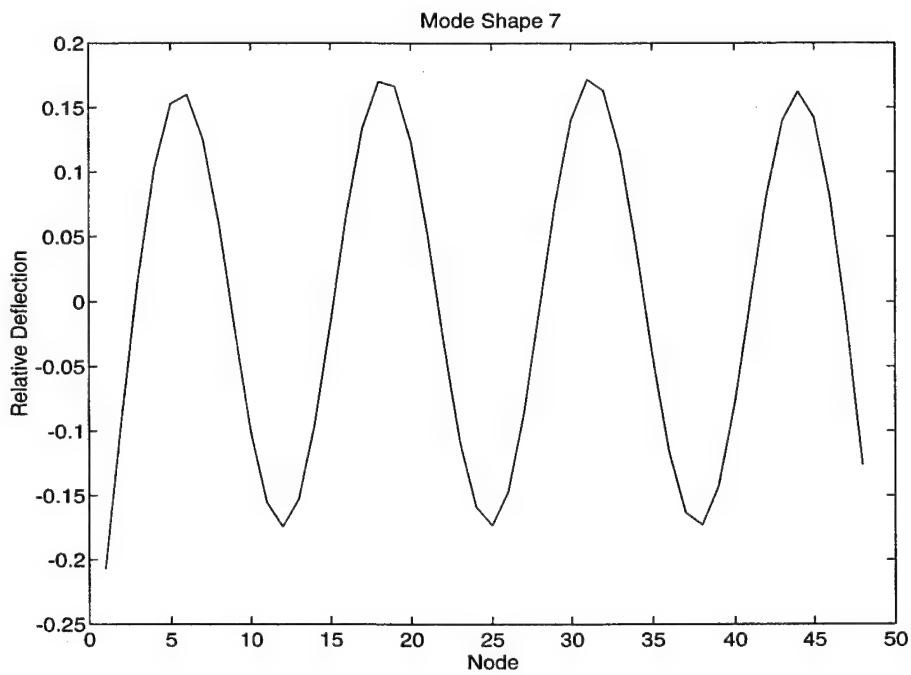


Figure B-8 Composite Beam Analytical Mode Shape 7

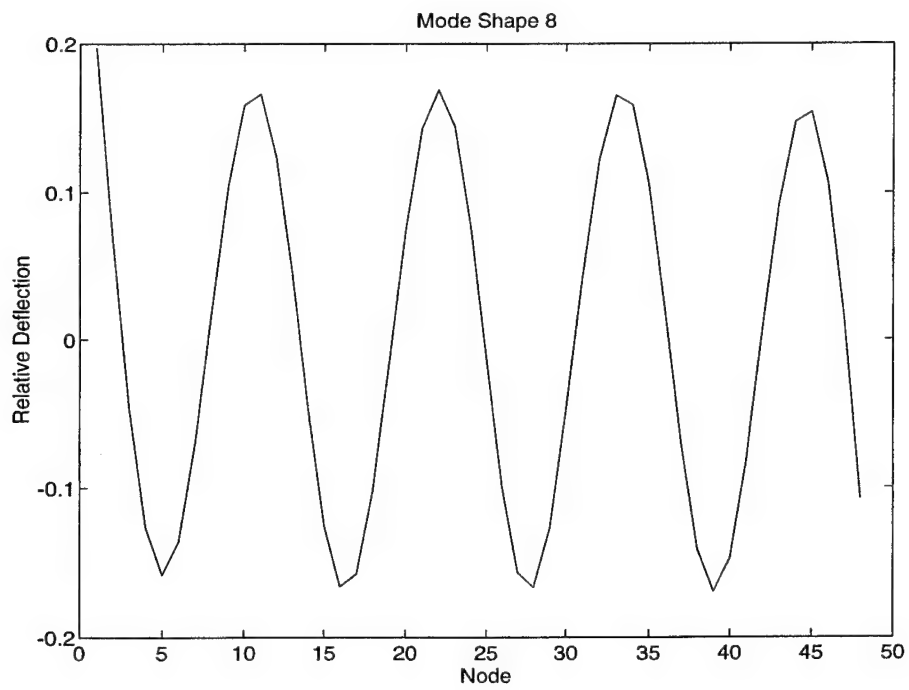


Figure B-9 Composite Beam Analytical Mode Shape 8

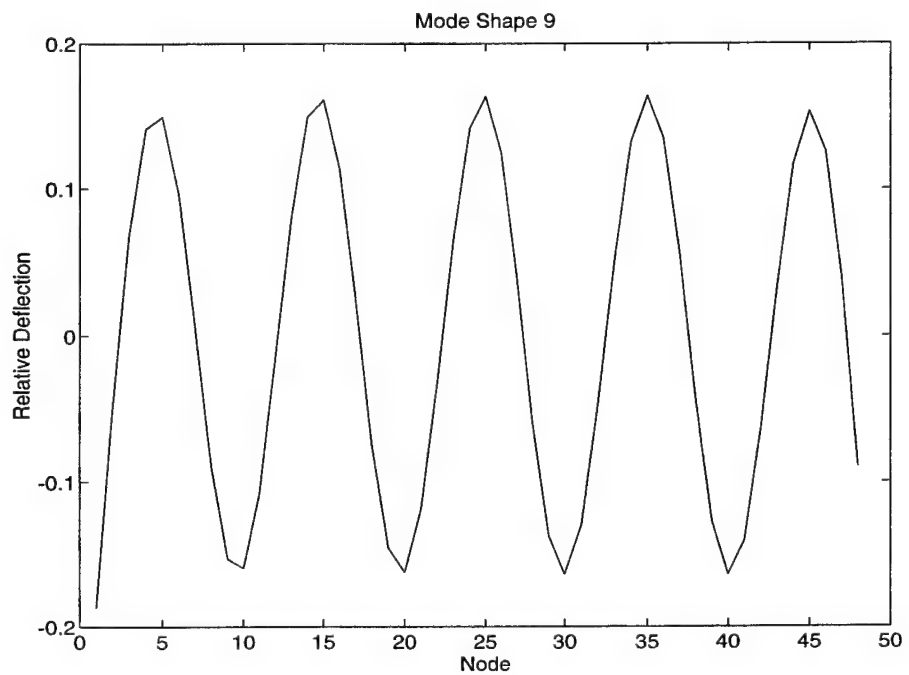


Figure B-10 Composite Beam Analytical Mode Shape 9

APPENDIX C. EXPERIMENTAL SETUP

The experimental setup involved the selection of test equipment and of test settings. The following equipment and software was used for measurement of the test pieces dynamic responses and signal processing or analysis:

- PCB load cell
- PCB accelerometers
- PCB Model 483A Amplifier
- Zonic Workstation 7000 Signal Analyzer
- HP Series 700 computer
- IDEAS Master Series 2.1 Software

Figure C-1 depicts the experimental setup. Calibration data for the measurement equipment is included on the following pages.

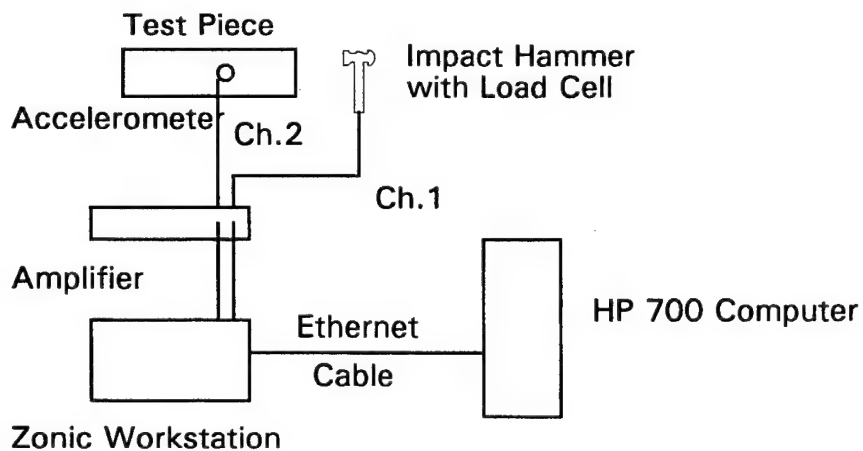


Figure C-1 Experimental Setup

PCB CALIBRATION CERTIFICATE



IMPULSE FORCE HAMMER

Model No. 086B03

Customer: NAVAL POSTGRADUATE

Serial No. 2194

SCHOOL

Range 0-500 lb

Linearity error < 1.0 %

Invoice No.:

Discharge Time Constant 2000 s

35777

Output Impedance 100 ohms

Output Bias 9.10 volts

Traceable to NBS through 737/236905 Calibration Specification MIL-STD 45662

Initials P-J Date: 5-22-86

Accelerometer: Model No. 302A07 Serial No. 7607 Sens. 9.91 mV/g

Pendulous Test Mass 1.05 lb (476 gram) including accelerometer

Hammer Sensitivity:

CONFIGURATION	Tip Extender	PLASTIC/VINYL NONE	PLASTIC/VINYL STEEL	
SCALING FACTOR (SENSITIVITY RATIO)	lb/g	1.03 (SEE NOTE)	0.98	
Accel/Force	(N/ms ⁻²)	0.47	0.44	
HAMMER SENSITIVITY	mV/lb	9.59	10.1	
	(mV/N)	2.15	2.26	

NOTES:

- The sensitivity ratio (Sa/Sf) is the scaling factor for converting structural transfer measurements into engineering units. Divide results by this ratio.
- Each specific hammer configuration has a different sensitivity. The difference is a constant percentage, which depends on the mass of the cap and tip assembly relative to the total mass of the head. Calibrating the specific hammer structure being used automatically compensates for mass effects.

Effective mass 0.265 with 302A07 attached and vinyl capped plastic tip.

PCB PIEZOTRONICS, INC. 3425 WALDEN AVENUE DEPEW, NEW YORK 14043-2495 TELEPHONE 716-684-0001 TWX 710-263-1371

Calibration Certificate

Per ISA-RP37.2

Model No. 336C04

Serial No. 11797

PO No. _____ Customer _____

Calibration traceable to NIST thru Project No. 822/251101-93

ICP® ACCELEROMETER

with built-in electronics

Calibration procedure is in compliance with MIL-STD-45662A and traceable to NIST.

CALIBRATION DATA

Voltage Sensitivity **96.3** mV/g
 Transverse Sensitivity **< 5.0** %
 Resonant Frequency **> 7** kHz
 Time Constant (NOM.) **0.5** s
 Output Bias Level **9.1** V

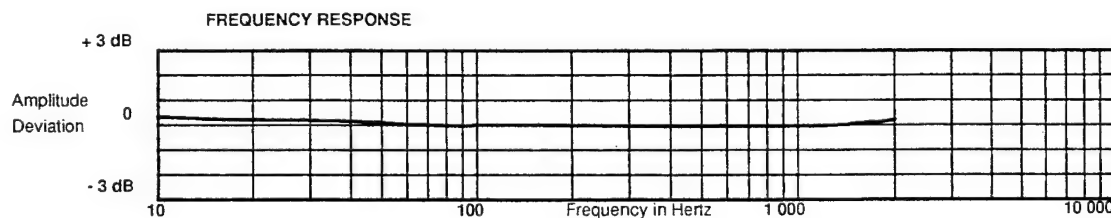
KEY SPECIFICATIONS

Range **50** ± g
 Resolution **0.001** g
 Temp. Range **0/+150** °F

METRIC CONVERSIONS:

ms⁻² = 0.102 g
 °C = 5/9 x (°F - 32)

Reference Freq.											
Frequency Hz	10	15	30	50	100	300	500	1000	2000		
Amplitude Deviation %	3.4	2.4	1.8	.8	0.0	-0.9	-0.9	-0.6	2.5		



Piezotronics, Inc. 3425 Walden Avenue Depew, NY 14043-2495 USA
 716-684-0001

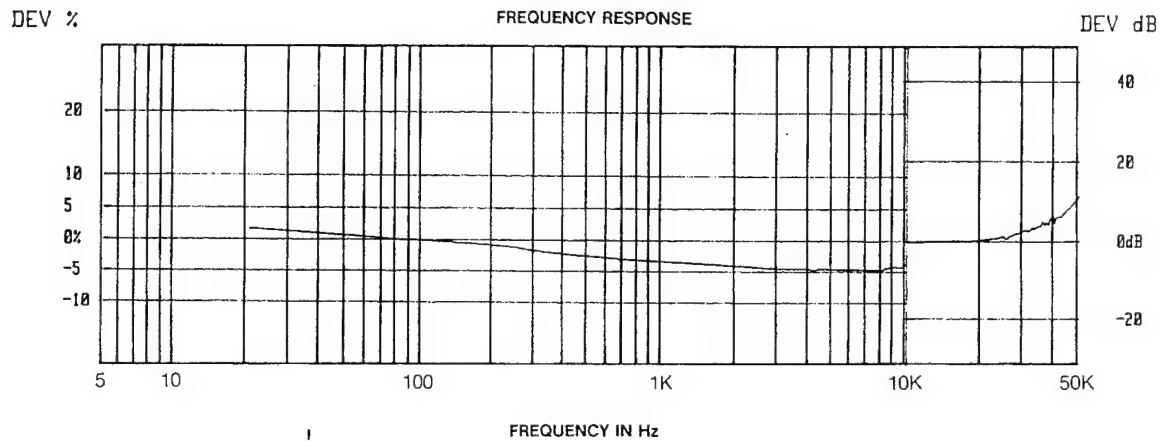
Date 2/17/94

Calibrated by J. Pashnow


CODE: CC-ENG

Calibration Data

ACCELEROMETER MODEL 2250A-10 SERIAL NO. BN01
 Sensitivity 10.10 mV/g @ 100 Hz 10 g's pK
 MAXIMUM TRANSVERSE SENSITIVITY: 1.3 %



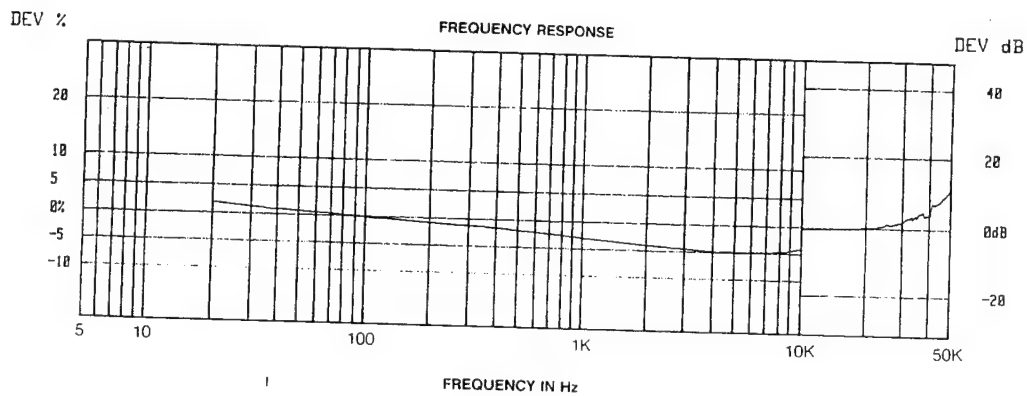
SJC

JUL 7 1986
 Date _____
 By (Signature) (Signature)
ENDEVCO 
 All calibrations are traceable to the National Bureau of Standards and in accordance with MIL-STD-45662. This certifies that this accelerometer meets all the performance, environmental and physical characteristics listed in Endevco* specifications.

16149

Calibration Data

ACCELEROMETER MODEL 2250A-10 SERIAL NO. BM96
 Sensitivity 10.12 mV/g @ 100 Hz 10 g's pK
 MAXIMUM TRANSVERSE SENSITIVITY: 1.0 %



SJC

Date DEC 20 1964
 By [Signature]

ENDEVCO

All calibrations are traceable to the National Bureau of Standards and in accordance with MIL-STD-45662. This certifies that this accelerometer meets all the performance, environmental and physical characteristics listed in Endevco's specifications.

APPENDIX D. AIRPLANE MODEL SPECIFICATIONS

A. PHYSICAL DIMENSIONS AND PROPERTIES

The airplane model used for testing consisted of three separate pieces joined together with fasteners. The three pieces are the wing, the tail, and the fuselage. The fuselage and the wing were single continuous pieces. The tail had two risers welded to the horizontal stabilizer. There were also two attachment fittings attached to the fuselage. The dimensions and mass of the airplane were measured. Piece dimensions and masses are included in Table D-1.

Name	Description	Dimensions (Inches)	Density (lbf*sec ² /in ⁴)
Wing	Rectangular Plate	21 x 6.02 x 0.25	0.000254
Body	Square cross section beam	1 x 1 x 24.25	0.000264
Tail	Horizontal rectangular plate	8.97 x 2.98 x 0.25	0.000397
Riser	Vertical rectangular plate	1.63 x 2.71 x 0.25	

Table D-1 Airplane Model Dimensions

The Young's modulus for all of the pieces was assumed to be 10×10^6 .

B. DYNAMIC RESPONSE

The configuration of the experimental excitation points is included as Figure D-1. The responses of the structure were measured at the starboard forward wing point and after port tail point. The experimentally obtained mode shapes are included as Figures D-2 through D-11.

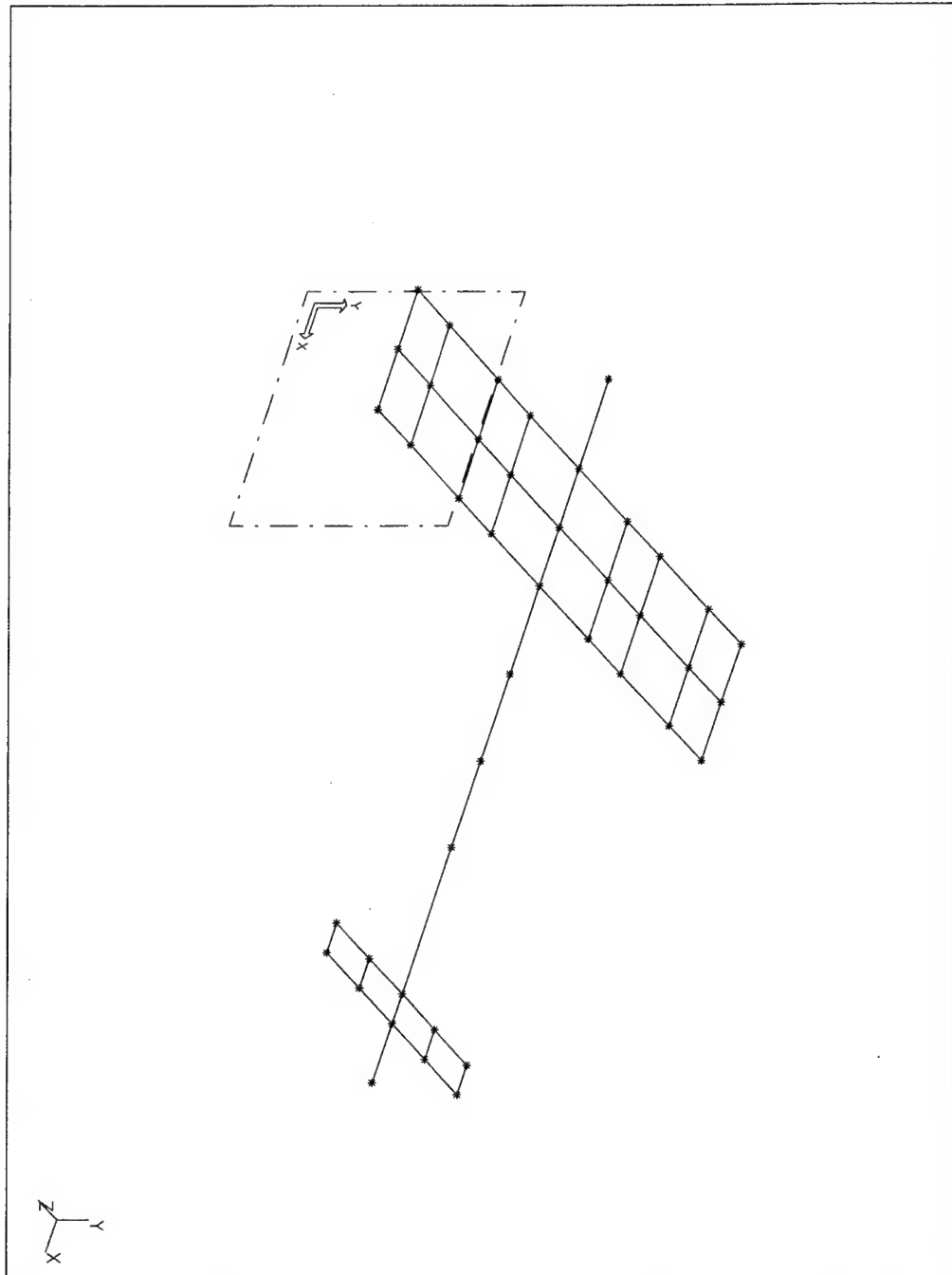


Figure D-1 Airplane Experimental Data Points

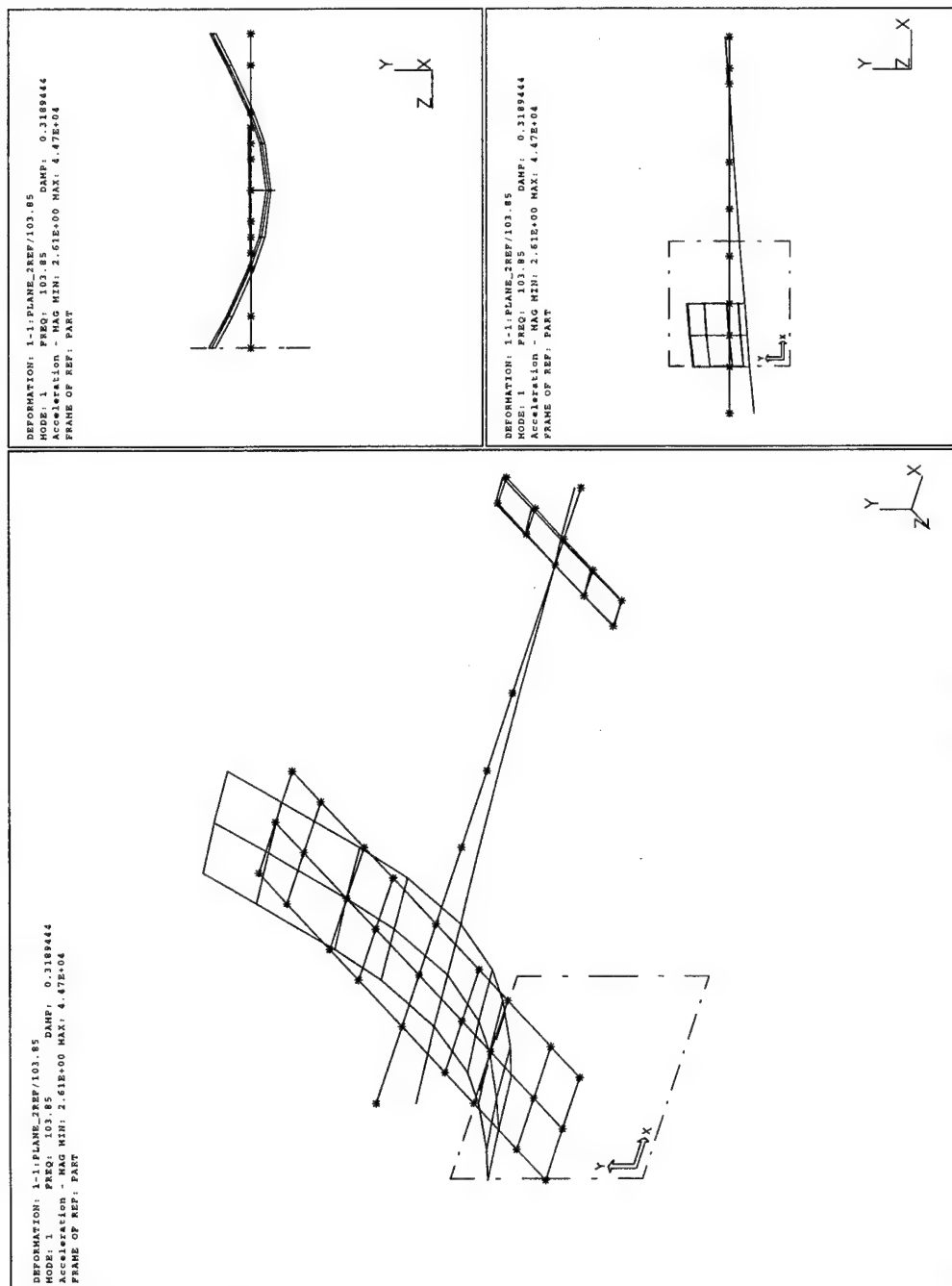


Figure D-2 Airplane Experimental Mode Shape 1

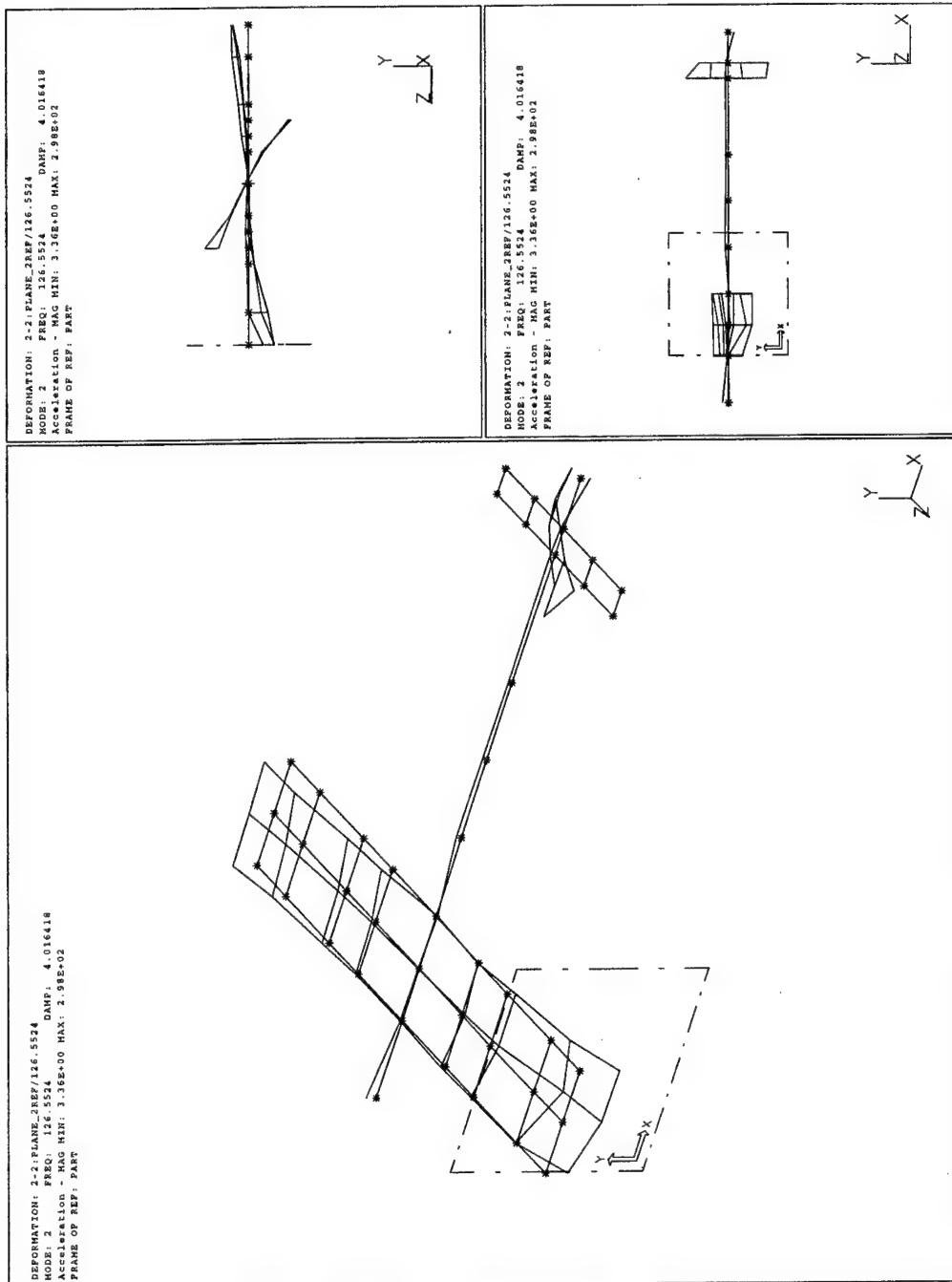


Figure D-3 Airplane Experimental Mode Shape 2

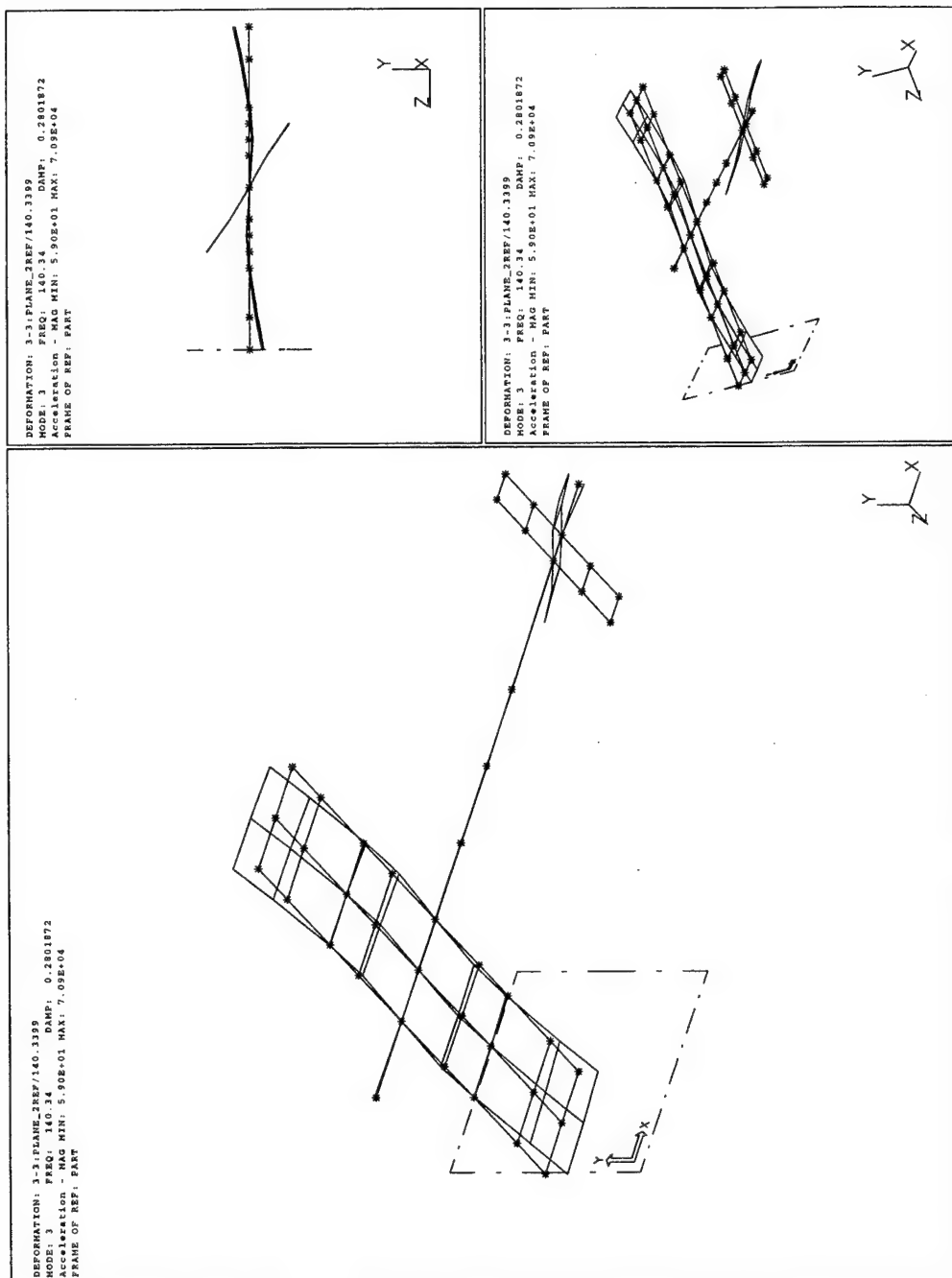
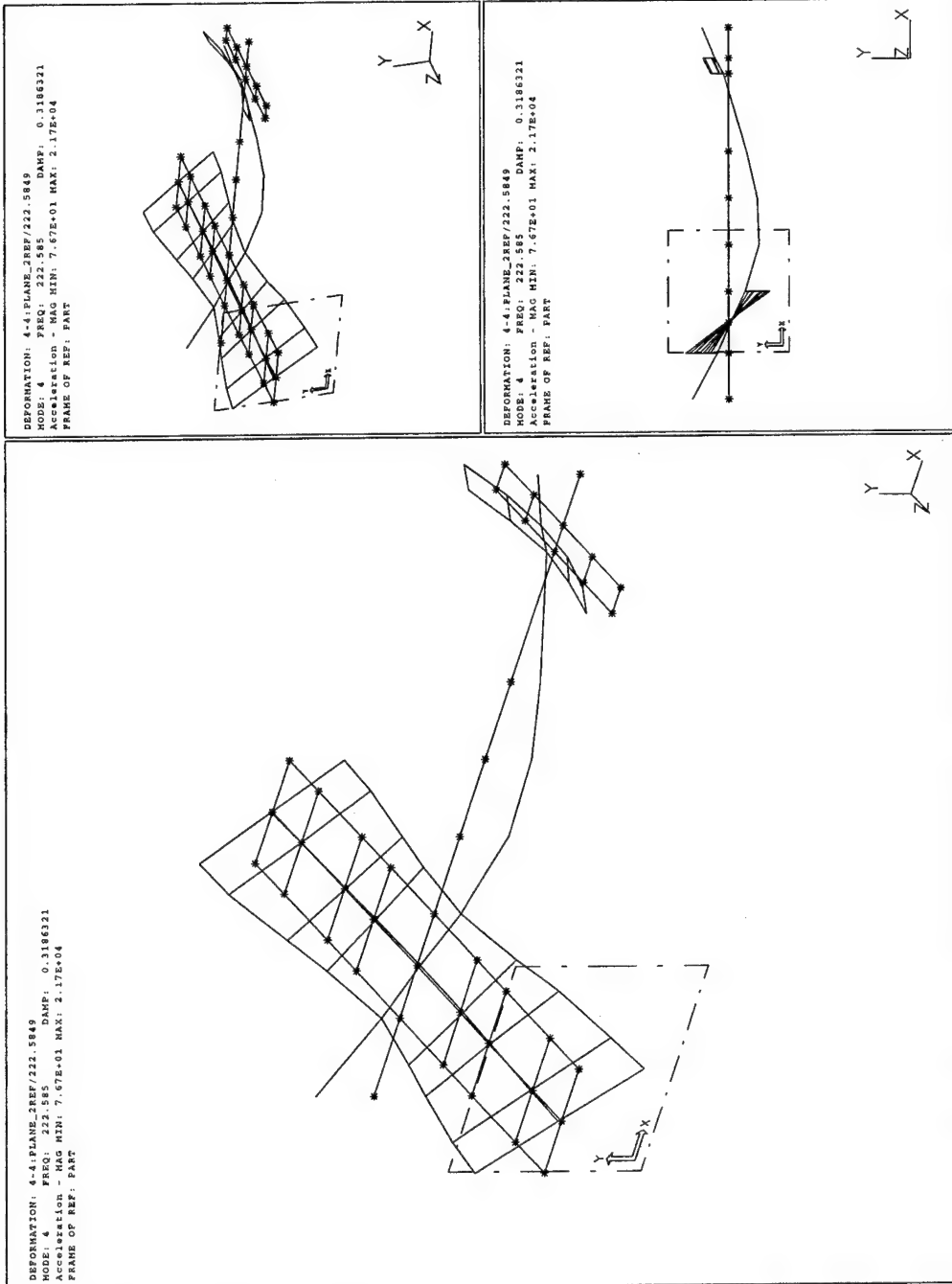


Figure D-4 Airplane Experimental Mode Shape 3

Figure D-5 Airplane Experimental Mode Shape 4



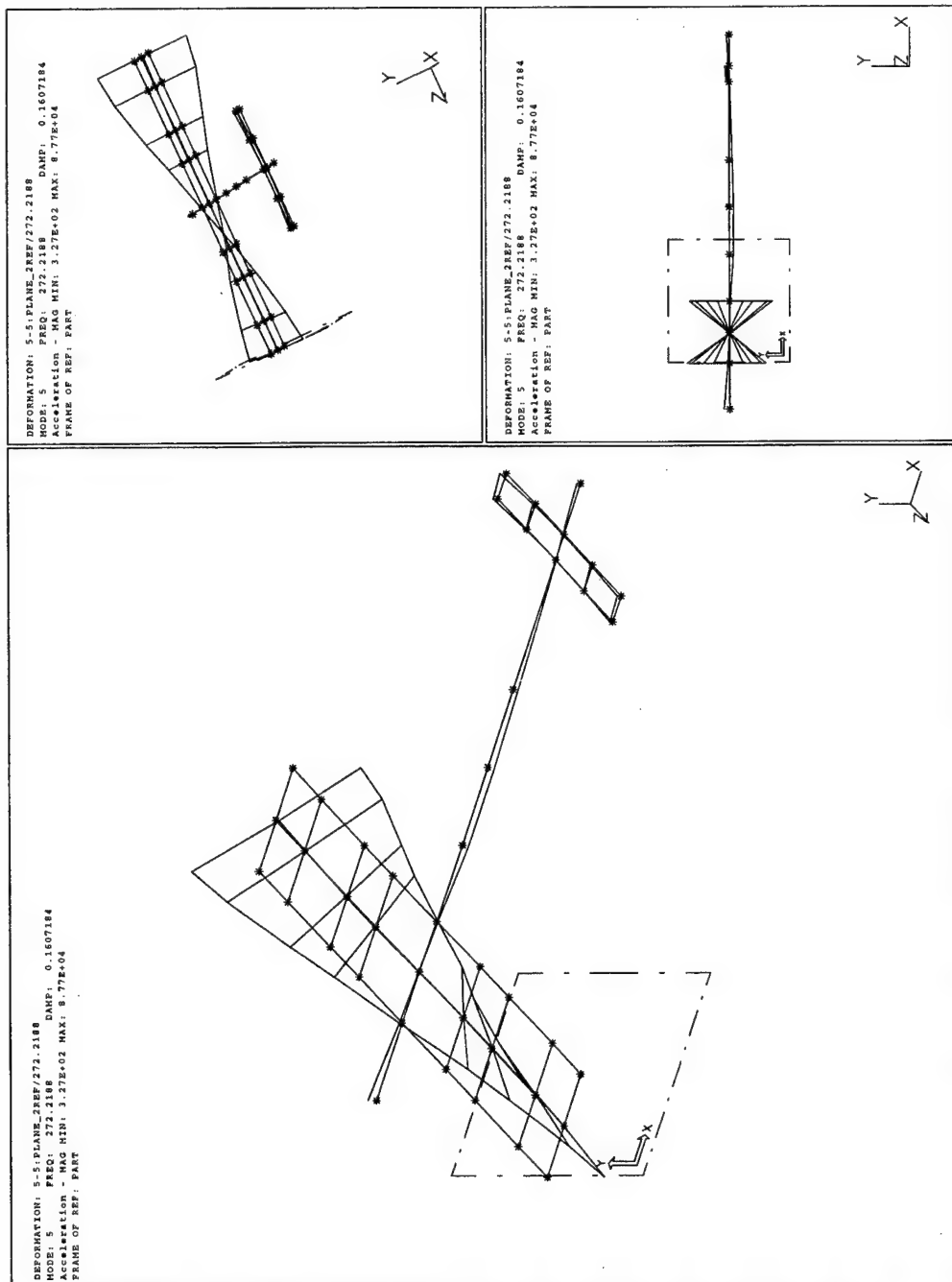
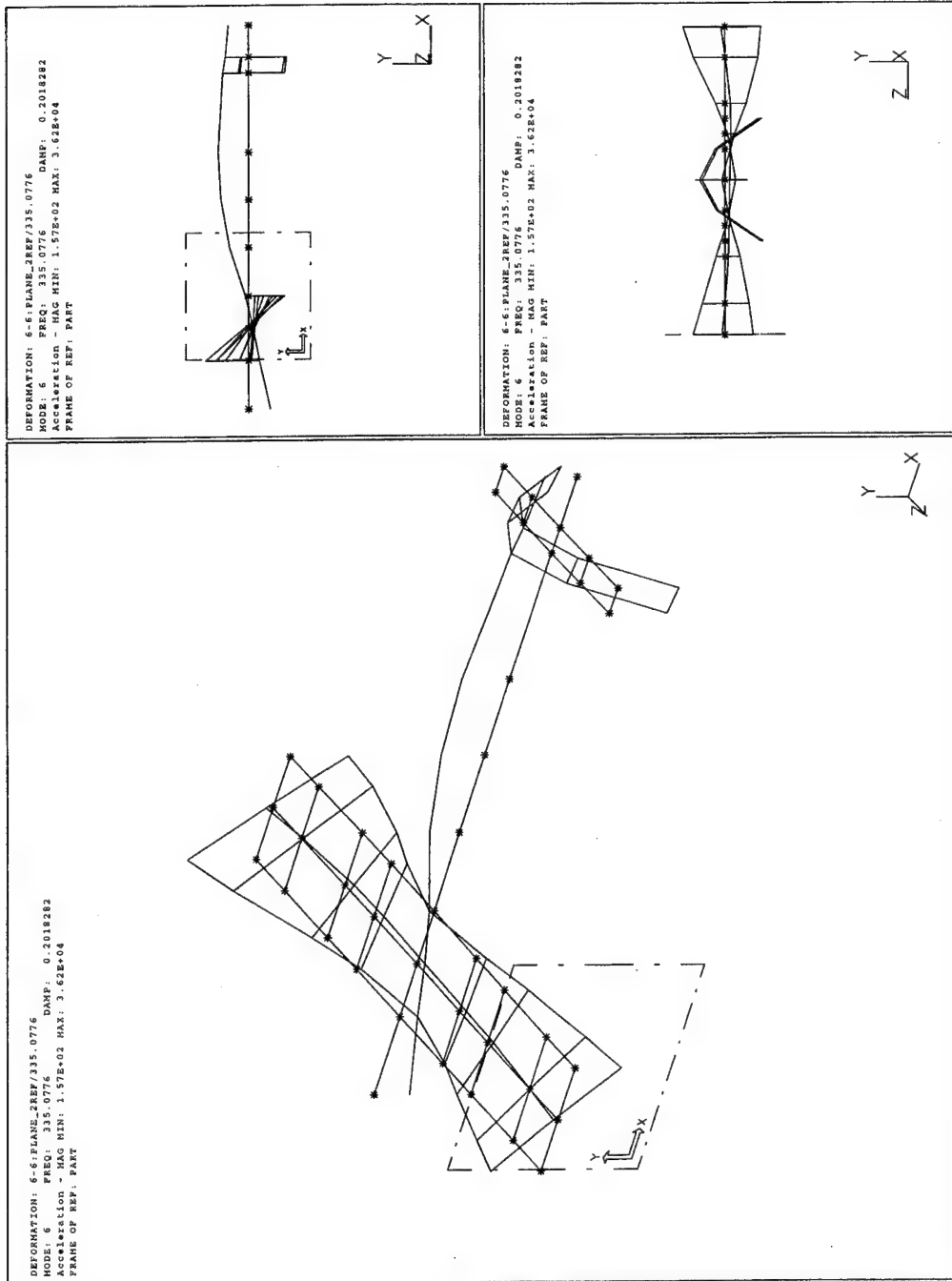


Figure D-6 Airplane Experimental Mode Shape 5

Figure D-7 Airplane Experimental Mode Shape 6



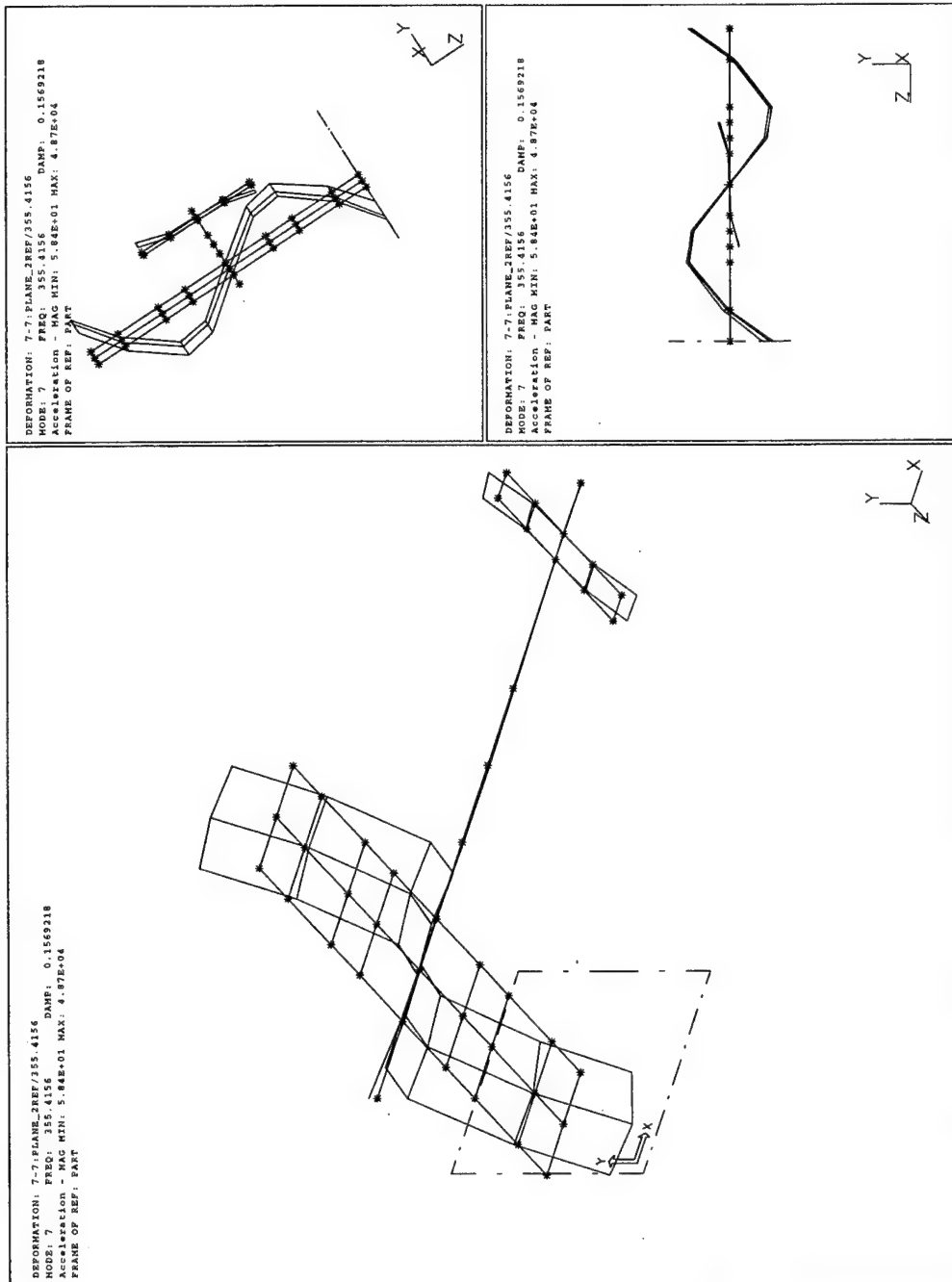
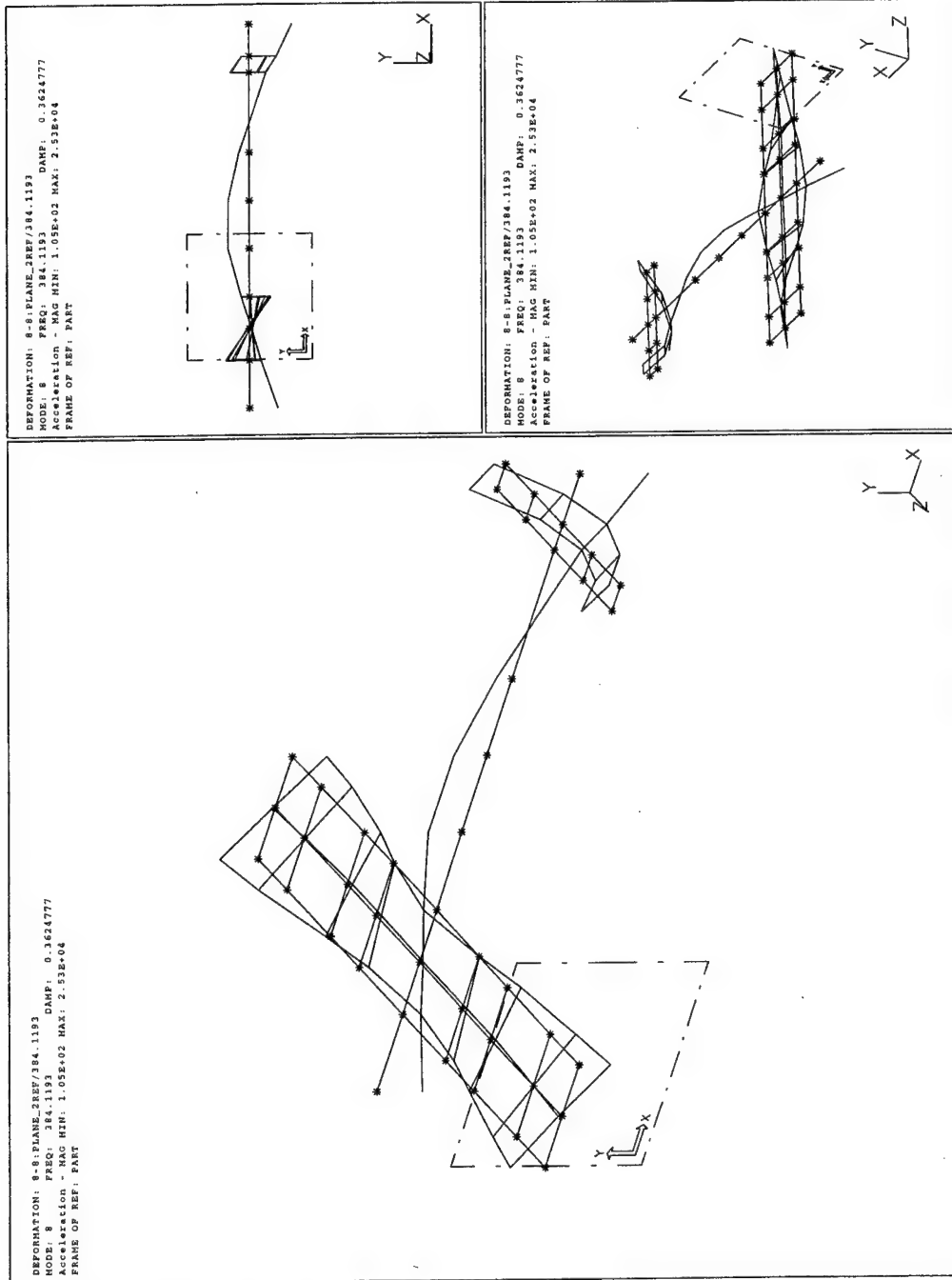


Figure D-8 Airplane Experimental Mode Shape 7

Figure D-9 Airplane Experimental Mode Shape 8



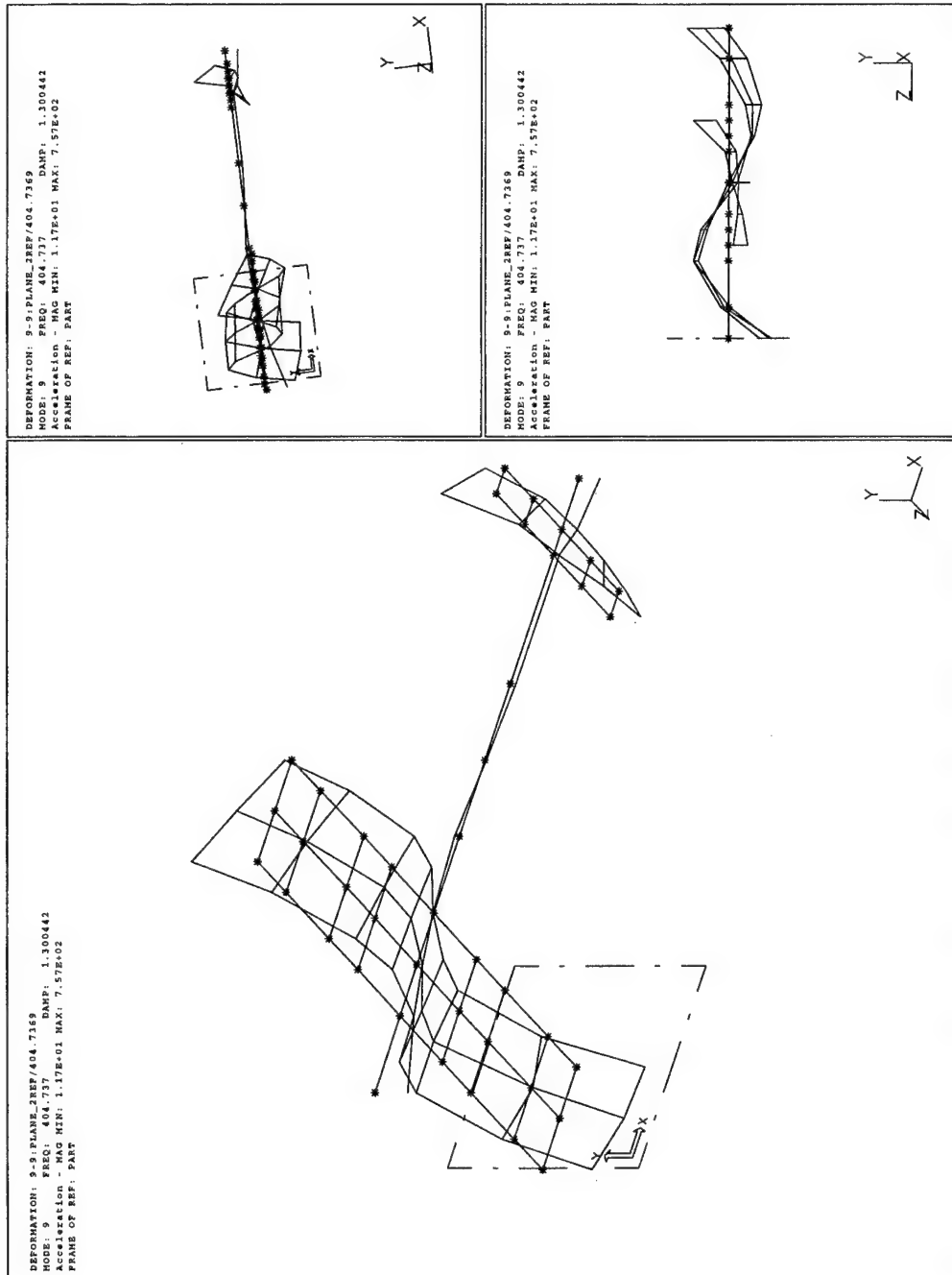
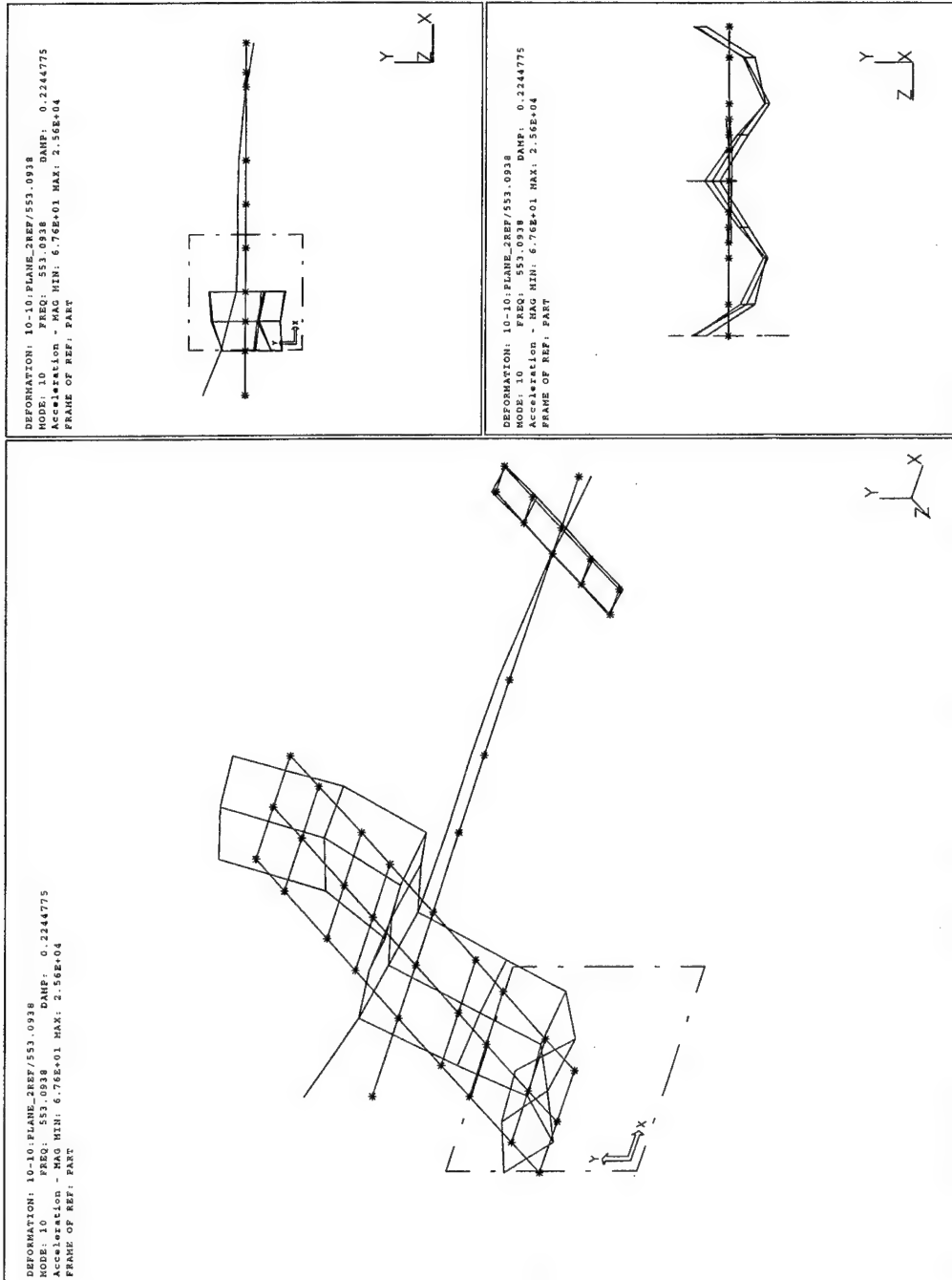


Figure D-10 Airplane Experimental Mode Shape 9



APPENDIX E. AIRPLANE FINITE ELEMENT MODEL

The finite element model built to study the airplane model was constructed with the IDEAS simulation software. The physical dimensions of the body, wing and tail were used to define the dimensions for the finite element model. The model consisted of 237 nodes, 200 elements, and two lumped masses. The wing and tail are represented by 174 thin shell elements. The tail risers were modeled to be the same width as the tail although that is not the case. The fuselage was represented by 26 beam elements. The beam elements were offset from the nodes to simplify the representation of the connection to the wing. The offsetting of the beam elements allowed the use of the same nodes for both wing elements and body elements. The two lumped masses represented the attachment bolts in the fuselage. Figure E-1 depicts the finite element model of the airplane. The first ten flexible modes of vibration were predicted by the model. The mode shapes predicted by the finite element model are included as Figures E-2 through E-11.

The model was used to solve for the predicated frequencies of all of the candidate solutions during model update. Each set of design variable changes were entered and new predictions run. The frequencies predicted, and the error from the experimental values are included in Table E-1.

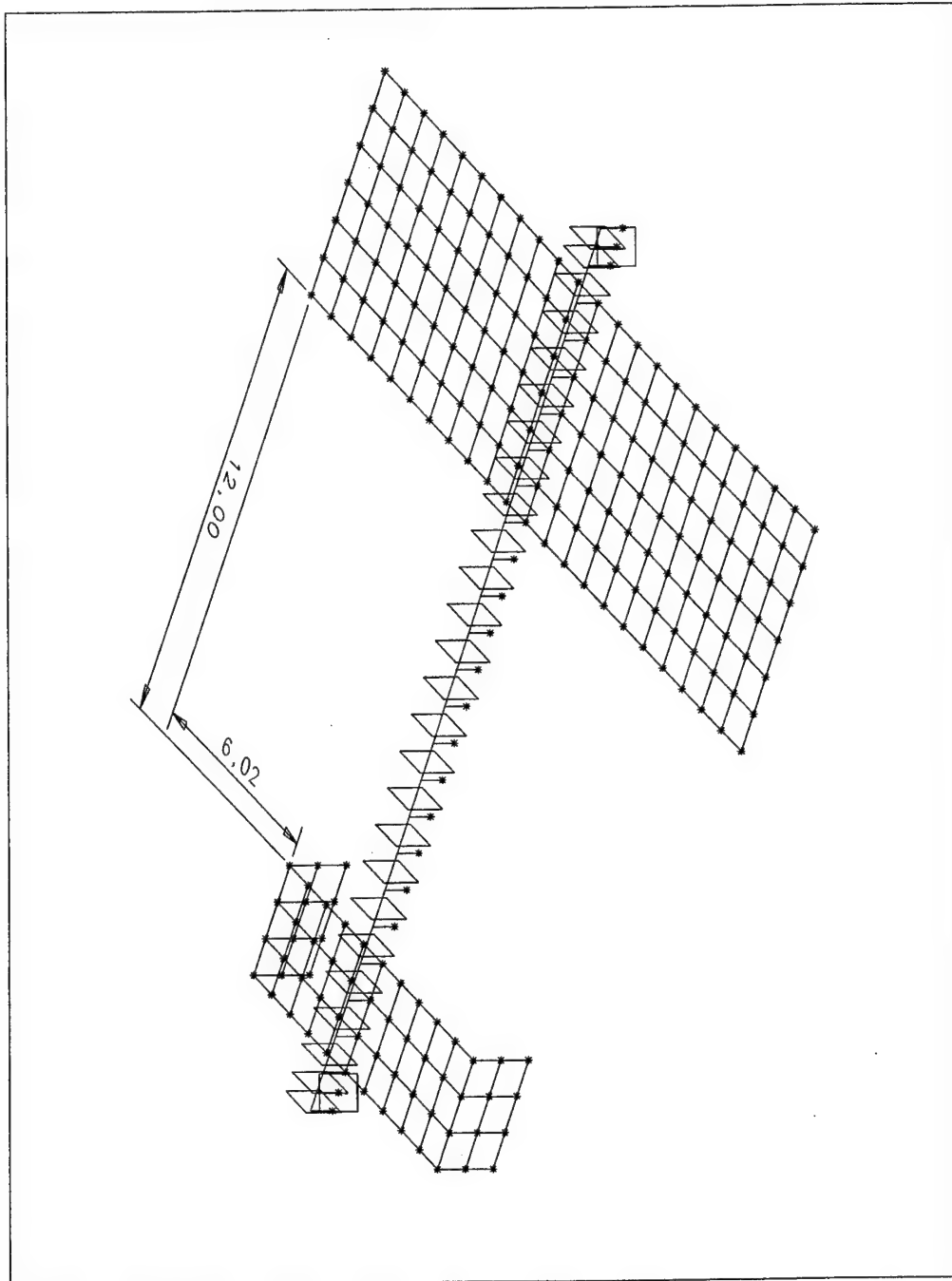


Figure E-1 Airplane Finite Element Model

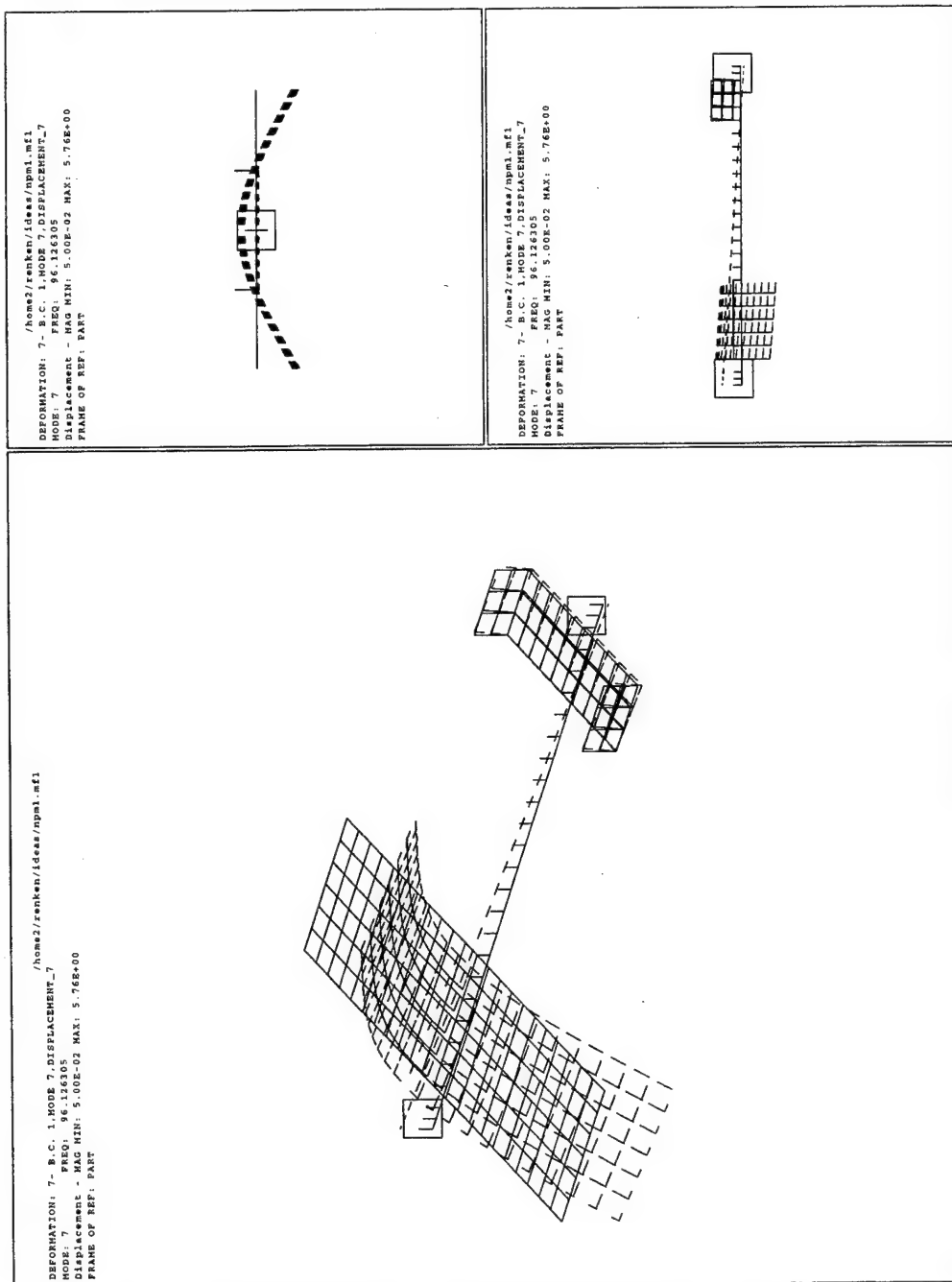
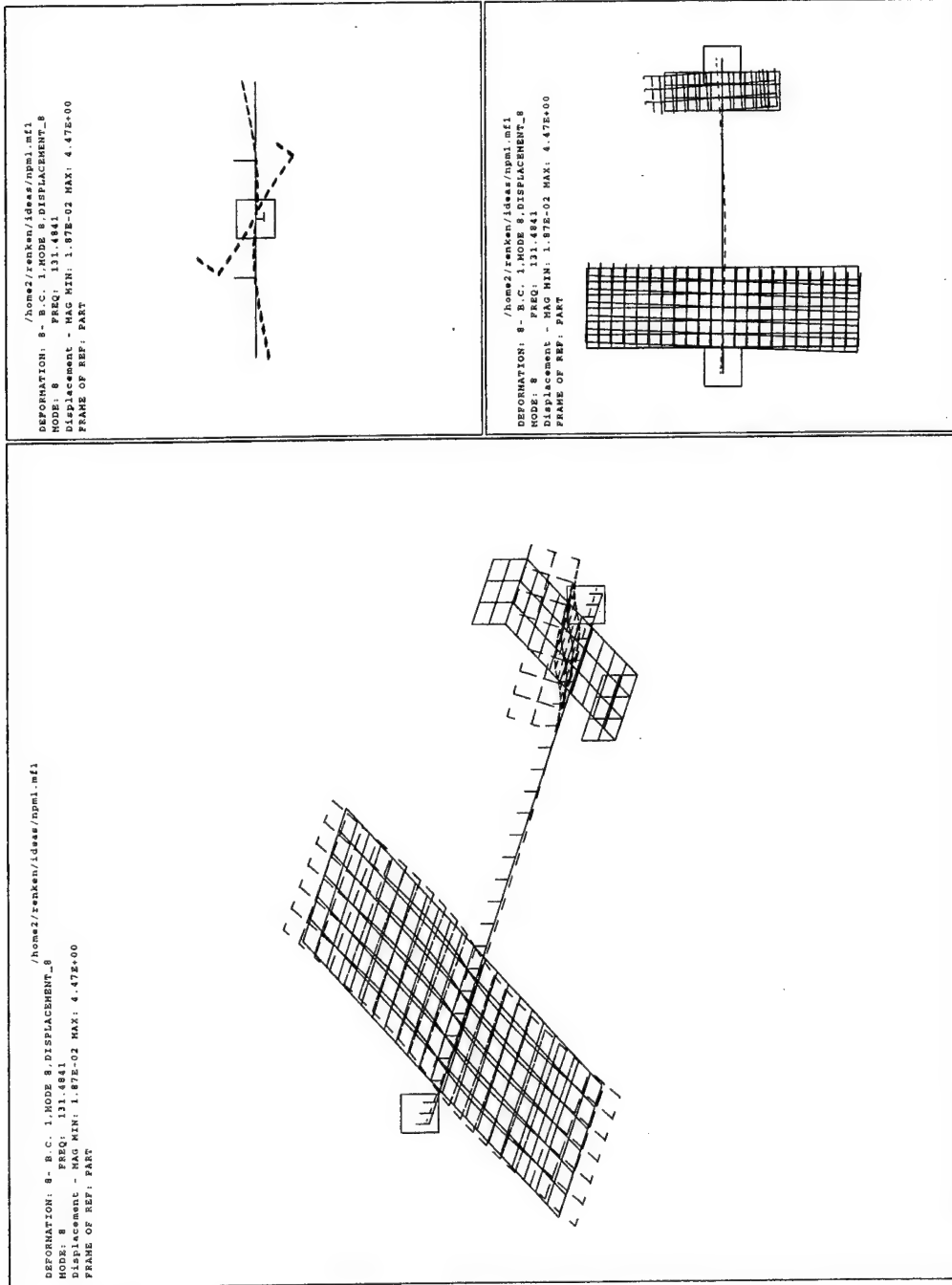


Figure E-2 Airplane Analytical Mode Shape 1

Figure E-3 Airplane Analytical Mode Shape 2



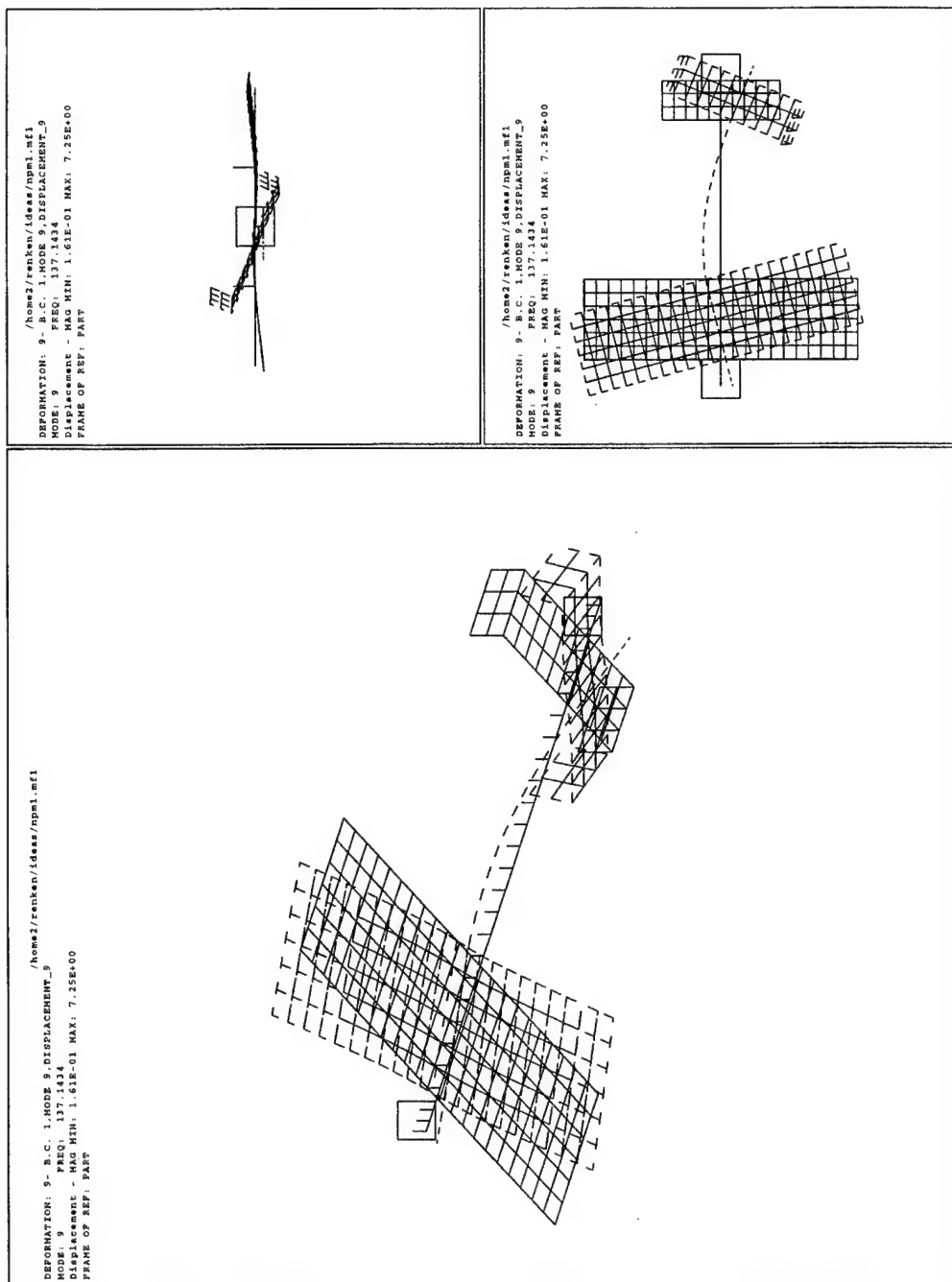
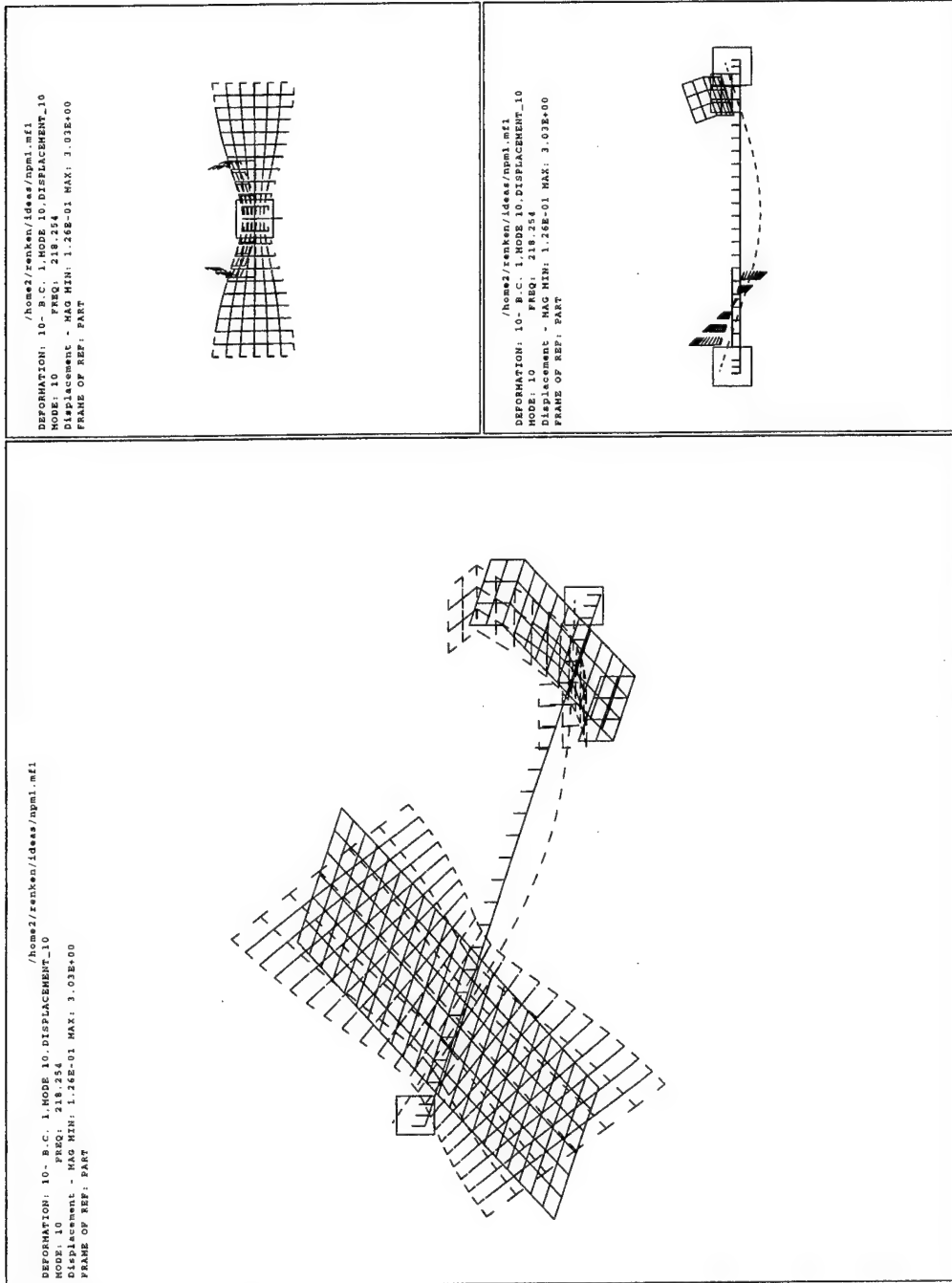


Figure E-4 Airplane Analytical Mode Shape 3

Figure E-5 Airplane Analytical Mode Shape 4



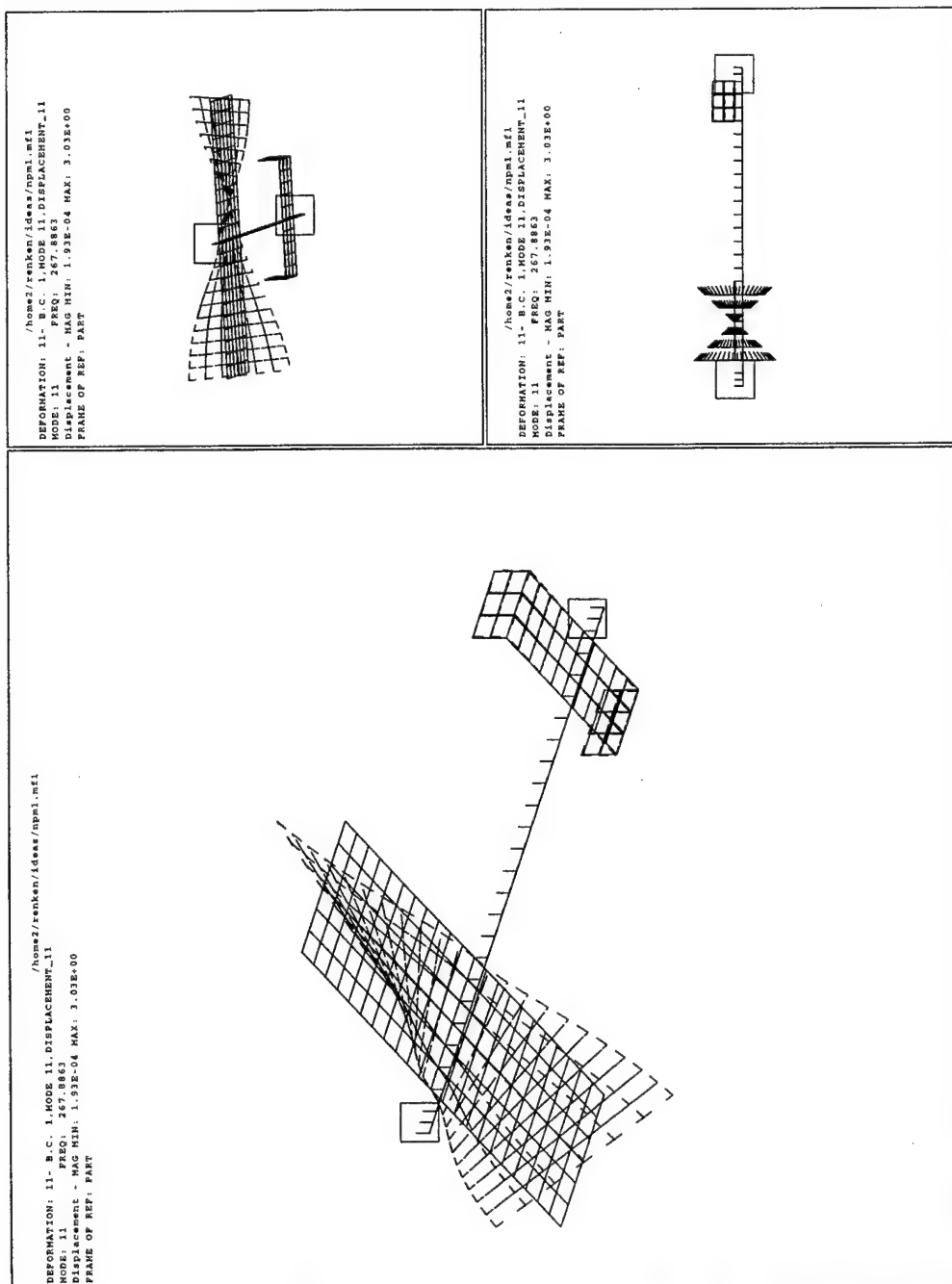
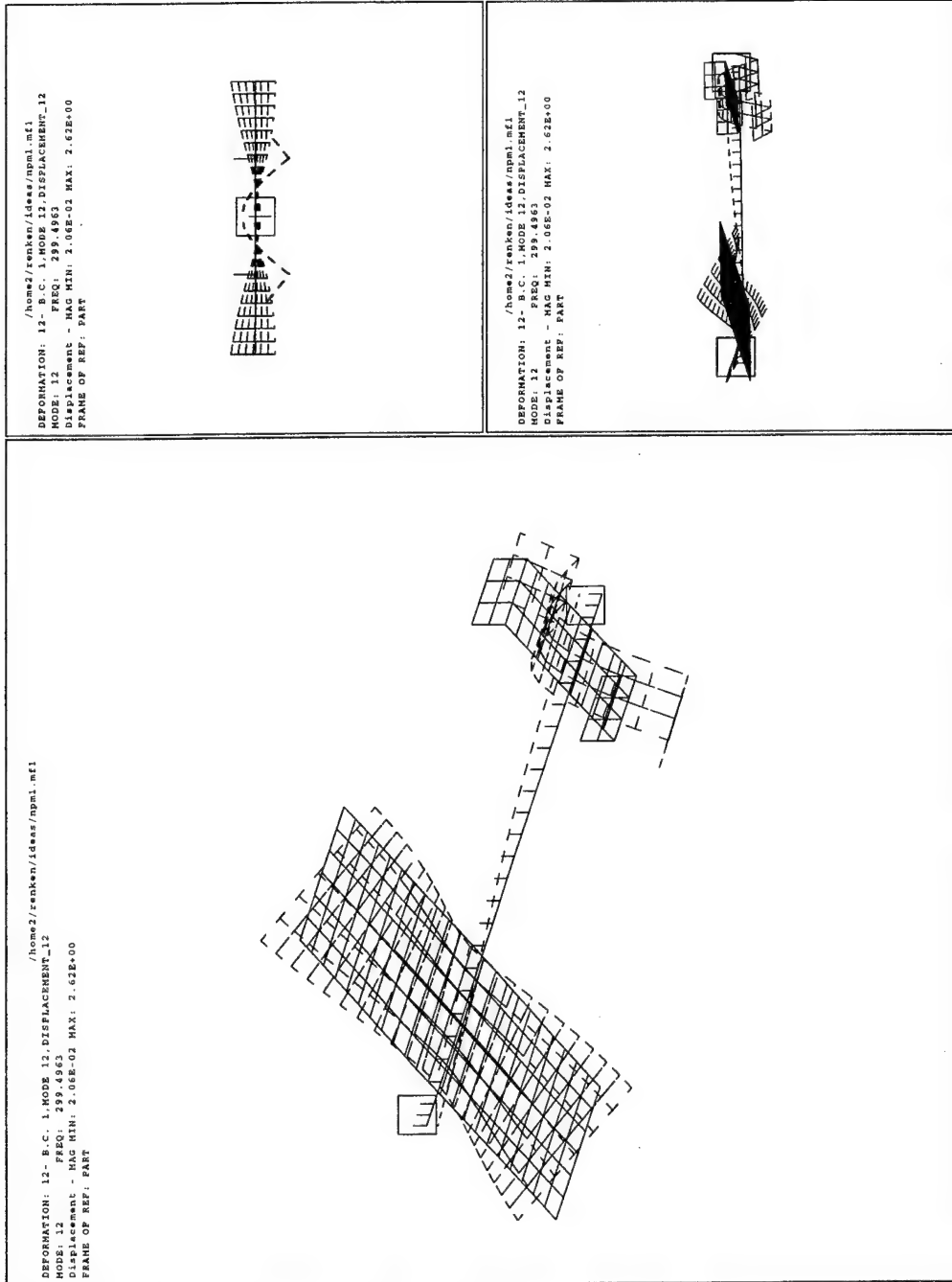


Figure E-6 Airplane Analytical Mode Shape 5

Figure E-7 Airplane Analytical Mode Shape 6



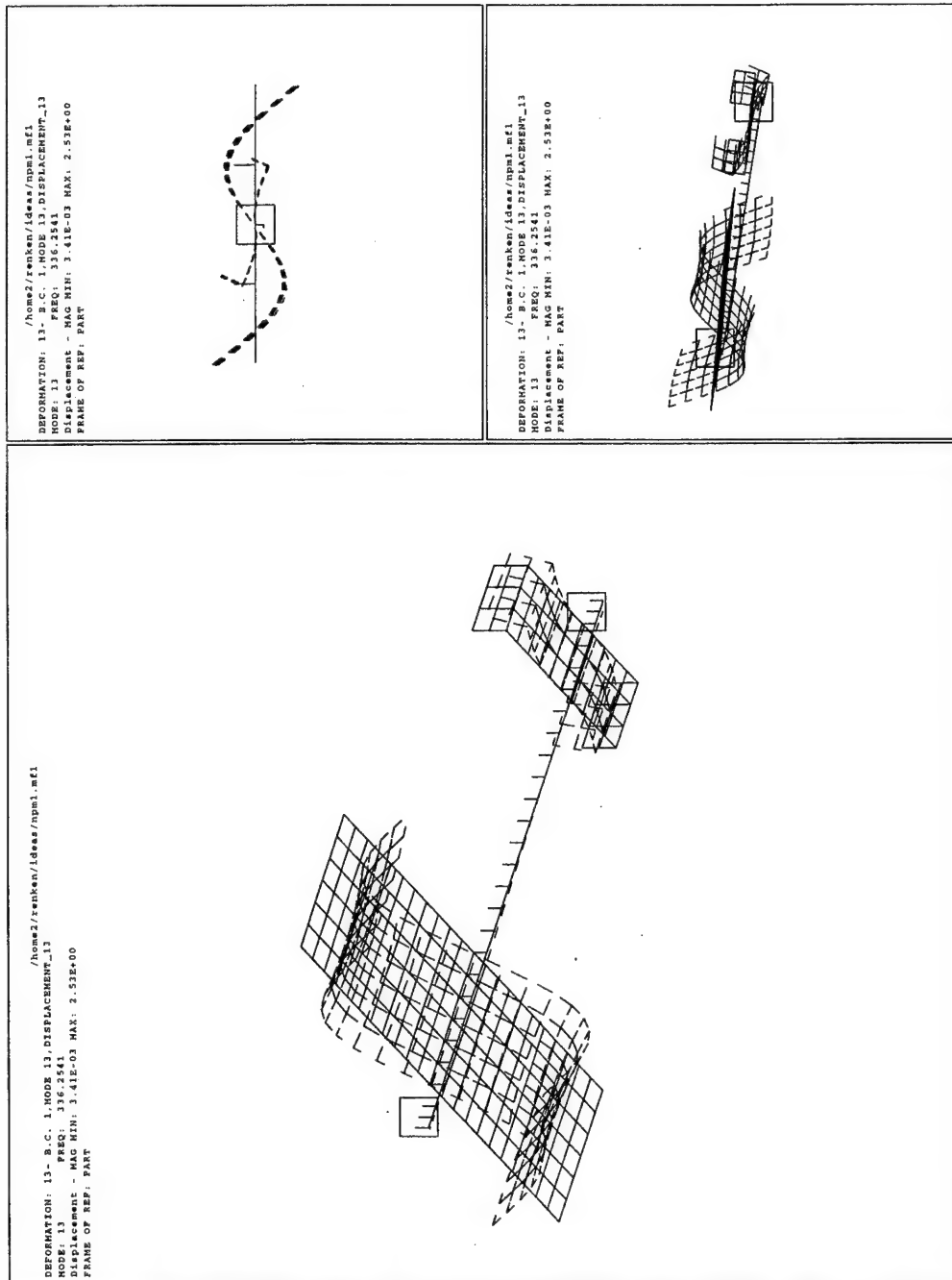
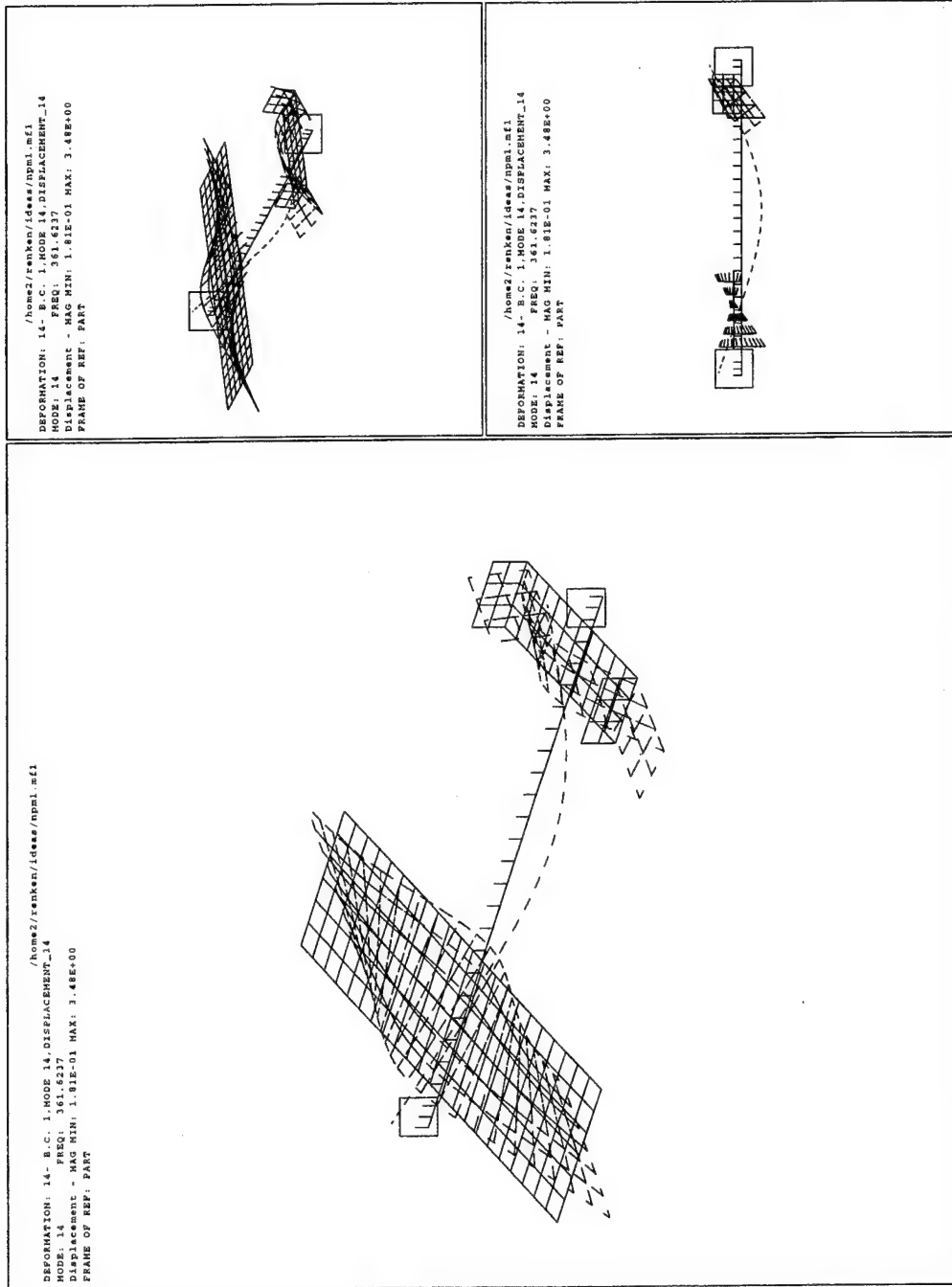


Figure E-8 Airplane Analytical Mode Shape 7

Figure E-9 Airplane Analytical Mode Shape 8



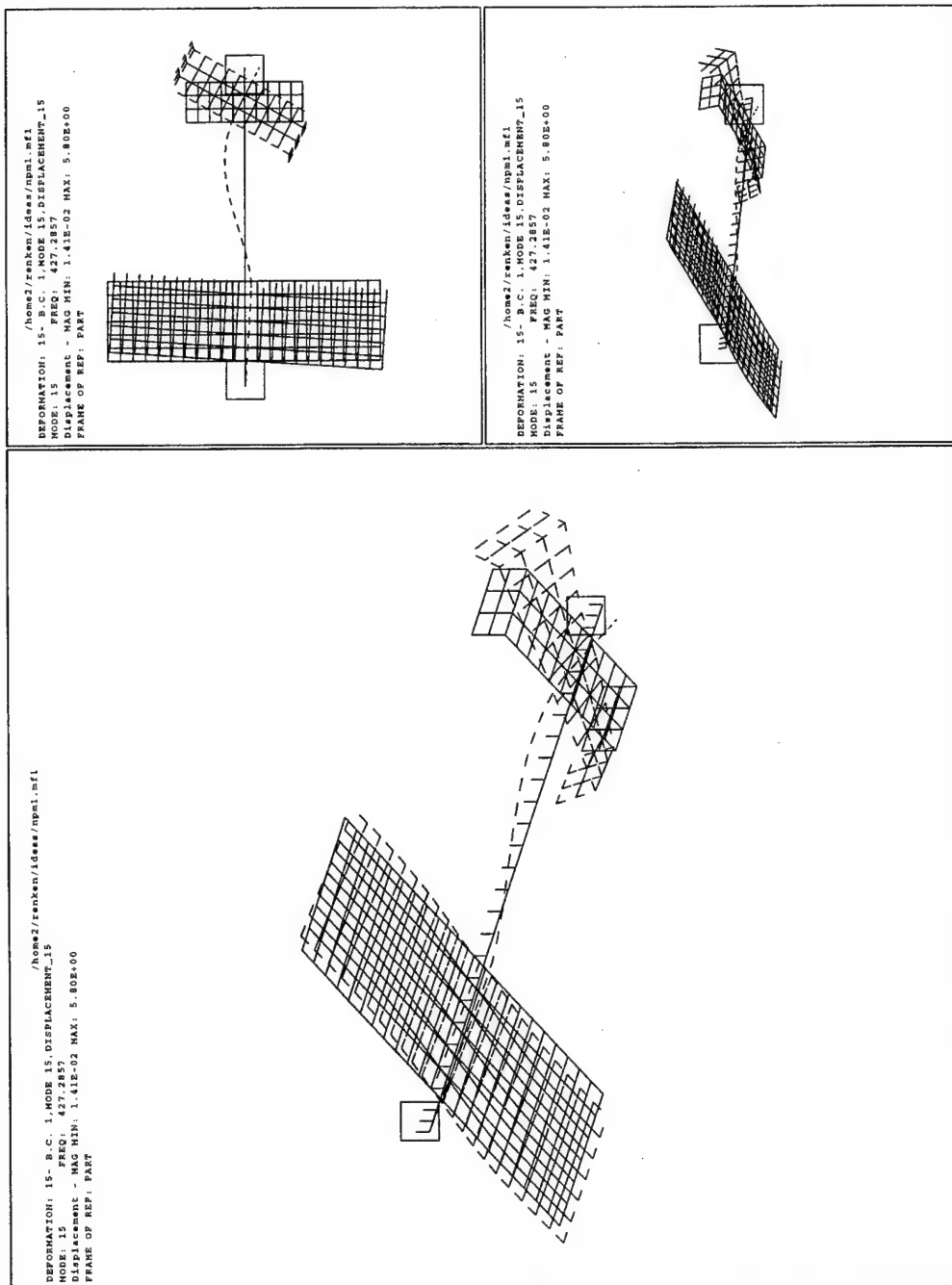
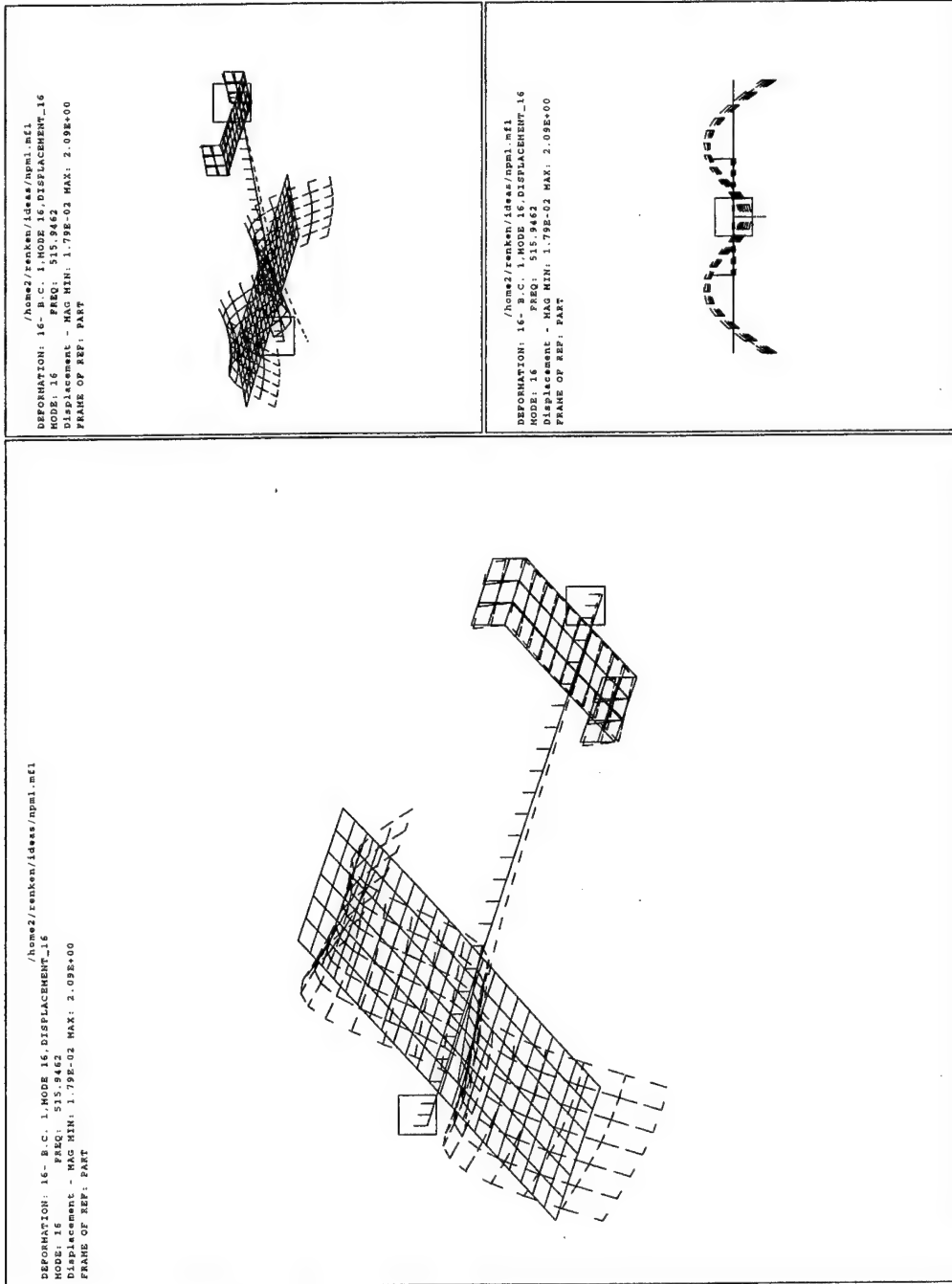


Figure E-10 Airplane Analytical Mode Shape 9

Figure E-11 Airplane Analytical Mode Shape 10



Update 1 - 8 Design Variables, 8 Frequencies (Modes 2 + 9 omitted)

Update 2 - 10 Design Variables, 8 Frequencies (Modes 2 + 9 omitted)

Update 3 - 7 Design Variables, 9 Frequencies (Mode 9 omitted)

Update 4 - 5 Design Variables, 10 Frequencies

AIRPLANE MODEL OPTIMIZATION					
FREQUENCY COMPARISON					
EXPERIMENTAL	ORIGINAL	UPDATE1	UPDATE2	UPDATE3	UPDATE4
103.906	96.7507	103.23	103.068	102.563	104.081
128.125	126.072	134.18	134.289	133.197	128.326
140.625	135.637	140.76	140.695	140.29	131.579
223.047	217.966	228.13	228.594	228.445	220.362
272.266	268.562	279.77	281.173	282.574	286.383
335.156	293.406	322.9	324.807	320.417	325.954
355.469	336.579	352.1	355.239	354.135	356.173
383.984	361.009	381.03	382.403	380.726	373.172
404.297	416.758	434.63	434.55	433.12	404.904
553.125	518.864	529.25	533.166	548.772	553.945
PERCENTAGE ERROR					
	ORIGINAL	UPDATE1	UPDATE2	UPDATE3	UPDATE4
	-6.88632	-0.65059	-0.8065	-1.29251	0.168421
	-1.602341	4.725854	4.810927	3.958634	0.156878
	-3.547022	0.096	0.049778	-0.23822	-6.43271
	-2.277995	2.278892	2.48692	2.420118	-1.20378
	-1.360434	2.756128	3.271433	3.786003	5.185003
	-12.45689	-3.6568	-3.08782	-4.39765	-2.74559
	-5.314106	-0.94776	-0.0647	-0.37528	0.198048
	-5.983322	-0.7693	-0.41174	-0.84847	-2.81574
	3.08214	7.502653	7.482865	7.129165	0.150137
	-6.194079	-4.31638	-3.60841	-0.78698	0.148249
Average error (abs)	4.870465	2.770037	2.608108	2.523305	1.920456
MAC Sum	9.4293	9.4991	9.508	9.5112	9.5734

Table E-1 Airplane Update Frequency Comparison

APPENDIX F. COMPOSITE BEAM TEST DATA

Both the undamaged and damaged composite beams were tested to obtain the experimental dynamic responses. The excitation force was applied at 25 points along the beam. These points corresponded to locations of finite element model nodes. Figure F-1 depicts the data point locations. Figures F-2 through F-10 are the first nine mode shapes for the damaged beam as determined from the experimental data and IDEAS software.

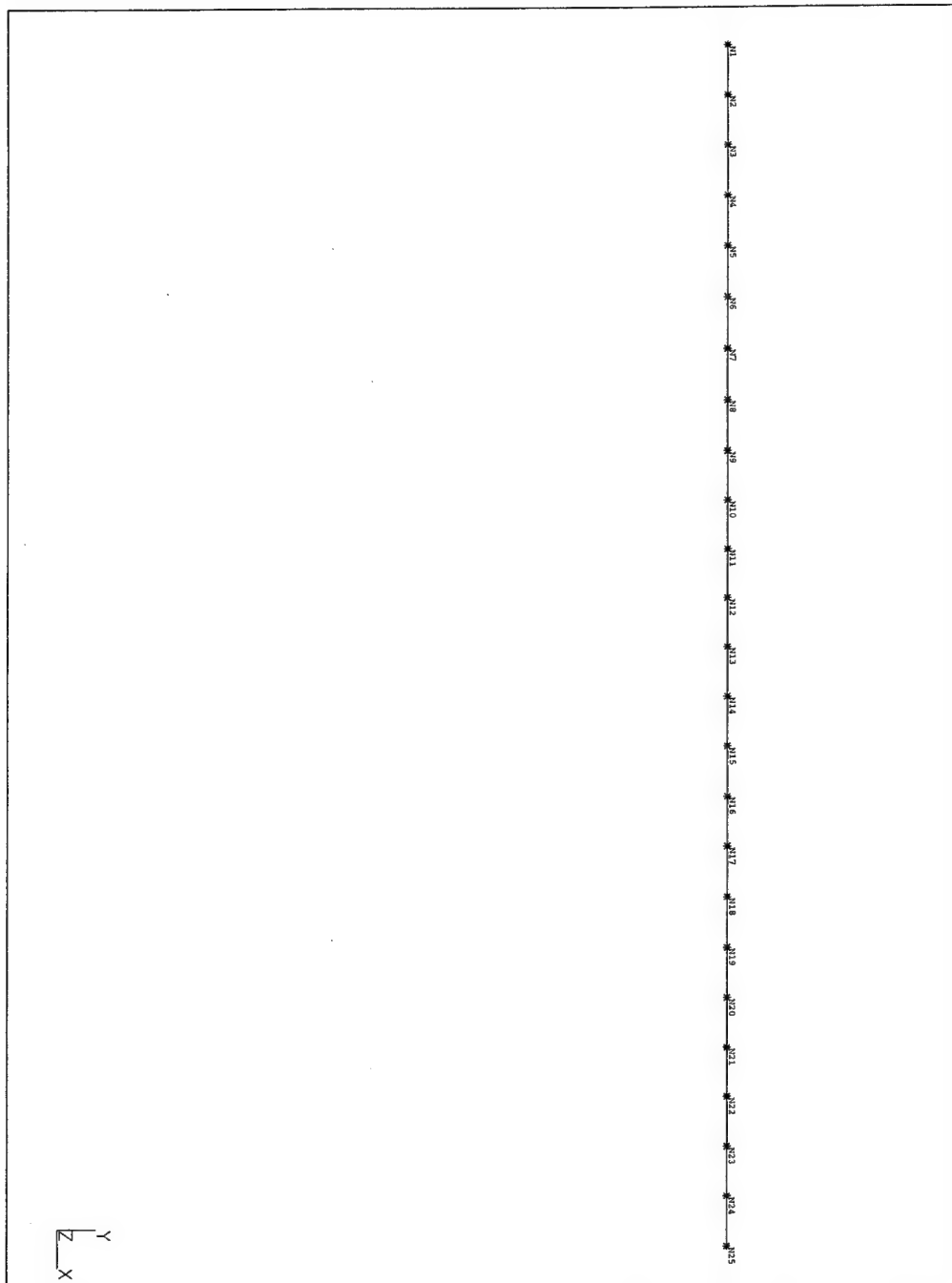


Figure F-1 Composite Beam Excitation Points

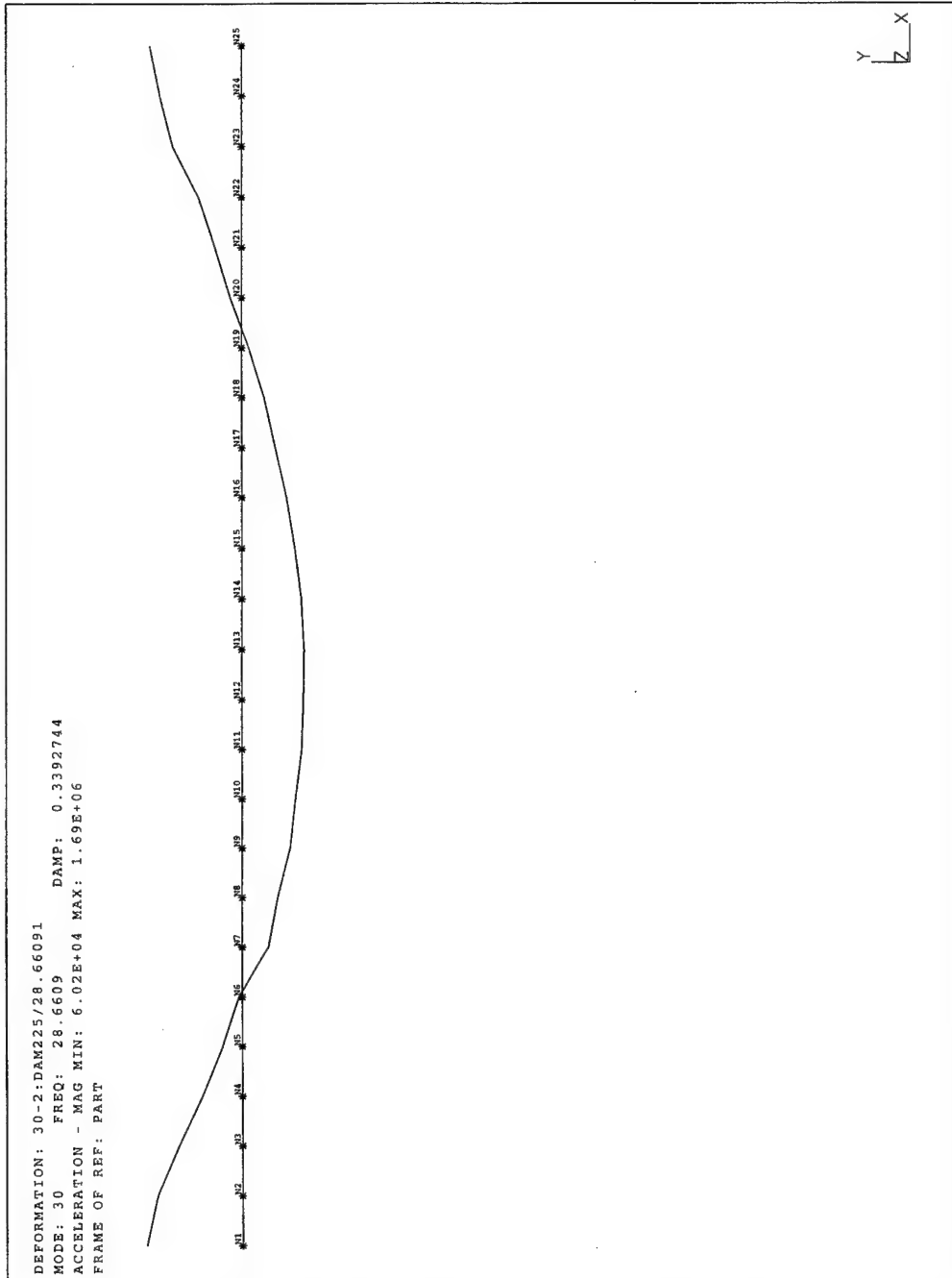


Figure F-2 Composite Beam Experimental Mode Shape 1

DEFORMATION: 31-3:DAM225/78.85377
MODE: 31 FREQ: 78.85377 DAMP: 0.1806784
ACCELERATION - MAG MIN: 7.18E+04 MAX: 1.86E+06
FRAME OF REF: PART

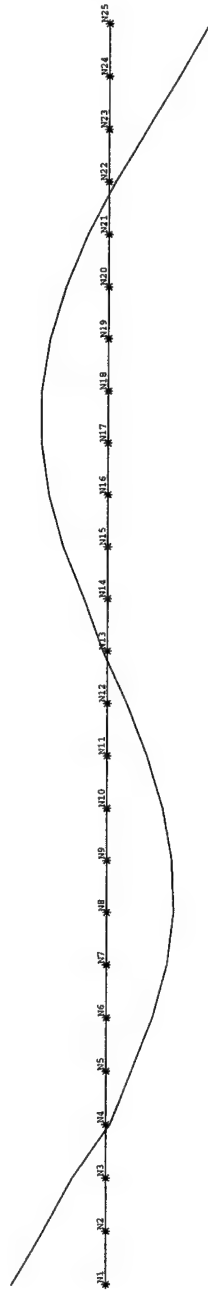


Figure F-3 Composite Beam Experimental Mode Shape 2

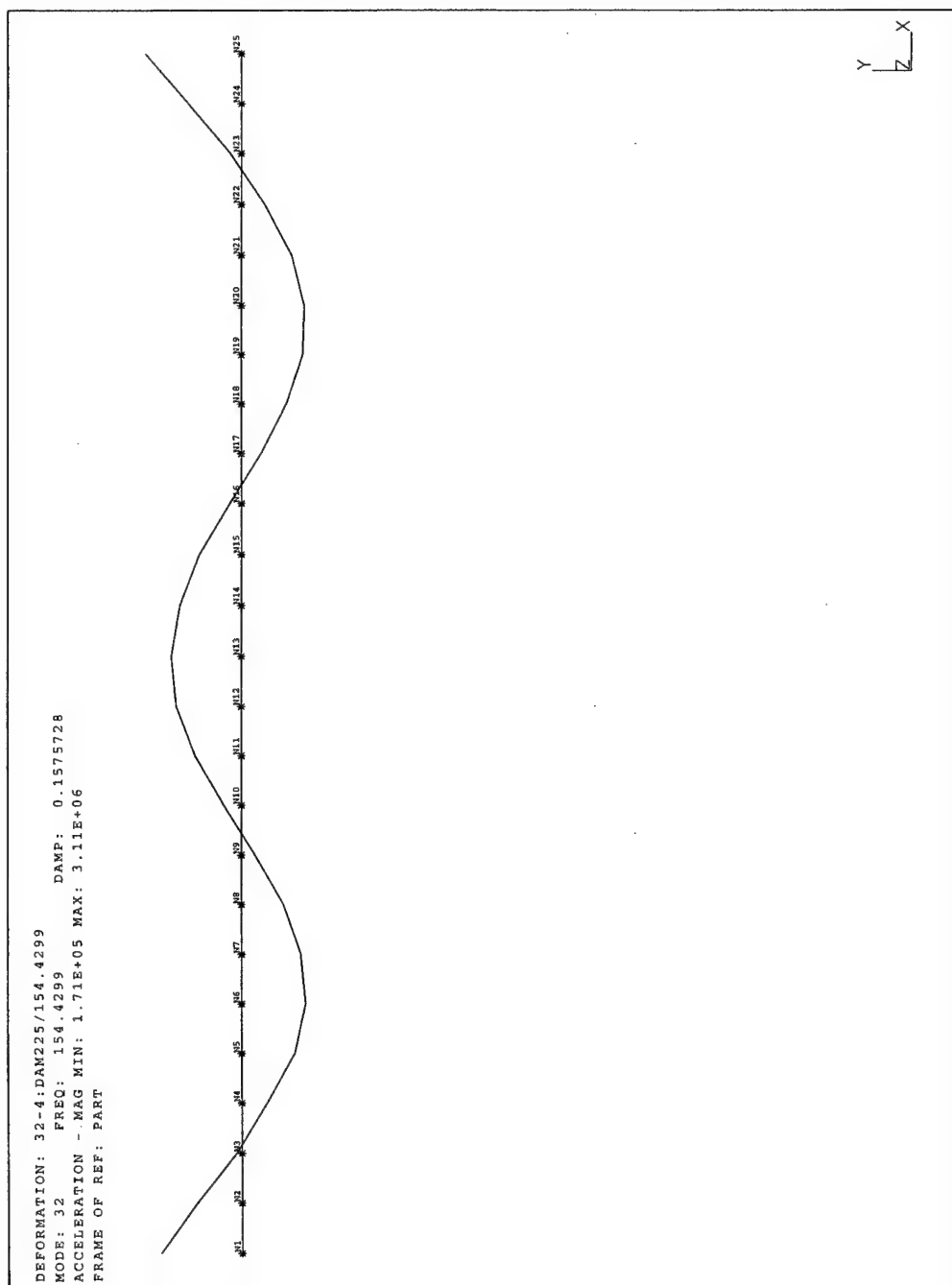


Figure F-4 Composite Beam Experimental Mode Shape 3

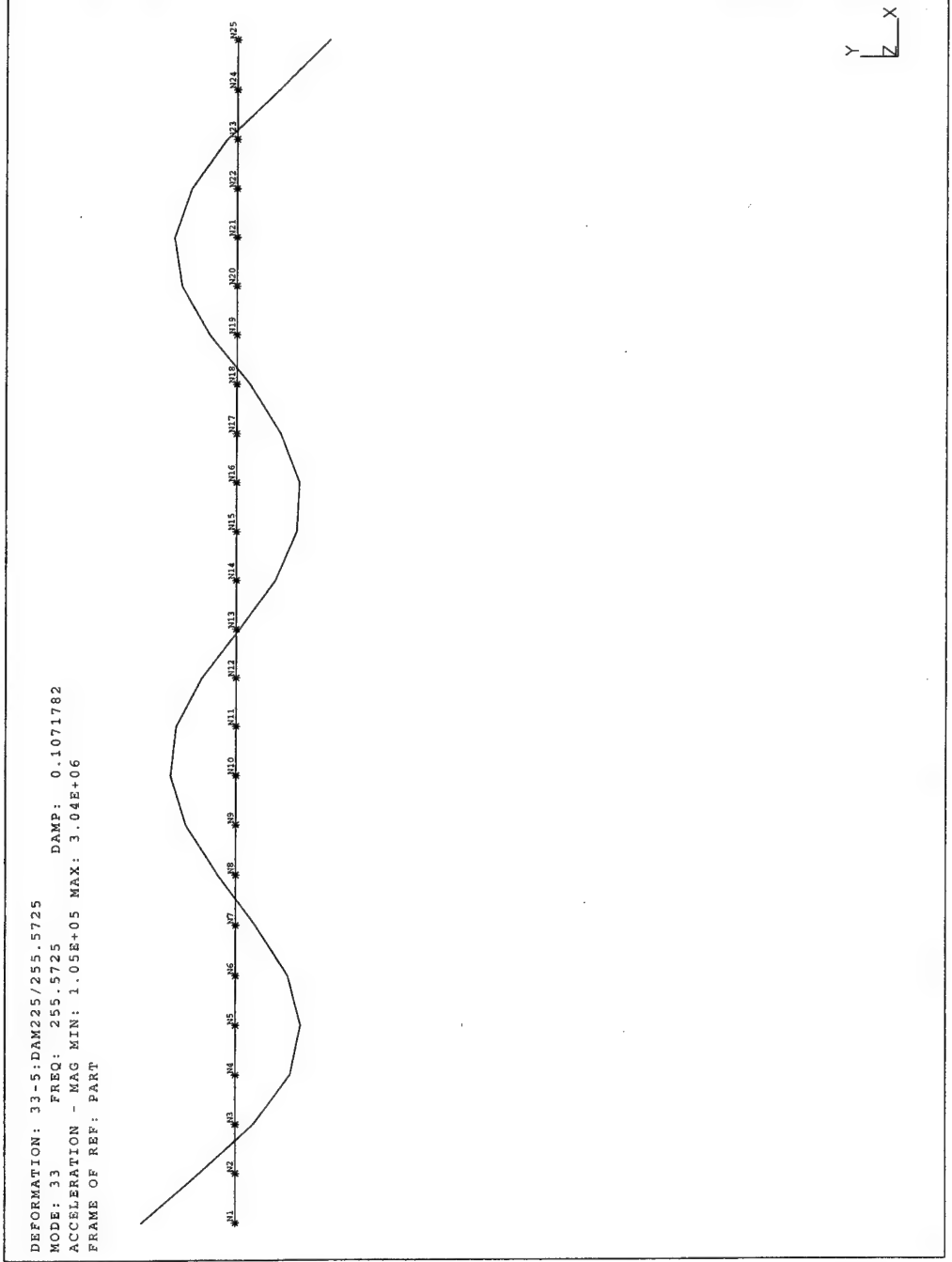


Figure F-5 Composite Beam Experimental Mode Shape 4

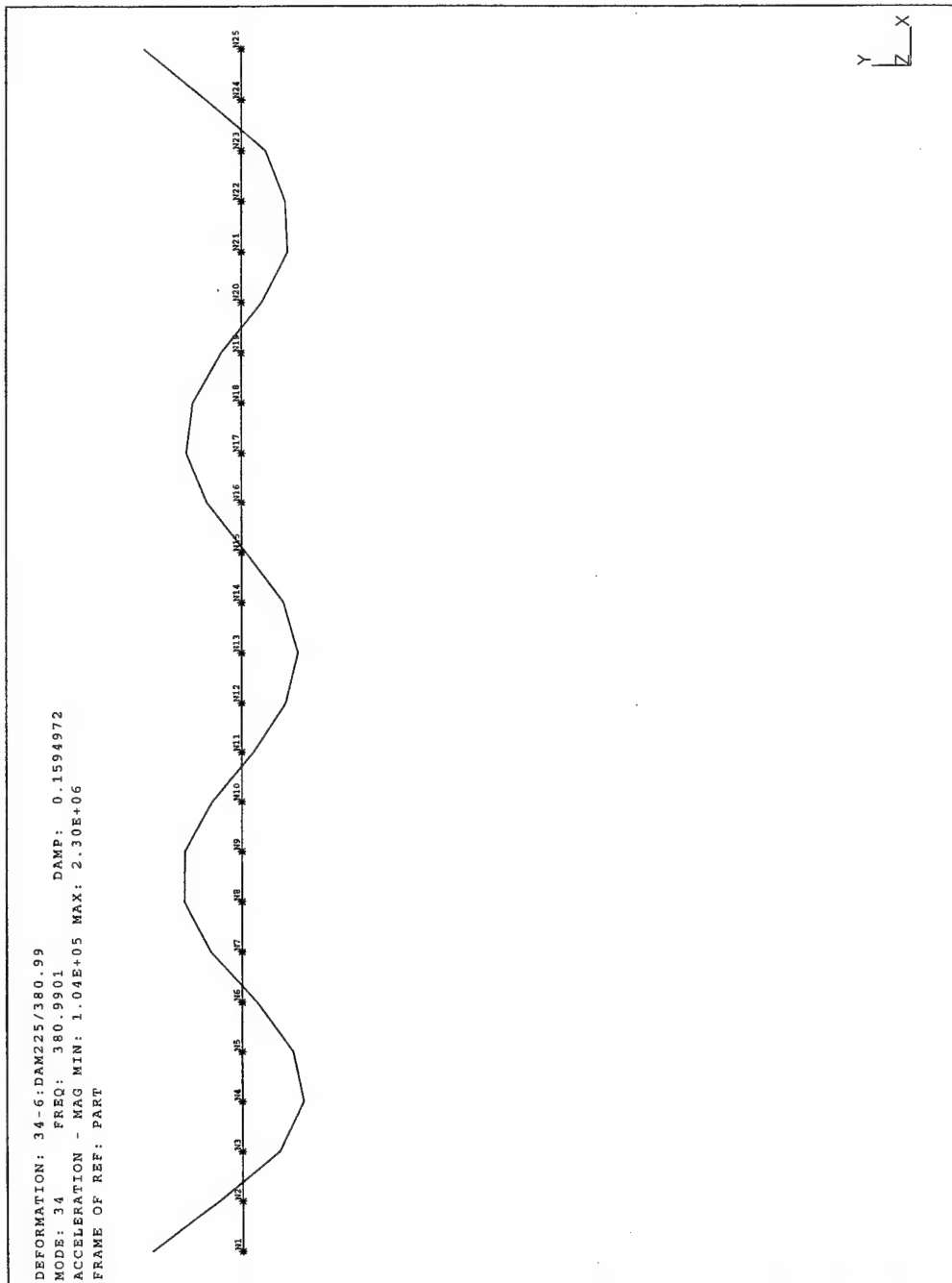


Figure F-6 Composite Beam Experimental Mode Shape 5

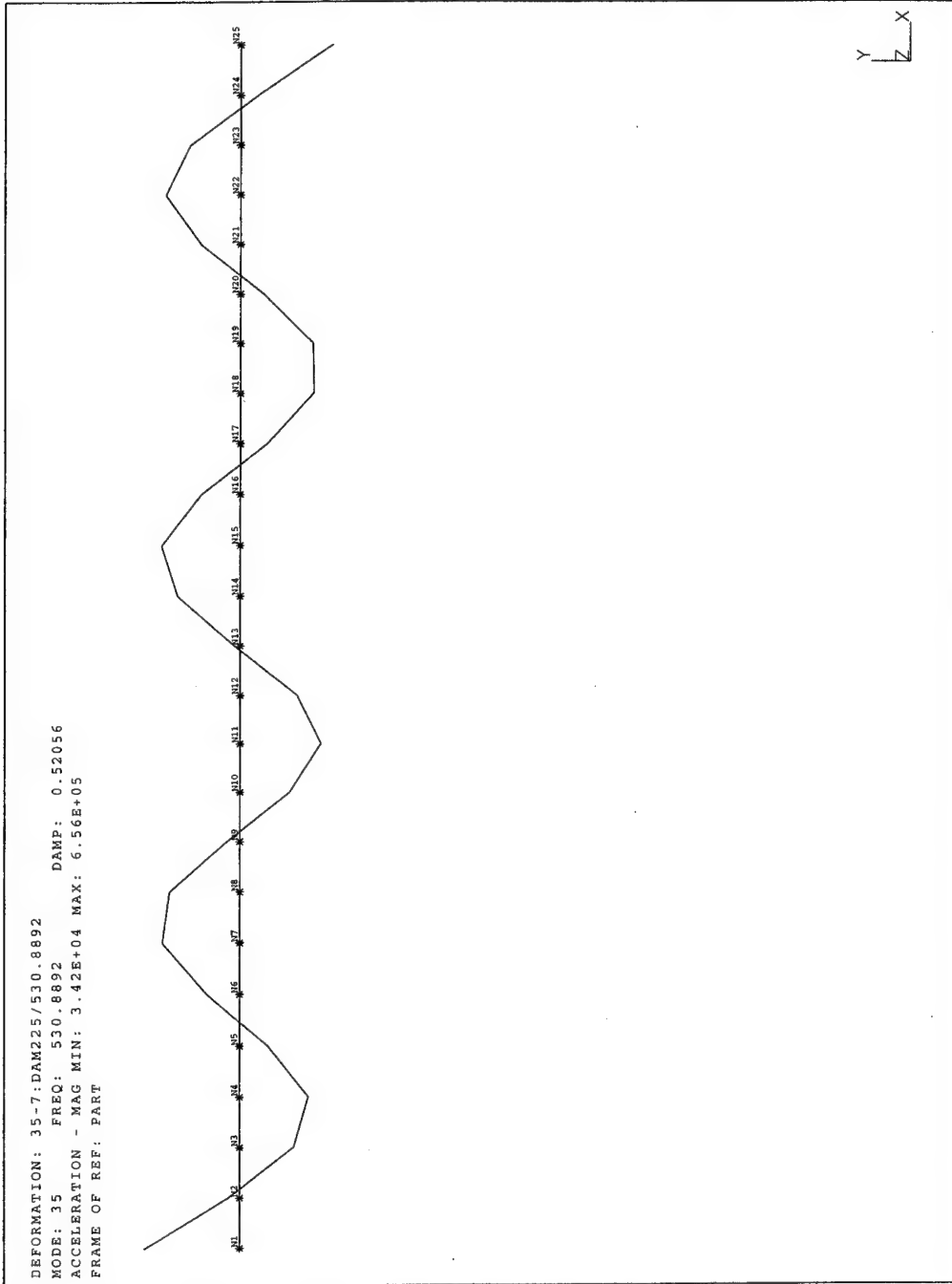


Figure F-7 Composite Beam Experimental Mode Shape 6

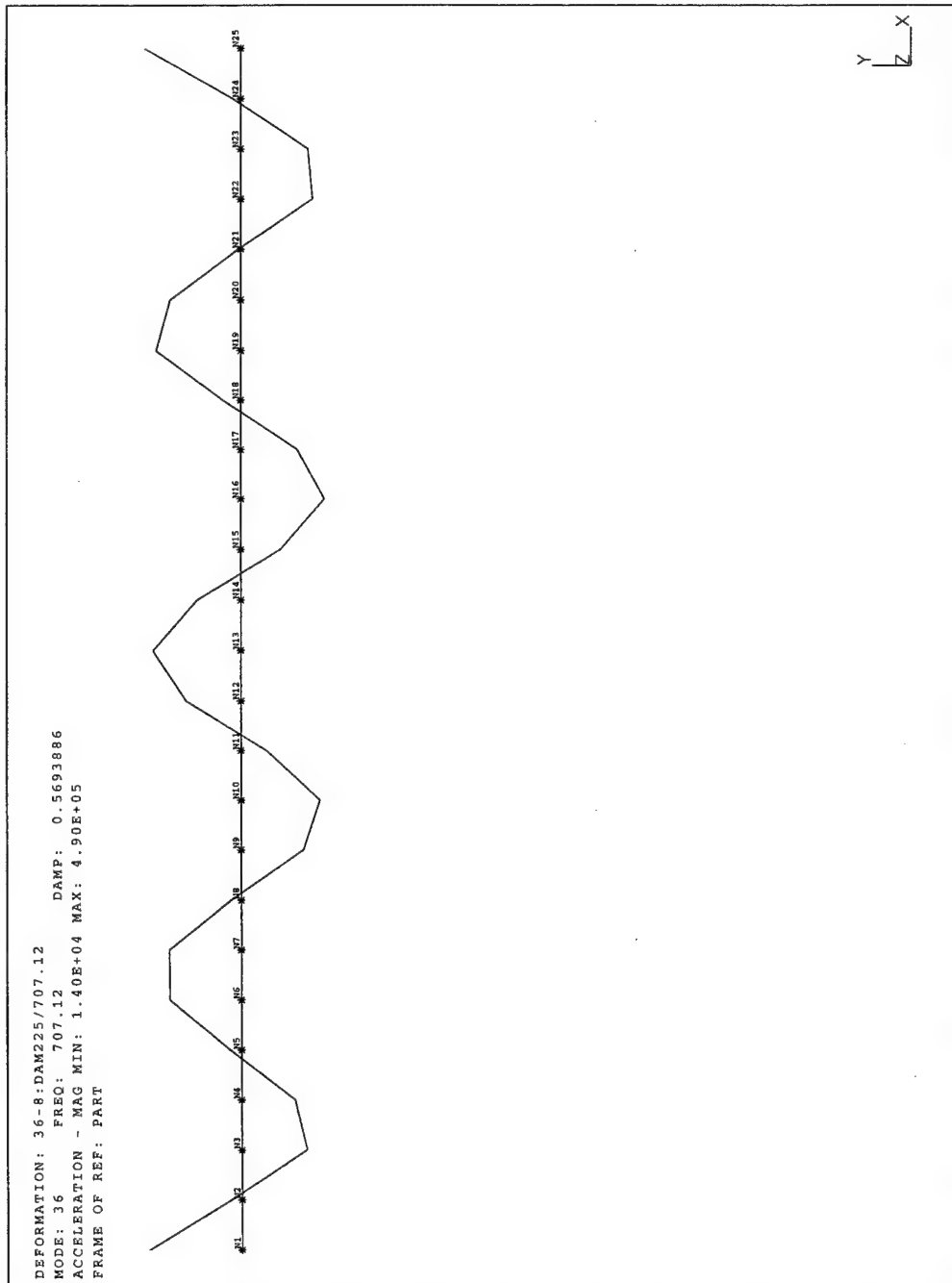


Figure F-8 Composite Beam Experimental Mode Shape 7

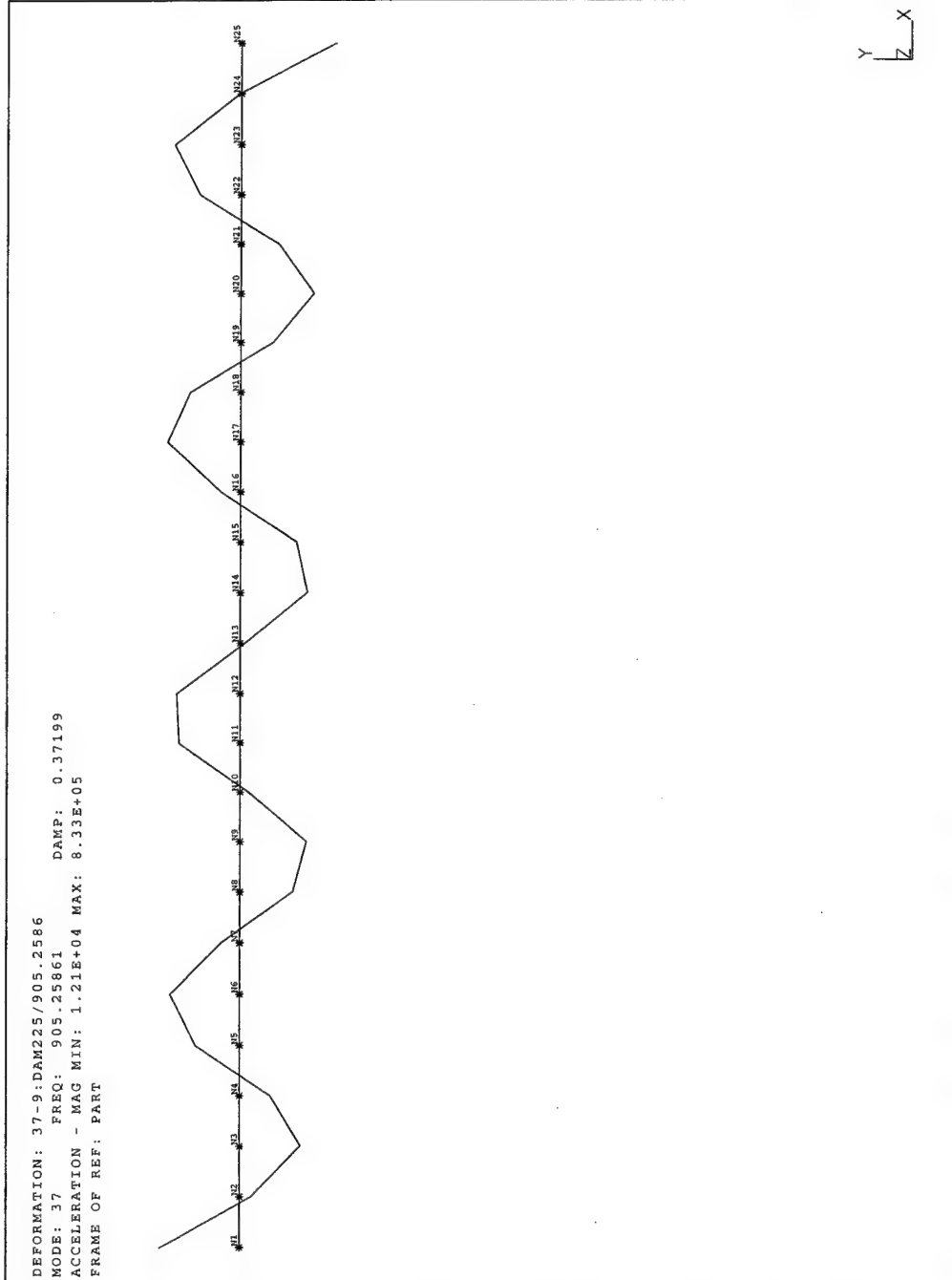


Figure F-9 Composite Beam Experimental Mode Shape 8

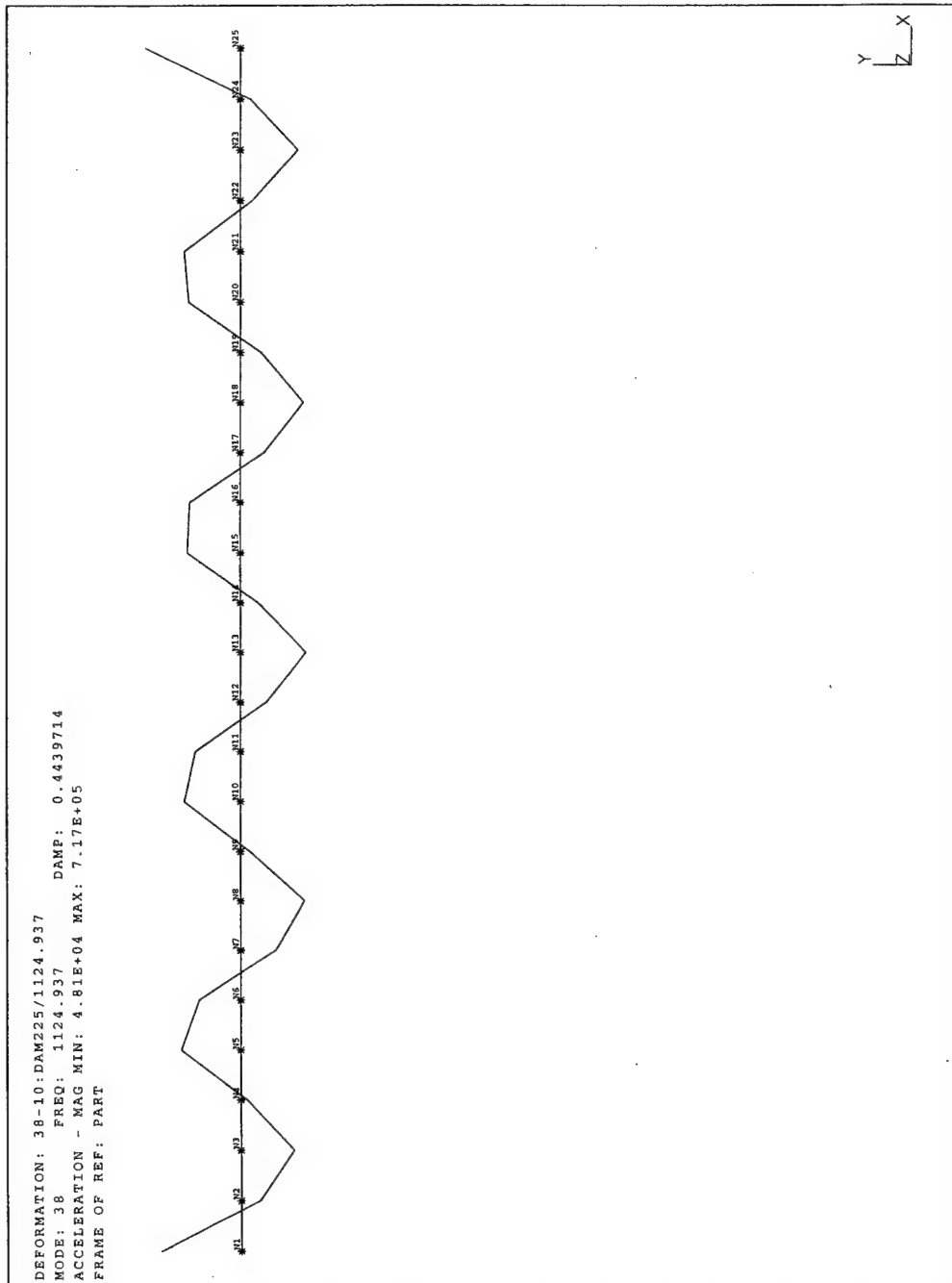


Figure F-10 Composite Beam Experimental Mode Shape 9

APPENDIX G. STEEL BEAM SPECIFICATIONS

A. PHYSICAL DIMENSIONS AND PROPERTIES

A steel beam was used to verify the damage localization procedure. The dimensions and the mass of the beam were measured. The original Young's modulus was assumed to be equal to a standard value for steel. The beam orientation for the simulations was as depicted in Figure G-1. The degrees of freedom for the beam were vertical translation, upward in the figure, and rotation around a vector out of the plane of the page.

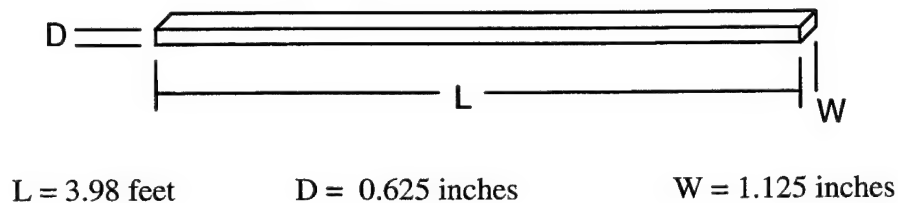


Figure G-1 Steel Beam

The original physical properties assumed for the beam were:

Young's modulus	$E = 30 \times 10^6$	PSI
mass density	$\rho = 0.00072$	lbf-sec ² /in ⁴

Young's modulus was updated using the optimization procedure and comparison to the undamaged beam's dynamic response. The updated value was:

Young's modulus	$E = 28.61 \times 10^6$	PSI
-----------------	-------------------------	-----

B. DYNAMIC RESPONSE

The damaged beam was tested to obtain the experimental dynamic responses. The excitation force was applied at 25 points along the beam. These points

corresponded to locations of finite element model nodes. Figure G-2 depicts the data point locations. Figures G-3 through G-11 are the first nine mode shapes for the damaged beam as determined from the experimental data and IDEAS software.

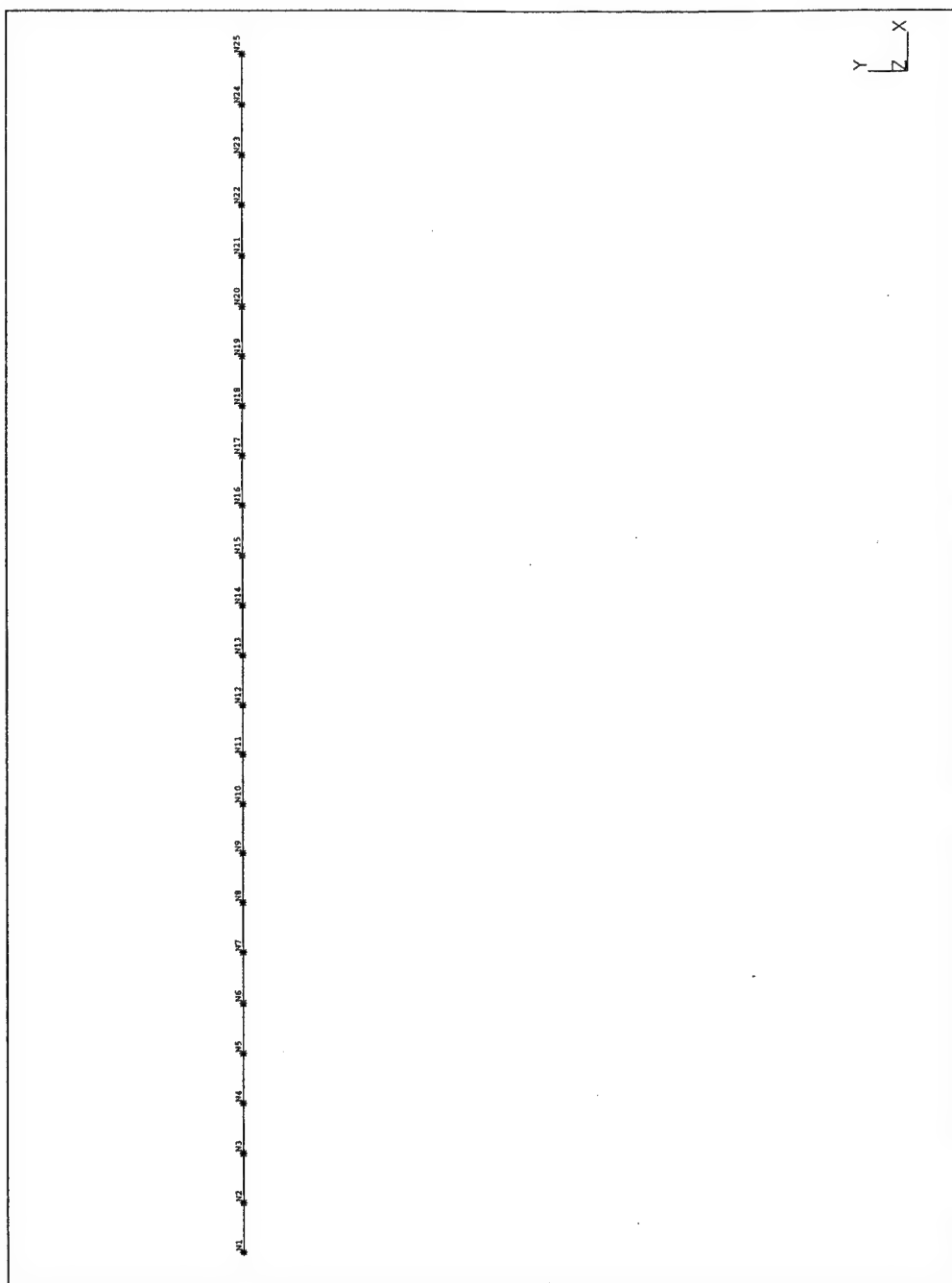


Figure G-2 Steel Beam Excitation Points

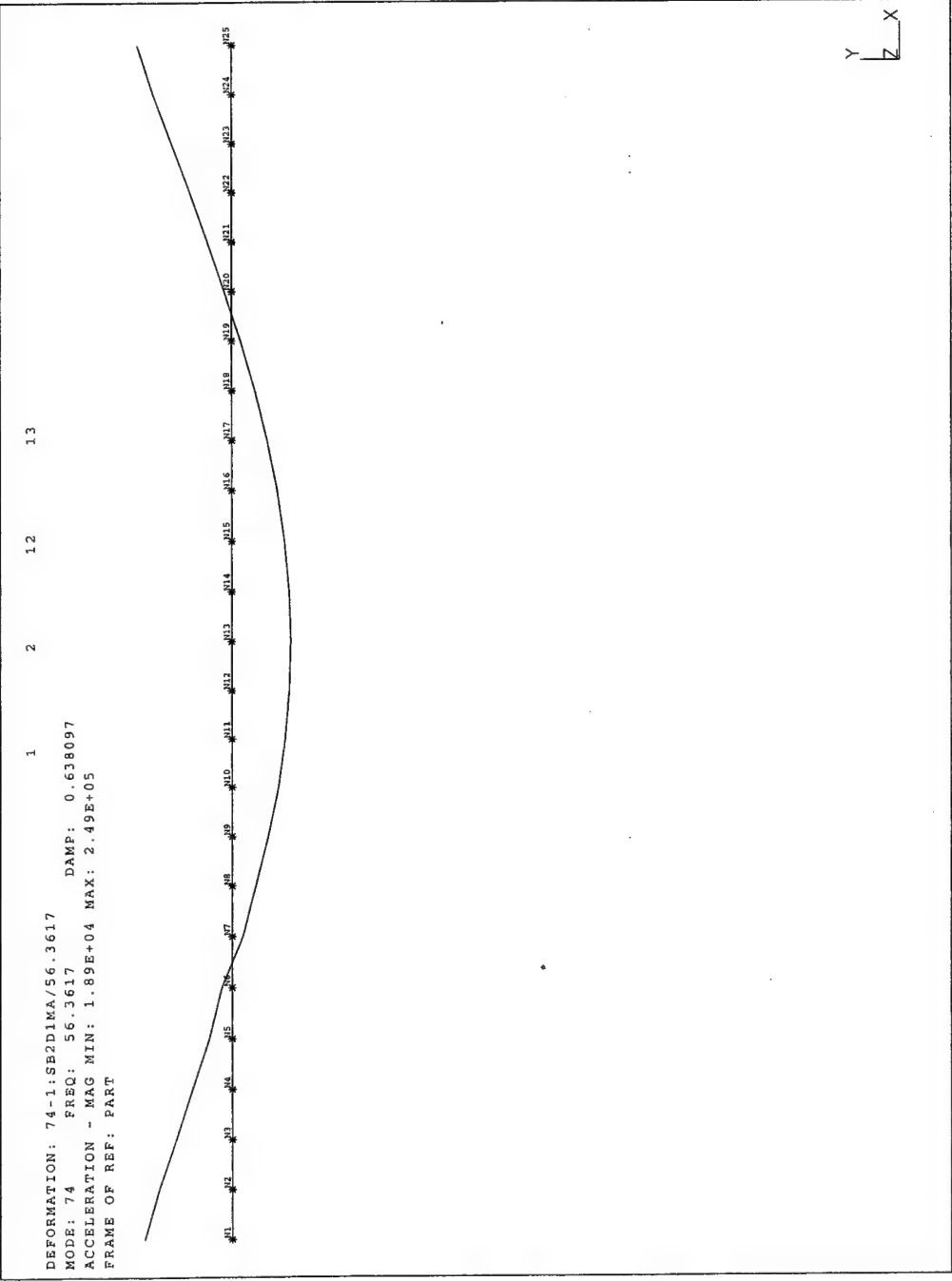


Figure G-3 Steel Beam Experimental Mode Shape 1

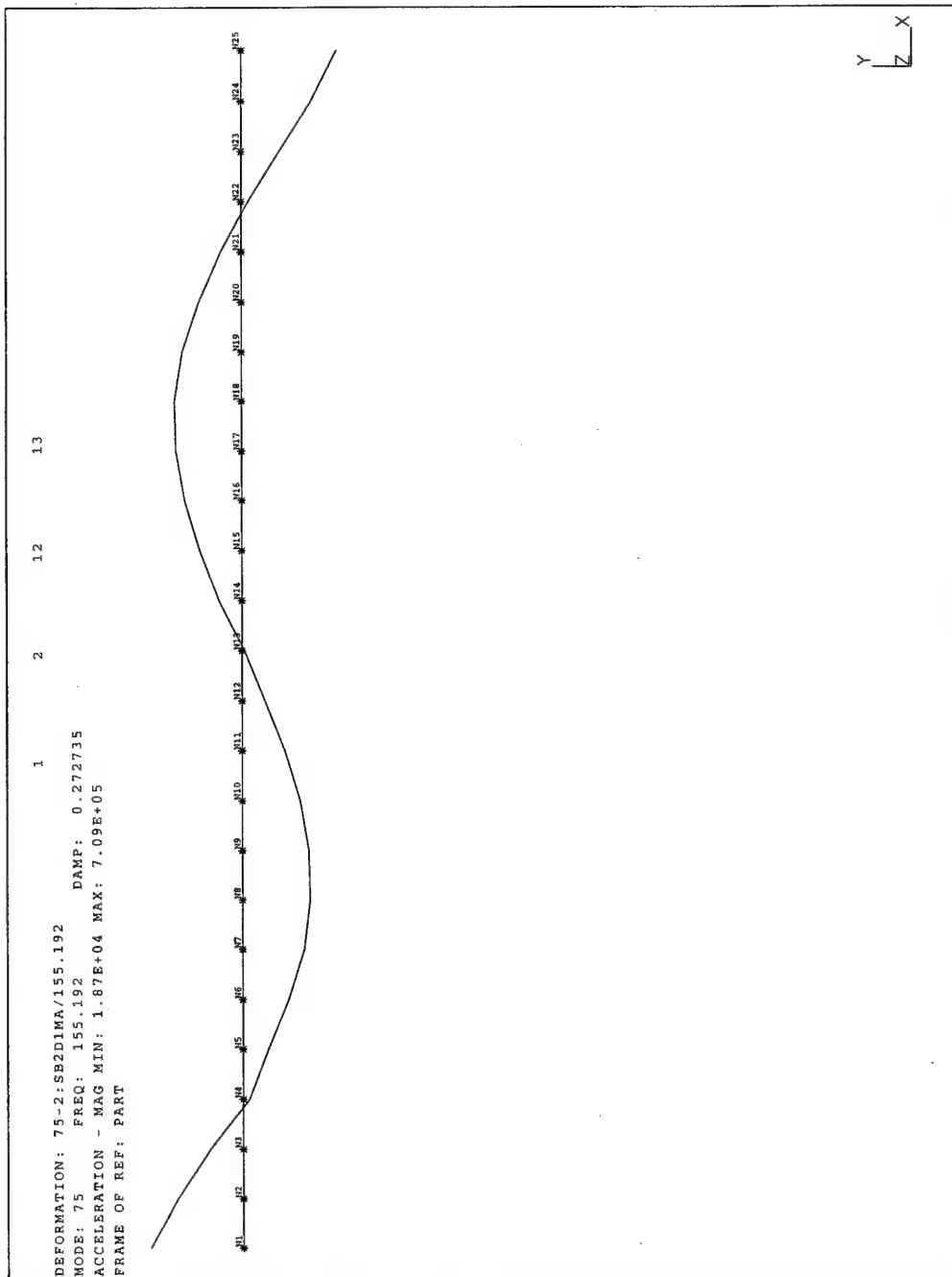


Figure G-4 Steel Beam Experimental Mode Shape 2

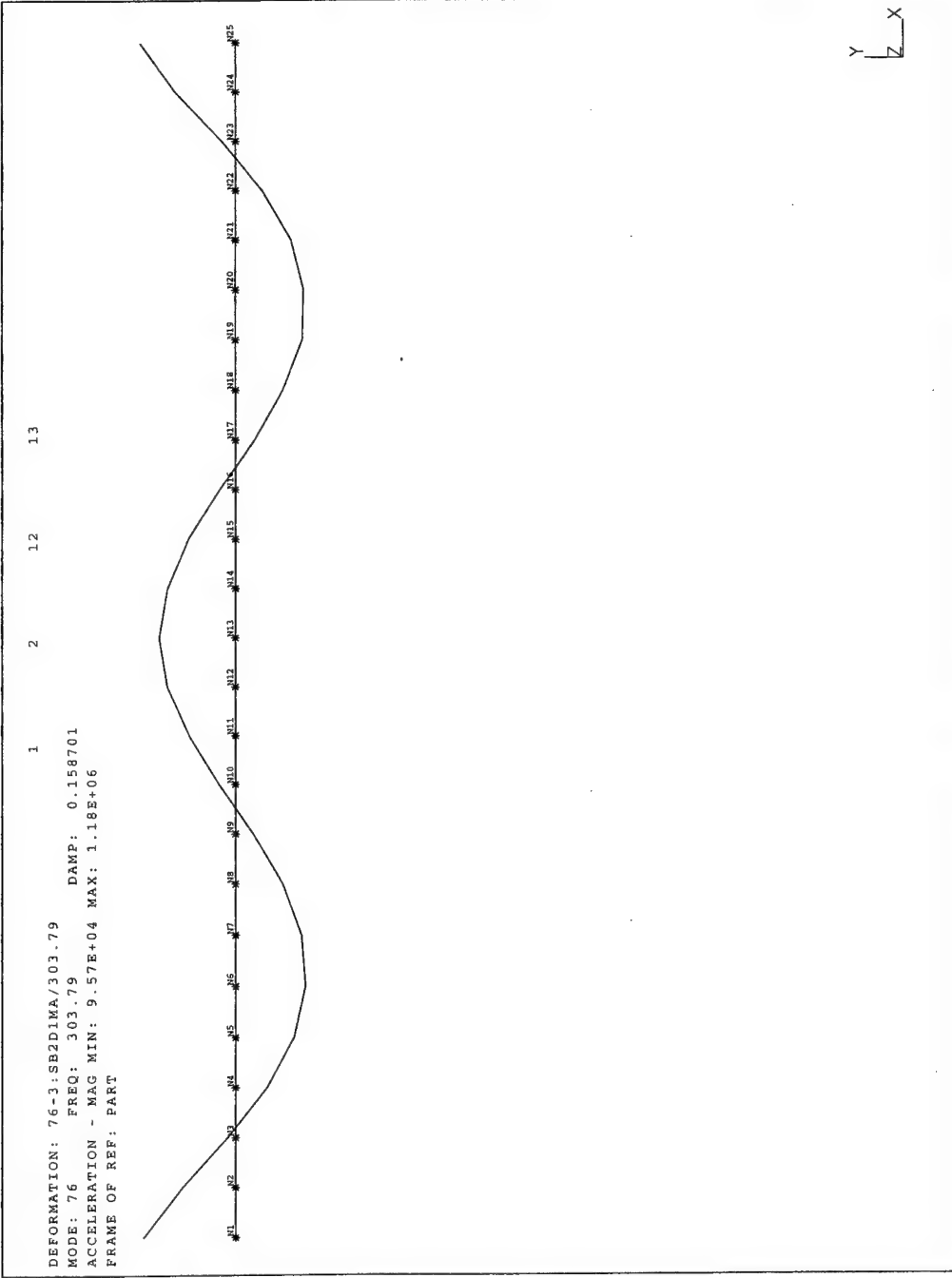


Figure G-5 Steel Beam Experimental Mode Shape 3

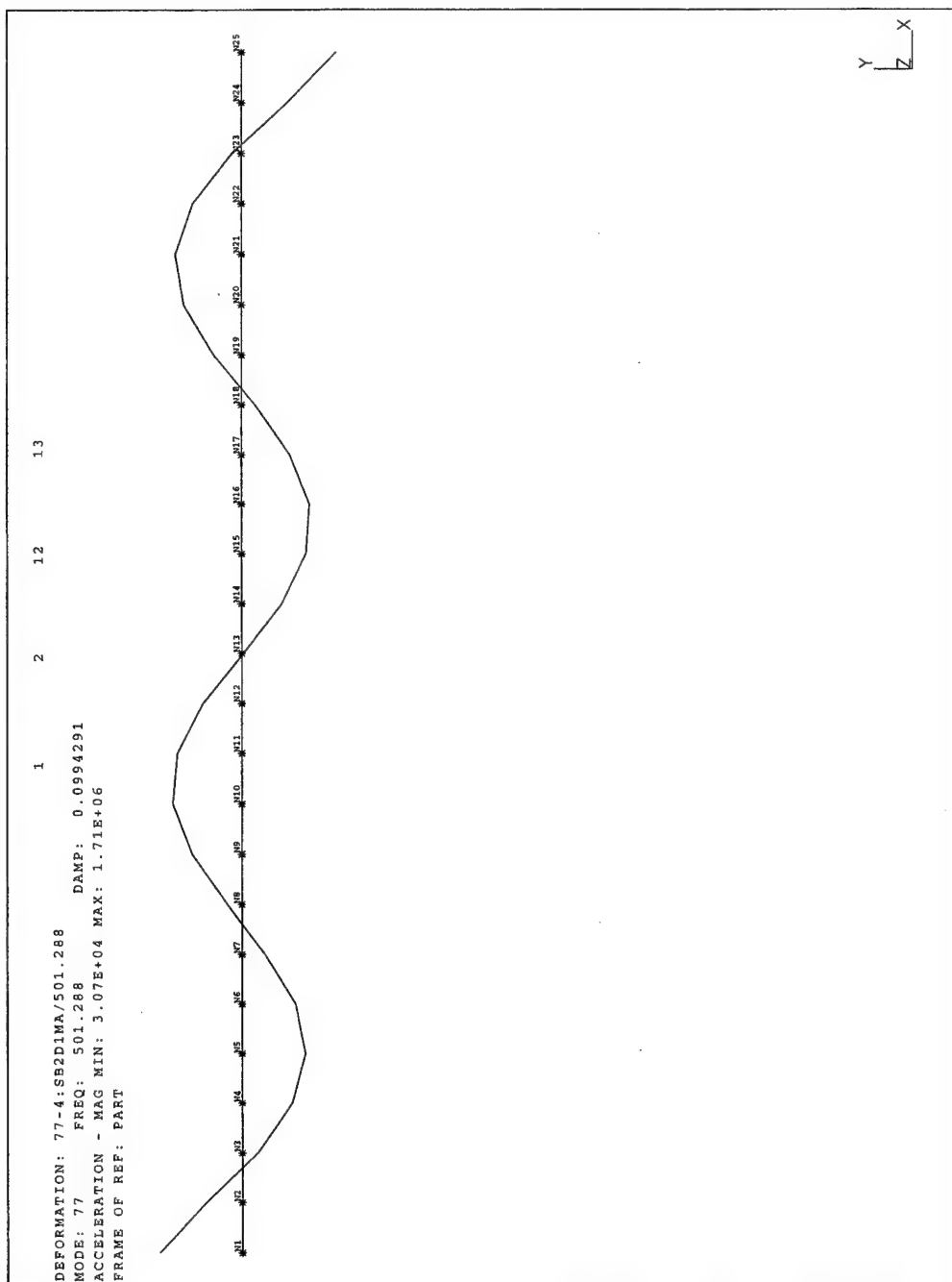


Figure G-6 Steel Beam Experimental Mode Shape 4

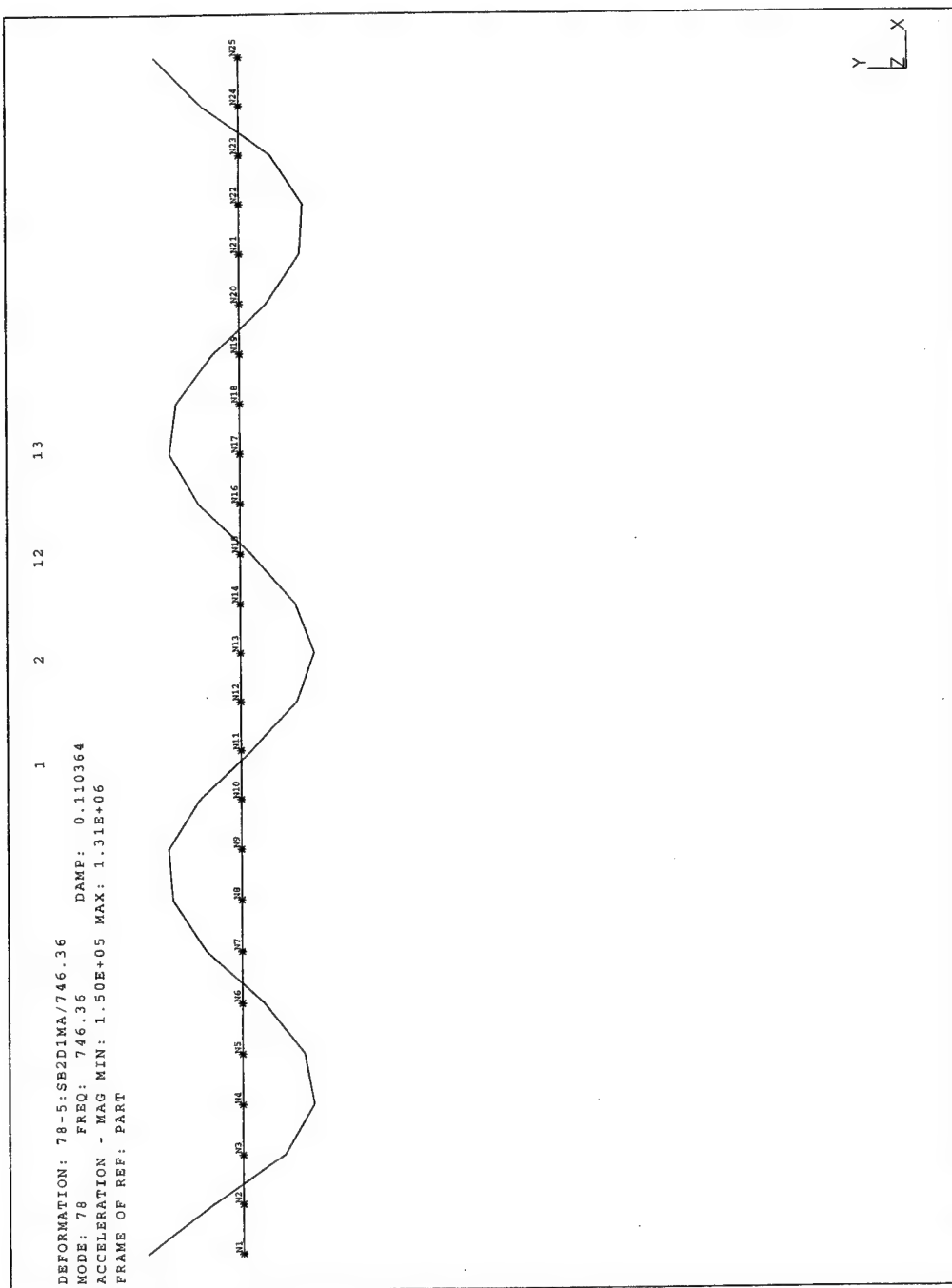


Figure G-7 Steel Beam Experimental Mode Shape 5

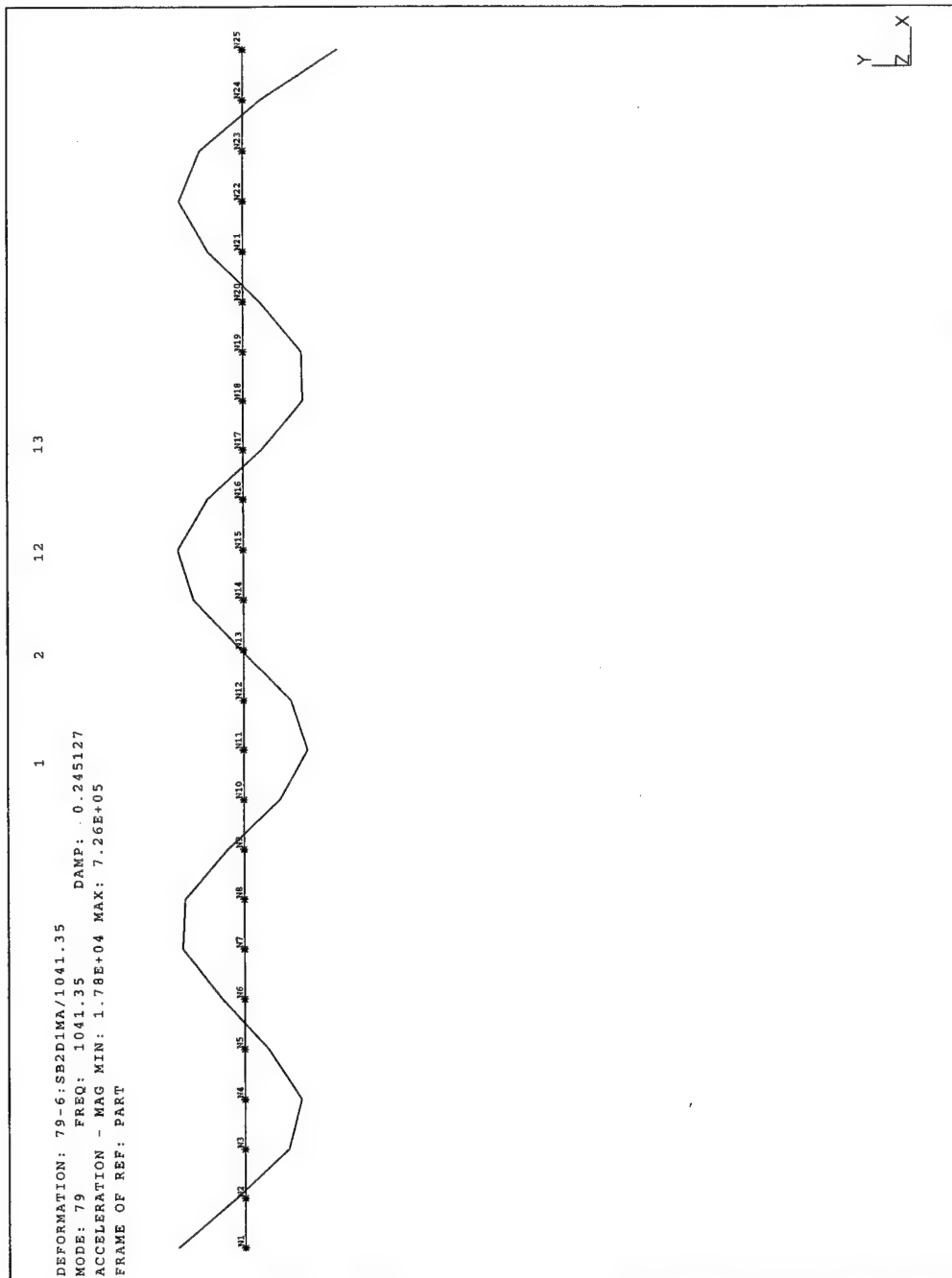


Figure G-8 Steel Beam Experimental Mode Shape 6

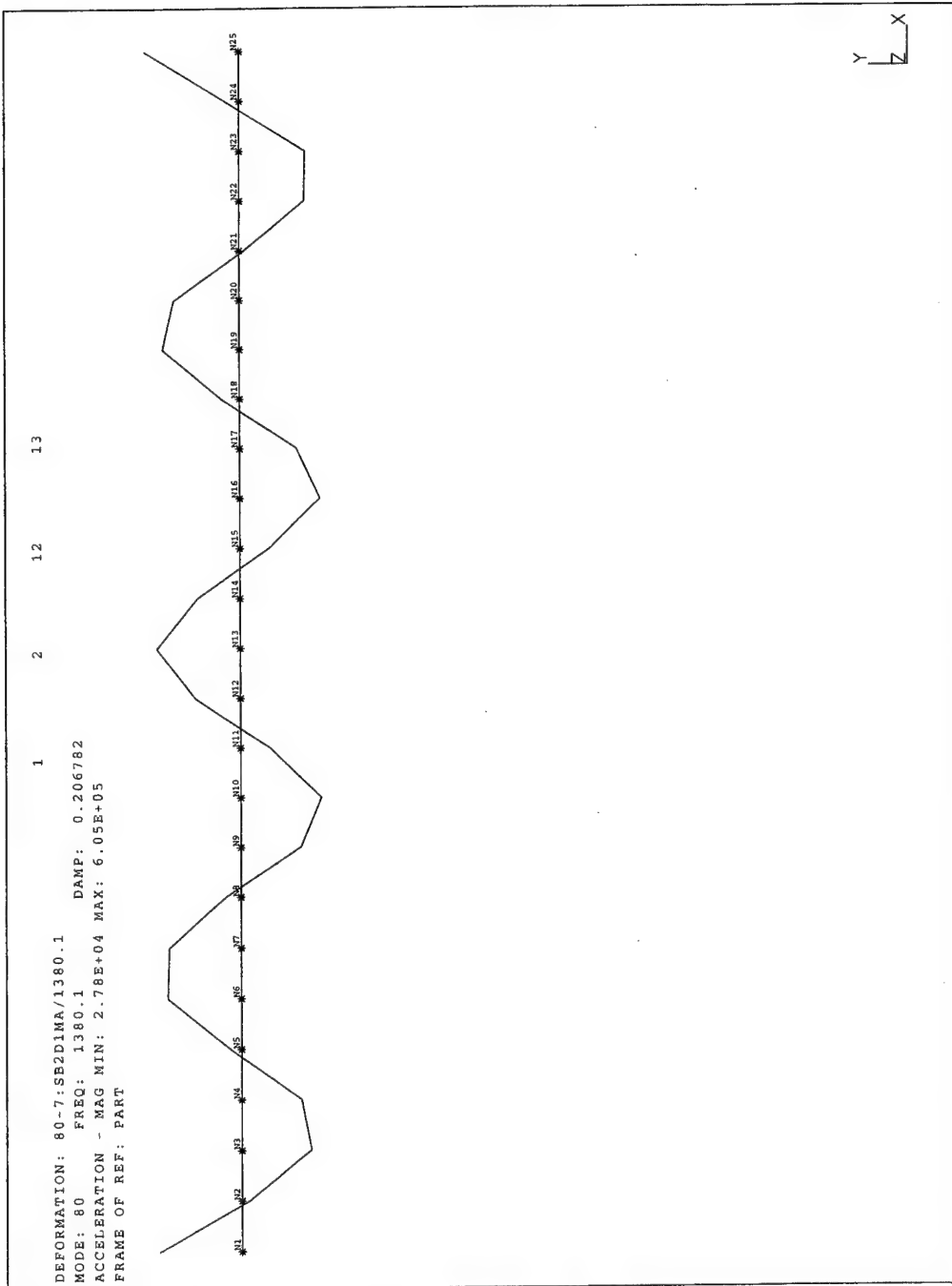


Figure G-9 Steel Beam Experimental Mode Shape 7

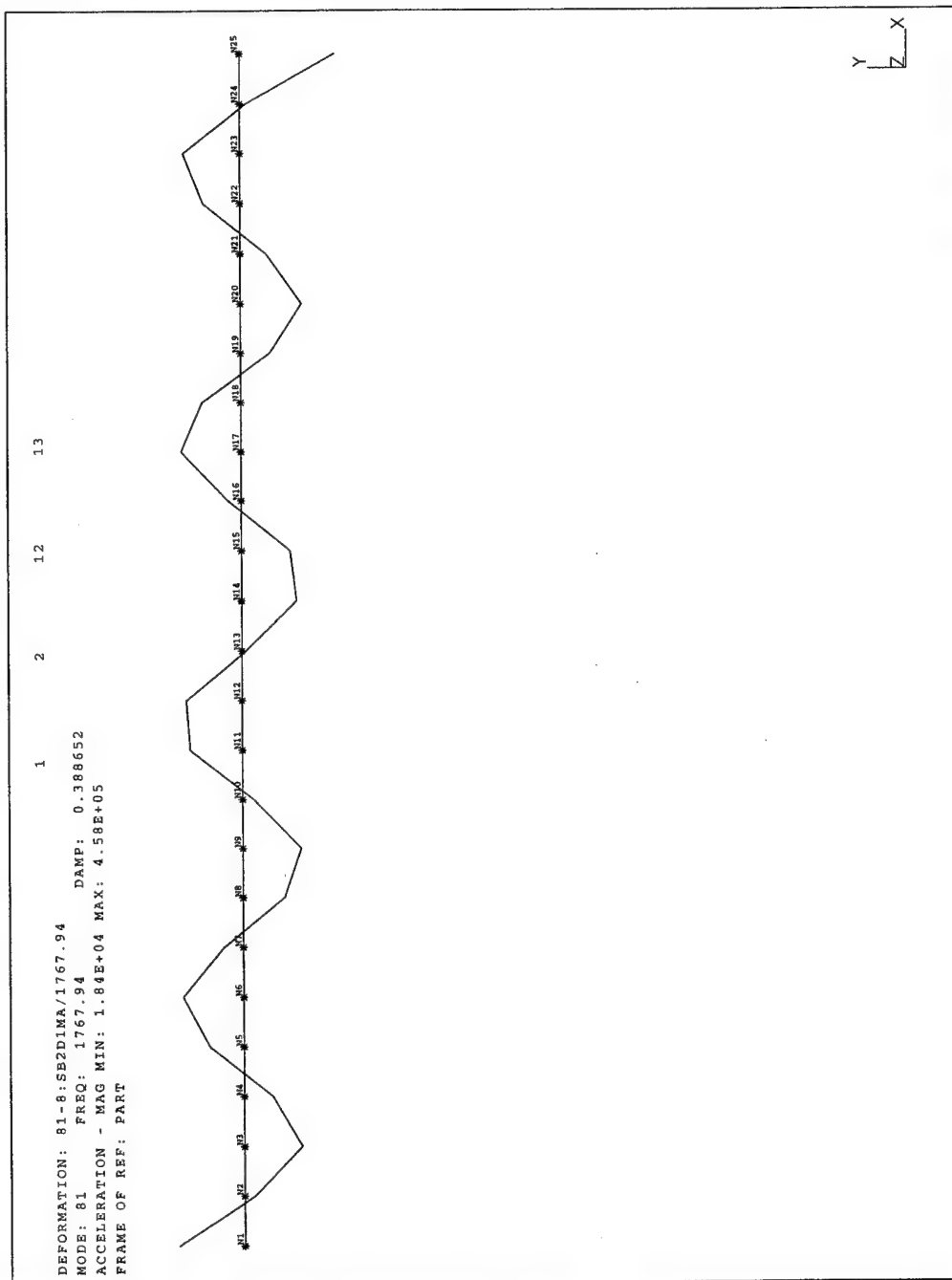


Figure G-10 Steel Beam Experimental Mode Shape 8

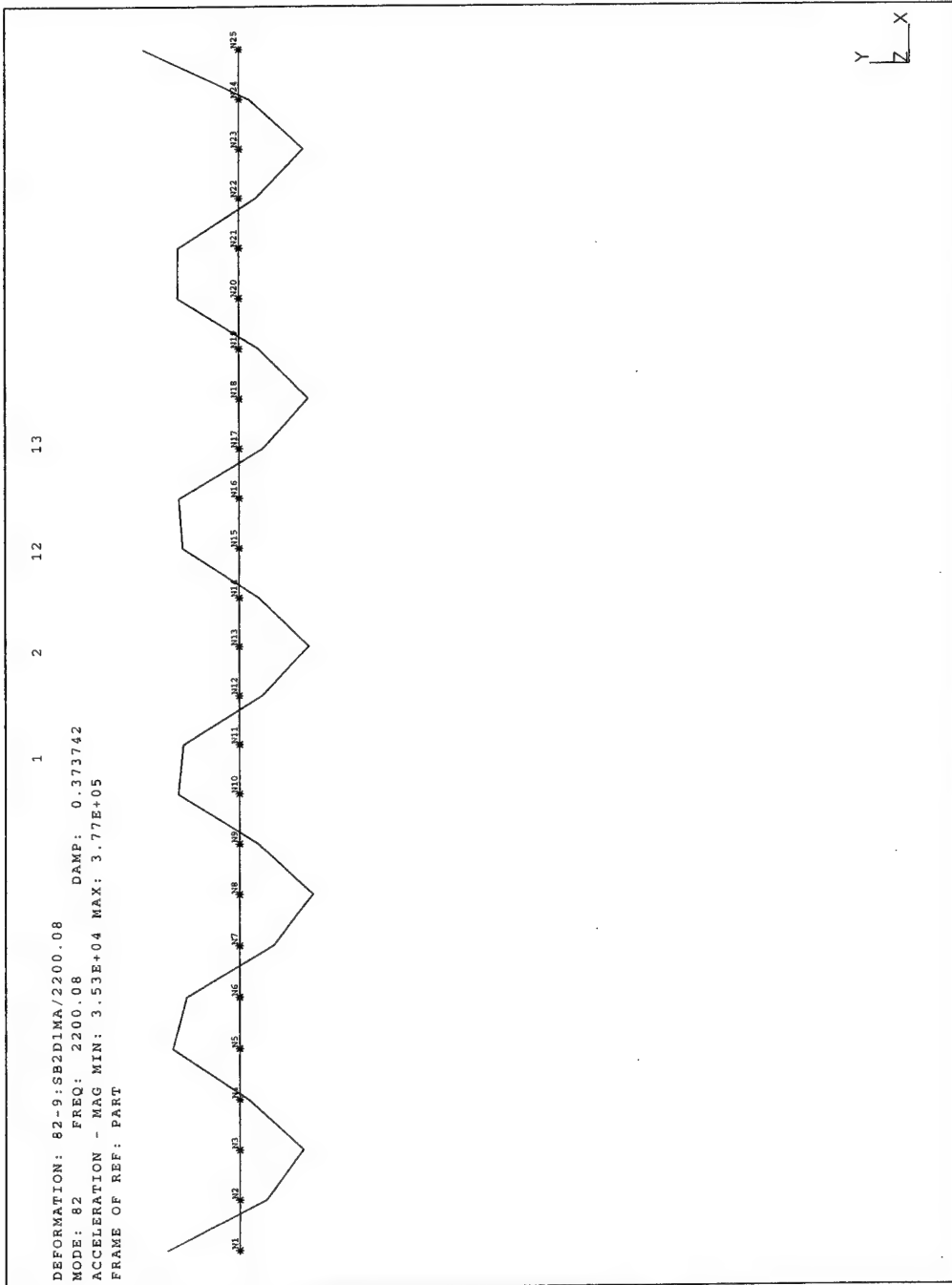


Figure G-11 Steel Beam Experimental Mode Shape 9

APPENDIX H. COMPUTER CODE

The following is a list and a brief description of MATLAB routines employed in this thesis. The different problems used similar routines modified to account for the test piece specifics and the application:

- FEMOD.M - develops finite element model and solution for a beam. Used to develop the beam finite element models and the simulated experimental data.
- GLOOPT.M - runs optimization routine for model updating and returns results. This program can be modified to run for the beam or any other model.
- DVMAT.M - develops the 2-level factorial combination matrix.
- OPTBEAM.M - inputs optimization process parameters such as limits and search method.
- OBJVAL.M - contains the objective function and constraints for optimization.
- CHECKW.N.M - calculates updated model natural frequencies and mode shapes for the beam trials for solution evaluation.
- CBLOC.M - divides designated region into sectors and runs localization routine for each sector.
- MODCOMP.M - calculates the Modal Assurance Criteria for active modes.
- DIRECT.M - does direct pseudo-inverse solution for the steel beam damage case. It also contains the reduction/expansion logic.

The codes are included in the following pages.

FEMOD.M

```
% develops finite element model for a beam

function [omega,T,gamma]=femod(dv)

nel=8;
nn=nel+1; % nn - number of nodes
dof=nn*2; % dof - number of degrees of freedom

% input beam dimensions

lt=10;
w=3;
d=10;

% calculate needed parameters

le=lt*12/nel; % le - element length
ar=w*d; % ar - cross sectional area
ve=ar*le; % ve - element volume
Iner=w*d^3/12; % Iner - moment of Inertia

% Construct geometric properties matrices

ke1=[12 6*le -12 6*le;
      6*le 4*le^2 -6*le 2*le^2;
      -12 -6*le 12 -6*le;
      6*le 2*le^2 -6*le 4*le^2];
ke=(Iner/le^3)*ke1;
me1=[156 22*le 54 -13*le;
      22*le 4*le^2 13*le -3*le^2;
      54 13*le 156 -22*le;
      -13*le -3*le^2 -22*le 4*le^2];
me=(ve/420)*me1;

% construct global matrices

kglo=zeros(dof,dof);
mglo=zeros(dof,dof);

% properties for the different elements (assumed homogenous)

for j=1:nel
```

```

        mod(j)=dv(1);
        rho(j)=dv(2);
    end

% designate element connectivity

for i=1:nel
    con=i+1;
    c1=(i*2)-1;
    c2=con*2;
    kglo(c1:c2,c1:c2)=kglo(c1:c2,c1:c2)+mod(i)*ke;
    mglo(c1:c2,c1:c2)=mglo(c1:c2,c1:c2)+rho(i)*me;
end

% set boundary conditions - zero the matrix elements which are
% constrained. Beam is cantilevered.

kact=kglo(3:dof,3:dof);
mact=mglo(3:dof,3:dof);

% solve for natural frequencies and mode shapes

[phi,lbd]=eig(mact\kact);
for j=1:dof-2;
    lambda(j)=lbd(j,j);
end
freqs=(sqrt(lambda));
[wn,I]=sort(freqs);
for j=1:dof-2;
    shnorm(:,j)=phi(:,I(j));
end
mtil=shnorm'*mact*shnorm;
for i=1:dof-2;
    alpha(i)=1./sqrt(mtil(i,i));
    shapes(:,i)=shnorm(:,i)*alpha(i);
end
wn=wn';

% compute sensitivities and Cauchy ratio equivalent

numdv=2*nel;
sens=zeros(dof-2,numdv);
gamma=zeros(dof-2,numdv);

```

```

counter=1;
for k=1:numdv
    tm=zeros(dof,dof);
    tk=zeros(dof,dof);
    if counter<=nel
        con=counter+1;
        c1=(counter*2)-1;
        c2=con*2;
        tk(c1:c2,c1:c2)=ke;
    else
        r=counter-numdv/2;
        con=r+1;
        c1=(r*2)-1;
        c2=con*2;
        tm(c1:c2,c1:c2)=me;
    end
    tkact=tk(3:dof,3:dof);
    tmact=tm(3:dof,3:dof);
    for g=1:dof-2

% sensitivity calculation

        mat=tkact-wn(g)^2*tmact;
        delw=shapes(:,g)*mat*shapes(:,g);
        sens(g,k)=sens(g,k)+delw;

% Cauchy ratio calculation

        for r=1:dof-2
            if r==g
                gam=0;
            else
                gam=-(shapes(:,r)*mat*shapes(:,g))^2/((wn(g)^2-
                    wn(r)^2)*delw);
            end
            gamma(g,k)=gamma(g,k)+gam;
        end
        mat=zeros(dof-2,dof-2);
    end
    counter=counter+1;
end

omega=wn(1:4);
T=sens(1:4,:);

```

GLOOPT.M

```
% Perform multiple iterations of optimization program for different combinations  
% of design variables. This particular code is set up to do the 8 element beam problem  
% with up to 16 design variables.
```

```
global size block Tb dv0 dvsc n dvvect omega measom prop
```

```
diary
```

```
% Determine Design variable matrix for iterations.
```

```
n=4;  
block=16/n;  
bimat=dvmat(n);
```

```
% Calculate FE model and Experimental Values
```

```
prop=[10e6 .000254];  
[omega,T,cauchy]=femod(prop);  
load moddat  
omega=omega  
prodv=[9.2e6 .000254]'  
[measom,measphi]=expmod(prodv);  
measom=measom  
startpt=[10e6 .000254]';
```

```
% solve optimization problem for each set of design variables
```

```
count=n/2;  
nrow=2^n-1;  
for i=1:nrow  
    dv=zeros(n,1);  
    stpt=zeros(n,1);  
    dvvect=bimat(i,:)  
    Tact=T;  
    cauchyact=cauchy;  
    ckdv=prodv;
```

```
% generate dv vector and initial values for the iteration. Also eliminate terms to account  
% for which design variables are in used
```

```
    for j=1:n  
        if j<=count
```

```

        if dvvect(j)==1
            dv(j)=prop(1);
            stpt(j)=startpt(1)-prop(1);
        else
            dv(j)=0;
        end
    else
        if dvvect(j)==1
            dv(j)=prop(2);
            stpt(j)=startpt(2)-prop(2);
        else
            dv(j)=0;
        end
    end
end
end

```

% eliminate unneeded dv information for the iteration

```

for j=n:-1:1
    if dvvect(j)==0
        dv(j)=[];
        stpt(j)=[];
        Tact(:,(j-1)*block+1:j*block)=[];
        cauchyact(:,(j-1)*block+1:j*block)=[];
        ckdv(j)=[];
    end
end
end

```

% scale design variables

```

scale=min(dv)/max(dv);
size=length(dv);
size1=length(Tact(1,:));
sc=zeros(size1);
for j=1:size1
    sc(j,j)=1;
end
for j=1:size
    if dv(j)/prop(1)==1
        for k=(j-1)*block+1:j*block
            sc(k,k)=scale;
        end
    end
end
end
end

```

```

Tb=Tact*inv(sc);

% scale design variable vector and starting point vector

dvsc=zeros(size);
for j=1:size
    if dv(j)/prop(1)==1
        dvsc(j,j)=scale;
    else
        dvsc(j,j)=1;
    end
end
dv0=dvsc*dv;
deldv0=dvsc*stpt;
diary

% enter constrained optimization routine

[optdv,senvexp,senveig,eigvexp,mac]=optbeam(dv,deldv0,measphi);
diary

% develop vector to calculate Cauchy ratio

ddv=zeros(size*block,1);
for l=1:size
    for j=1:block
        start=(l-1)*block;
        ddv(start+j)=optdv(l)-dv(l);
    end
end

% print out solution data

optdv=optdv
data=[senvexp senveig eigvexp] % this is frequency comparison data
pctdiff=(optdv-ckdv)./ckdv*100
macsum=sum(mac);
for j=1:length(ddv)
    cauchyrat(:,j)=cauchyact(:,j)*ddv(j);
end
ratio=max(abs(cauchyrat(1:4,:)));
dvposit=1;
for j=1:n
    if dvvect(j)==1

```

```
        output(i,j)=optdv(dvposit);
        dvposit=dvposit+1;
    else
        output(i,j)=0;
    end
end
output(i,n+1)=macsum;
end
diary off
```

DVMAT.M

% develops matrix to track design variable combinations. Returns a matrix with ones
% and zeros in a binary type code.

```
function [bimat]=dvmat(n)

nrow=2^n;
bimat=zeros(nrow,n);
for i=1:n
    counter=2^(i-1);
    part1=zeros(counter,1);
    part2=ones(counter,1);
    fill(1:counter,1)=part1;
    fill(counter+1:counter*2,1)=part2;
    size=length(fill);
    for j=1:nrow/(2*counter)
        bimat((j-1)*size+1:j*size,i)=fill;
    end
end
bimat(1,:)=[];
```

OPTBEAM.M

```
% provides information needed by the optimization process

function[optdv,senvexp,senveig,eigvexp,mac]=optbeam(dv,deldv0,expsh)

global dvsc measom newom prop

% sets limits and defines information for the constrained optimization routine

ll=-.1*dv;
ul=.1*dv;
options=[];
options(1)=1;
options(2)=1e-8;
options(3)=1e-8;
options(6)=2;
options(14)=1000;

% enters the optimization routine

[optdel]=constr('objval',deldv0,options,ll,ul);

% scales the solution back to original basis and adds to original value

optdel=dvsc\optdel;
optdv=dv+optdel;

% updates FEM

[eigomega,newphi]=checkwn(optdel,prop);

% compares frequencies Sensitivity update vs experimental , Sensitivity update vs
% eigen re-solve, and eigen re-solve vs experimental (percentage basis)

senvexp=max(abs((measom-newom)./measom))*100;
senveig=max(abs((eigomega-newom)./eigomega))*100;
eigvexp=max(abs((measom-eigomega)./measom))*100;

% calculates MAC

[mac]=modcomp(expsh,newphi);
```

OBJVAL.M

% computes objective function and constraint values

function [value,con]=objval(deldv)

global size block Tb newom measom dv0 omega

% expands a single dv value up to number of linked variables, i.e. 1 E value up to 8
% elements

```
m=length(deldv);
ddv(m*block,1)=zeros;
for i=1:m
    for j=1:block
        ddv((i-1)*block+j)=deldv(i);
    end
end
```

% calculates sensitivity update

```
diff=Tb*ddv;
newom=sqrt(omega.^2+diff);
```

% calculates Objective function

```
subval1=5*sum(abs((measom-newom)./measom));
subval2=block*sum(abs(deldv./dv0));
value=subval1+subval2;
```

% calculates constraint value (none in this case)

```
con=[];
```

CHECKWN.M

% calculates updated frequencies and mode shapes based on optimization solution

function [wnnew,shapes]=checkwn(deldv,dv)

global n block dvvect

% define beam parameters (same as baseline model

```
nel=8;
nn=nel+1; % nn - number of nodes
dof=nn*2; % dof - number of degrees of freedom
lt=10;
w=3;
d=10;
```

% expands dv vector up to fill 16 values (8 for E, 8 rho)

```
for i=1:n
    for j=1:block
        if i<=n/2
            num=(i-1)*block+j;
            mod(num)=dv(1);
        else
            num=(i-n/2-1)*block+j;
            rho(num)=dv(2);
        end
    end
end
```

% adds change in design variables to original values

```
count=1;
for w=1:n
    if dvvect(w)==1
        if w<=n/2
            for j=(w-1)*block+1:w*block;
                mod(j)=mod(j)+deldv(count);
            end
        else
            q=w-n/2;
            for j=(q-1)*block+1:q*block;
```

```

                                rho(j)=rho(j)+deldv(count);
                                end
                                end

                                count=count+1;
                                end
                                end

le=lt*12/nel; % le - element length
ar=w*d;      % ar - cross sectional area
ve=ar*le;    % ve - element volume
Iner=w*d^3/12; % Iner - moment of Inertia

% calculates elemental mass and stiffness matrices

ke=[12 6*le -12 6*le;
    6*le 4*le^2 -6*le 2*le^2;
    -12 -6*le 12 -6*le;
    6*le 2*le^2 -6*le 4*le^2];
ke=(Iner/le^3)*ke;
me=[156 22*le 54 -13*le;
    22*le 4*le^2 13*le -3*le^2;
    54 13*le 156 -22*le;
    -13*le -3*le^2 -22*le 4*le^2];
me=(ve/420)*me;

% assembles global matrices

kglo=zeros(dof,dof);
mglo=zeros(dof,dof);
or i=1:nel
    con=i+1;
    c1=(i*2)-1;
    c2=con*2;
    kglo(c1:c2,c1:c2)=kglo(c1:c2,c1:c2)+mod(i)*ke;
    mglo(c1:c2,c1:c2)=mglo(c1:c2,c1:c2)+rho(i)*me;
end

% define boundary conditions

kact=kglo(3:dof,3:dof);
mact=mglo(3:dof,3:dof);

% solve eigen problem

```

```

[phi,lbd]=eig(mact\kact);
for j=1:dof-2;
    lambda(j)=lbd(j,j);
end
freqs=(sqrt(lambda));
[wn,I]=sort(freqs);
for j=1:dof-2;
    shnorm(:,j)=phi(:,I(j));
end
mtil=shnorm'*mact*shnorm;
for i=1:dof-2;
    alpha(i)=1./sqrt(mtil(i,i));
    shapes(:,i)=shnorm(:,i)*alpha(i);
end

wn=wn';
wnnew=wn(1:4);

```

CBLOC.M

```
% Perform multiple iterations of optimization program for composite beam
% to localize damage
```

```
global Tbca dv anfreq exfreqd newfreq
```

```
% Call model data
```

```
load cb8;      % composite beam data file
anfreq=omega/2/pi;
load('exfreqd.dat')
load cddamdat; % damaged composite beam data file
```

```
% solve optimization
```

```
dv=6.7576e6;
count=length(anfreq);
c=8*pi^2;
```

```
% convert sensitivities from delta lambda to delta frequency
```

```
for i=1:count
    Tb(i,:)=T(i,+)/c/anfreq(i);
end
```

```
% Enter the section of the beam to be investigated
% there must be at least 3 elements
```

```
le=input('Enter the first element of the region of interest - ');
re=input('Enter the last element of the region of interest - ');
```

```
% sum the sensitivities for the three sections
```

```
numel=re-le+1;
step=fix(numel/3);
leftover=rem(numel,3);
if leftover==0
    lb(1)=le;
    lb(2)=le+step;
    rb(1)=lb(2)-1;
    lb(3)=lb(2)+step;
    rb(2)=lb(3)-1;
    rb(3)=re;
```

```

elseif leftover==1
    lb(1)=le;
    lb(2)=le+step;
    rb(1)=lb(2)-1;
    lb(3)=lb(2)+step+1;
    rb(2)=lb(3)-1;
    rb(3)=re;
elseif leftover==2
    lb(1)=le;
    lb(2)=le+step+1;
    rb(1)=lb(2)-1;
    lb(3)=lb(2)+step;
    rb(2)=lb(3)-1;
    rb(3)=re;
end
lb(4)=le;
rb(4)=re;

% sum elements of sensitivity matrix for the three sections and
% the whole sector

temp=Tb(:,lb(1):rb(1))';
if lb(1)==rb(1)
    Tbc(:,1)=temp';
else
    Tbc(:,1)=sum(temp)';
end
temp=Tb(:,lb(2):rb(2))';
if lb(2)==rb(2)
    Tbc(:,2)=temp';
else
    Tbc(:,2)=sum(temp)';
end
temp=Tb(:,lb(3):rb(3))';
if lb(3)==rb(3)
    Tbc(:,3)=temp';
else
    Tbc(:,3)=sum(temp)';
end
Tbc(:,4)=Tbc(:,1)+Tbc(:,2)+Tbc(:,3);

% solve the optimization problem for each section

for i=1:4

```

```

    Tbca=Tbc(:,i);
    deldv0=0;

% enter optimization (values the same as previous applications)

    [optdv,ufreq,pctdiff,mcf]=dlopt(dv,deldv0,xshp,lb(i),rb(i));

    solvec(i)=optdv;
    update(:,i)=ufreq;
    pctd(:,i)=pctdiff;
    modalc(:,i)=mcf;
    end

% print results, DV values and MAC sums

solvec=solvec
modalc=modalc

% add different combinations of mode MAC's

total(1,:)=sum(modalc);
total(2,:)=sum(modalc(1:4,:));
total(3,:)=sum(modalc(5:8,:));
total(4,:)=sum(modalc(1:2,:));
total(5,:)=sum(modalc(3:4,:));
total(6,:)=sum(modalc(5:6,:));
total(7,:)=sum(modalc(7:8,:));
total(8,:)=sum(modalc(1:6,:));
total(9,:)=sum(modalc(3:8,:));

```

MODCOMP.M

% calculated modal assurance criterion

function [factor]=modcomp(old,new);

factor=zeros(8,1);

for i=1:8

 top=old(:,i)'*new(:,i);

 b1=old(:,i)'*old(:,i);

 b2=new(:,i)'*new(:,i);

 factor(i)=top^2/(b1*b2);

end

DIRECT.M

% this function solves for design variable difference with the pseudo-inverse method

function [optdv,mcf]=direct(dv,Tbca,olshp,lb,rb)

global anfreq exfreqd aset oset Ttype mact kact compshp red_shapes

% solve for dv value

```
delfreq=exfreqd-anfreq;
optdel=Tbca\delfreq;
optdv=dv+optdel;
```

```
[eigomega,mupd,kupd,upshp]=ckwn(optdel,lb,rb);
```

% select transformation matrix method

```
%[kstat,mstat,T_static]=fstatic_tam(kupd,mupd,oset,aset);
[kstat,mstat,T_static]=firstam(kupd,mupd,oset,aset);
```

% generate shape vectors

```
count=length(aset);
ndof=length(oset)+count;
```

if Ttype==1 % for reduction of analytical to experimental size

```
compshp=olshp;
[wnred,red_shapes]=shgen(mstat,kstat);
```

elseif if Ttype==2 % extraction method

```
compshp=olshp;
for i=1:count
    red_shapes(i,:)=upshp(aset(i,:))'
end
```

elseif if Ttype==3 % expand experimental up to analytical size

```
% [kstat1,mstat1,T_static1]=fstatic_tam(kact,mact,oset,aset);
[kstat1,mstat1,T_static1]=firstam(kact,mact,oset,aset);
compshp=upshp;
phi_exp=T_static1*olshp;
```

```

start=ndof-count;
for i=1:count % unpartitioning shape vector
    red_shapes(aset(i),:)=phi_exp(start,:);
    t=(i-1)*3;
    red_shapes(aset(i)+1:aset(i)+3,:)=phi_exp(t+1:t+3,:);
end
red_shapes(99,100)=[];

end

eig=eigomega/2/pi;
eigvexp=(eig-esfreqd)./exfreqd*100;

% calculating MAC

[mcf]=modcomp(compshp,red_shapes);

```

APPENDIX I. IDEAS CONVERSION INFORMATION

The IDEAS simulation software provides finite element modeling capability with a graphic end. The program allows the user to build and solve models. To allow for conversion between IDEAS and other software some conversions were necessary. The following will provide a walk through of those measures.

A. SENSITIVITY CONVERSION

The equation developed for frequency sensitivities in Chapter II, Equation (2.11), defines the frequency sensitivity as a change in lambda per change in design variable. This was the method used in the MATLAB code. IDEAS on the other hand computes the frequency sensitivity on a change in frequency per change in design variable basis. The conversion from one to the other is developed as follows by substituting for lambda:

$$\frac{\partial \lambda}{\partial DV} = \frac{\partial (2\pi f)^2}{\partial DV} = 4\pi^2 \frac{\partial f^2}{\partial DV} = 4\pi^2 (2f) \frac{\partial f}{\partial DV} \quad (I.1)$$

$$\frac{\partial \lambda}{\partial DV} = 8\pi^2 f \frac{\partial f}{\partial DV} \quad (I.2)$$

This allows the conversion of sensitivities on a lambda basis to a frequency basis. The other issue is the units of the denominator. IDEAS outputs sensitivities in the unit system designated within the model file, so if English units are designated the output file will be in English units.

B. MODE SHAPE NORMALIZATION AND MODAL MASSES

IDEAS normalizes the output mode shapes in a different fashion than MATLAB. MATLAB normalizes mode shapes so that the magnitude of the modes shape vector is one. For the models used in this thesis, English units were used, so that the nominal units

of the mode shape vector were inches for deflection and radians for rotation. Modal mass is in $\text{lbf} \cdot \text{sec}^2/\text{in}$. IDEAS normalizes mode shapes so that the magnitude of the largest single element in the modal matrix is one. The program outputs the modes shapes in metric units, so that deflections are in meters and rotations are in radians. In order to convert MATLAB data to the same format as IDEAS data the following procedure is used:

- convert active mass matrix from $\text{lbf} \cdot \text{sec}^2/\text{in}$ to kg

$$\frac{\text{lbf} \cdot \text{sec}^2}{\text{in}} * \frac{12\text{in}}{\text{ft}} * \frac{14.159\text{kg}}{\text{slug}} \quad (\text{I.3})$$

- convert translations in modal matrix from inches to meters (odd rows of matrix)

$$\text{in} * \frac{2.54\text{cm}}{\text{in}} * \frac{\text{m}}{100\text{cm}} \quad (\text{I.4})$$

- renormalize mode shape matrix so that largest term is one

$$\{\phi_i\}^R = \frac{\{\phi_i\}}{\max(\phi_i)} \quad (\text{I.5})$$

- Calculate modal mass with renormalized modal matrix and mass matrix

LIST OF REFERENCES

1. Flanigan, C.C., "Test Analysis Correlation Using Design Sensitivity and Optimization - Does It Work?", Society of Automotive Engineers, Inc., 1988.
2. Lubber, W., Sensburg, O., "Identification of Errors and Updating in Analytical Models Using Test Data", 13th International Modal Analysis Conference, Nashville, TN, 1995, pp. 407-413.
3. Dascotte, E., Stroble, J., Hua, H., "Sensitivity-Based Model Updating Using Multiple Types of Simultaneous State Variables", 13th International Modal Analysis Conference, Nashville, TN, 1995, pp. 1035-1040.
4. Vanderplaats, G., Numerical Optimization Techniques for Engineering Design, pp. 79, 88, 93, 97-100, McGraw-Hill, Inc., 1984
5. Allemang, R.J., Brown, D.L., "A Correlation Coefficient for Modal Vector Analysis", 1st International Modal Analysis Conference, , 1982, pp. 110-116.
6. Barker, T.B., Quality by Experimental Design, pp. 51-60, Marcel Dekker, Inc., 1994.
7. Hemez, F.M., Farhat, C., "Structural Damage Detection Via a Finite Element Model Updating Methodology", Modal Analysis, The International Journal of Analytical and Experimental Modal Analysis, Volume 10, Number 3, July 1995.
8. Crema, L.B., Castellani, A., Coppotelli, G., "Generalization of Non-destructive Damage Evaluation Using Modal Parameters", 13th International Modal Analysis Conference, Nashville, TN, 1995, pp. 429-434.
9. Lam, H.F., Ko, J.M., Wong, C.W., "Detection of Damage Location Based on Sensitivity Analysis", 13th International Modal Analysis Conference, Nashville, TN, 1995, pp. 1499-1505.
10. Zongbou Li, Houghton, J.R., "Damage Location in Structures Using Vibration Data and It's Sensitivity to Measurement Errors", 13th International Modal Analysis Conference, Nashville, TN, 1995, pp. 1418-1424.
11. Brandon, J.A., "Second-order Design Sensitivities to Assess the Applicability of Sensitivity Analysis", Journal of the American Institute of Aeronautics and Astronautics, Volume 29, Number 1, January 1991, pp. 135-139.
12. Guyan, R.J., "Reduction of Stiffness and Mass Matrices", Journal of the American Institute of Aeronautics and Astronautics, Vol. 3, February 1965, p. 380.

13. O'Callahan, J., "A Procedure for an Improved Reduction System (IRS) Model", 7th International Modal Analysis Conference, Las Vegas, NV, 1989.
14. Campbell, M., "Structural Damage Detection Using Frequency Domain Error Localization", Master's Thesis, Naval Postgraduate School, December 1994.
15. IDEAS Master Series 2.1 Manuals

INITIAL DISTRIBUTION LIST

	No. Copies
1. Defense Technical Information Center 8725 John J. Kingman Rd., STE 0944 Ft. Belvoir, VA 22060-6218	2
2. Library, Code 13 Naval Postgraduate School Monterey, California 93943-5101	2
3. Professor J.H. Gordis, Code ME/GO Department of Mechanical Engineering Naval Postgraduate School Monterey, California 93943	3
4. Naval Engineering Curricular Office Code 34 Naval Postgraduate School Monterey, California 93943-5000	1
5. LCDR Jay A. Renken, USN Naval Sea Systems Command (PMS-303) 2531 Jefferson Davis Highway Arlington, VA 22242-5160	2